Research Paper

Geosphere, published online on 5 February 2016 as doi:10.1130/GES01198.1

GEOSPHERE

GEOSPHERE; v. 12, no. 2

doi:10.1130/GES01198.1

11 figures; 2 tables; 1 supplemental file

CORRESPONDENCE: jenseriklundsnee@gmail.com

CITATION: Lund Snee, J.-E., Miller, E.L., Grove, M., Hourigan, J.K., and Konstantinou, A., 2016, Cenozoic paleogeographic evolution of the Elko Basin and surrounding region, northeast Nevada: Geosphere, v. 12, no. 2, doi:10.1130/GES01198.1.

Received 2 May 2015
Revision received 7 December 2015
Accepted 23 December 2015

Cenozoic paleogeographic evolution of the Elko Basin and surrounding region, northeast Nevada

J.-E. Lund Snee[1,*], E.L. Miller[1], M. Grove[1], J.K. Hourigan[2], and A. Konstantinou[3]

[1]Department of Geological Sciences, 450 Serra Mall Building 320, Room 118, Stanford University, Stanford, California 94305, USA
[2]Department of Earth and Planetary Sciences, 1156 High Street, Room A232, University of California, Santa Cruz, Santa Cruz, California 95064, USA
[3]Oil and Gas Engineering Department, University of Nicosia, 46 Makedonitissas Avenue, Engomi, P.O. Box 24005, 1700 Nicosia, Cyprus

ABSTRACT

Geologic mapping, supported by $^{40}Ar/^{39}Ar$ and U-Pb geochronology and geochemistry of sedimentary and volcanic rocks, reveals the details of the Cenozoic depositional and tectonic history of the eastern Piñon Range and central Huntington Valley in the north-central Basin and Range Province, Nevada (USA). Cretaceous to Miocene supracrustal successions were studied in detail in order to compare the geologic evolution of the upper crust near the Ruby Mountains–East Humboldt Range (RMEH) metamorphic core complex (MCC) with the magmatic, metamorphic, and deformational history of the deep crust in the developing MCC. During the well-documented Late Cretaceous–Oligocene history of partial melting and infrastructure development within the RMEH, surface deposits in Huntington Valley reflect general tectonic quiescence, with evidence for the development of the shallow Elko Basin, minor extension, and eruption of southward-younging ignimbrite flare-up volcanism. Thin, discontinuous successions of Cretaceous–early Cenozoic sedimentary strata were locally blanketed by rhyodacite ignimbrites, domes, and subvolcanic intrusions of the Robinson Mountain volcanic field between 38.5 and 36.8 Ma. This magmatic event represents the first local expression of Cenozoic volcanism linked to the ignimbrite flare-up, and its onset occurred slightly after a renewal of partial melting in the RMEH beginning ca. 42 Ma. The volcanic section was subsequently tilted ~10°–15° west before ca. 33.9 ± 0.4 Ma. Although melting continued at depth in the RMEH until after 30 Ma, there was no eruption of volcanic rocks after Robinson Mountain volcanism. An additional ≥10°–15° of westward tilting occurred between 31.1 ± 0.3 Ma and ca. 24.4 Ma, as bracketed by the 31 Ma tuff of Hackwood Ranch (which was probably erupted from a distant caldera) and an angular unconformity beneath the overlying Miocene Humboldt Formation. Neither of these tilting events and unconformities appears to represent significant (>~1 km each) extension, but they could be surface expressions of magmatism, metamorphism, and crustal flow at depth. The Humboldt Formation includes >2000 m of sediment deposited mostly between ca. 16 and 12 Ma, with deposition lasting until at least ca. 8.2 Ma. Humboldt Formation sediments thicken eastward, toward the west-dipping fault that bounds the RMEH, and are interpreted as a basin that developed in the hanging wall of this fault system. Motion on this normal fault system led to the exhumation of metamorphic and igneous rocks of the core complex ~10 m.y. after the documented cessation of partial melting, high-temperature metamorphism, and intrusion of granitoids into the deep crust ca. 29 Ma. Metamorphic clasts and a detrital zircon signature thought to represent RMEH provenance are first detected in 14.2 Ma or younger sediments.

INTRODUCTION

The northern Basin and Range Province (BRP) of western North America (Fig. 1A) has had a protracted history of Cenozoic east-west–directed extension that also involved the uplift of anomalous exposures of deeper crustal rocks in metamorphic core complexes (MCCs) (e.g., Coney, 1980; Armstrong, 1982; Coney and Harms, 1984; Dickinson, 2006, 2013; Colgan, 2013). Despite decades of study, there is still much disagreement on the exact timing, nature, and geodynamic setting for the uplift of metamorphic rocks in MCCs (e.g., discussions in Wells et al., 2012; Miller et al., 2012).

Quantitative geobarometry of metamorphic rocks in northern BRP core complexes yields data that require uplift of some of these rocks from at least 35 km depth, perhaps in more than one stage of extension, beginning in the Late Cretaceous to early Cenozoic (e.g., Hodges et al., 1992; McGrew and Snee, 1994; Lewis et al., 1999; McGrew et al., 2000; Wells and Hoisch, 2008; Cooper et al., 2010; Wells et al., 2012; Hallett and Spear, 2014, 2015; Willis, 2014). These data have implications for crustal thicknesses at the end of crustal shortening in the Mesozoic and whether the crust had become thick enough to collapse gravitationally prior to Basin and Range extension, as proposed by Vandervoort and Schmitt (1990), Hodges and Walker (1992), Camilleri and Chamberlain (1997), Sonder and Jones (1999), DeCelles and Coogan (2006), Wells and Hoisch (2008), and Wells et al. (2012). The major structures proposed by these authors to have operated during the Cretaceous to Paleogene extensional events have not been clearly identified as surface-breaking features except in one place (Camilleri, 1996; Camilleri et al., 1997). Maps of rock units and structures beneath the reconstructed Cenozoic unconformity have also not found clear evidence for these structures (e.g., Gans and Miller, 1983; Van Buer et al., 2009; Konstantinou et al.,

*Present address: Department of Geophysics, 397 Panama Mall, Mitchell Building, 3rd Floor, Stanford University, Stanford, CA, 94305-2210, USA.

Geosphere, published online on 5 February 2016 as doi:10.1130/GES01198.1

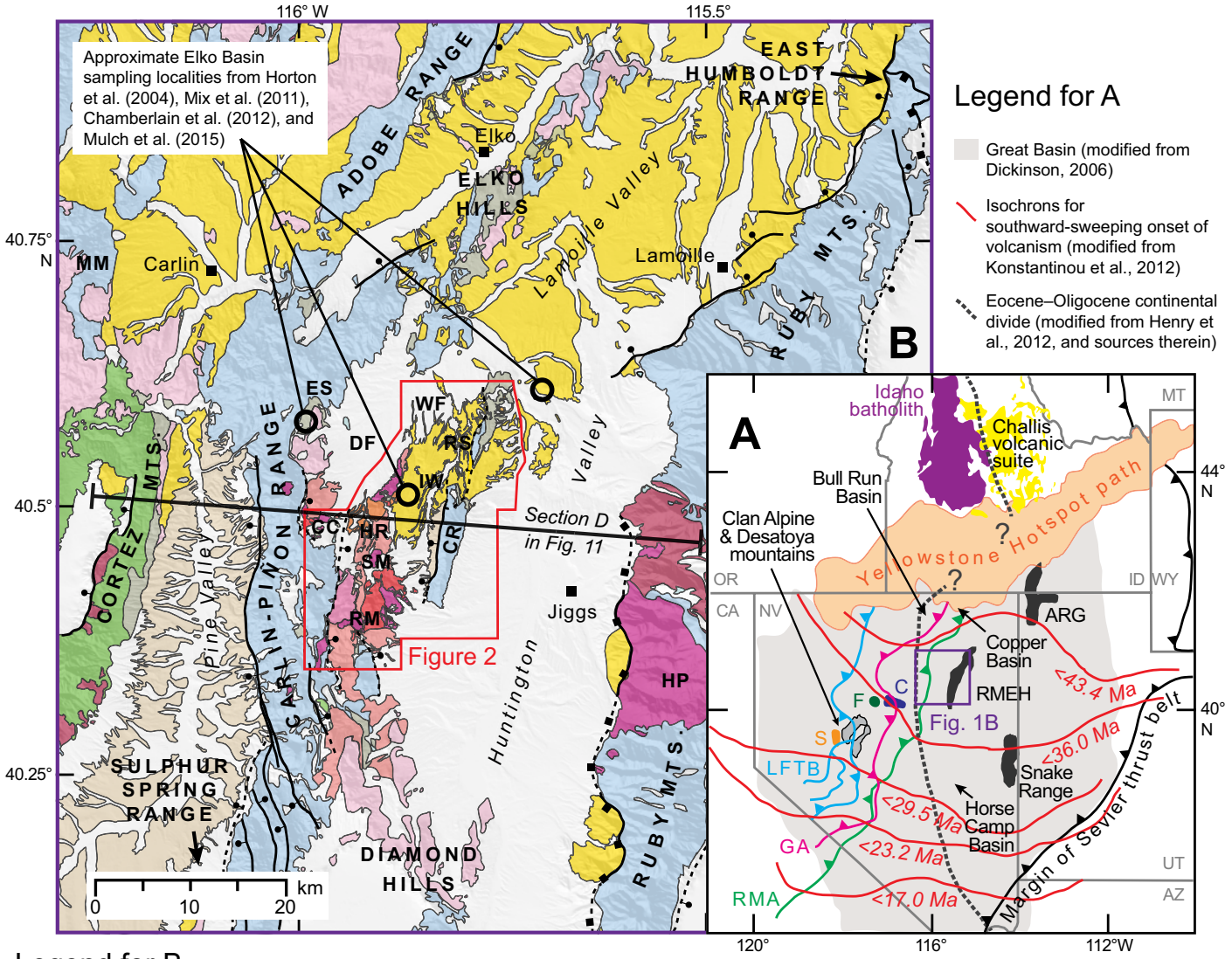

Legend for A

- Great Basin (modified from Dickinson, 2006)
- Isochrons for southward-sweeping onset of volcanism (modified from Konstantinou et al., 2012)
- Eocene–Oligocene continental divide (modified from Henry et al., 2012, and sources therein)

Legend for B

- Normal fault (from Colgan et al., 2010, and references therein, and this study)
- Detachment fault (from Colgan et al., 2010, and references therein)
- Quaternary sediments
- Latest Neogene–Quaternary Hay Ranch Formation
- Miocene sedimentary rocks
- Oligocene tuff of Hackwood Ranch
- Eocene ignimbrites
- Eocene felsic to mafic lavas
- Eocene plutonic rocks and subvolcanic intrusions
- Undifferentiated Cenozoic igneous rocks
- Cretaceous to Eocene sedimentary rocks
- Jurassic and Cretaceous plutonic rocks
- Jurassic volcanic and sedimentary rocks
- Undifferentiated Paleozoic rocks

Figure 1. (A) Index map of the Great Basin region showing the location of the study area and salient features discussed in the text. RMEH—Ruby Mountains–East Humboldt Range metamorphic core complex; ARG—Albion–Raft River–Grouse Creek Range metamorphic core complex; C—Caetano caldera; F—Fish Creek Mountains caldera; S—Stillwater complex calderas, including the Elevenmile Canyon and Poco Canyon calderas; LFTB—Luning-Fencemaker thrust belt; GA—Golchonda allochthon; RMA—Roberts Mountains allochthon. Great Basin boundaries and eastern margins of Golchonda and Roberts Mountains allochthons are modified from Dickinson (2006). Luning-Fencemaker thrust belt is modified from Best et al. (2009); Sevier thrust front is after DeCelles (2004); Eocene–Oligocene paleodivide is modified from Henry et al. (2012); extent of Idaho batholith and Challis volcanic field is modified from Chetel et al. (2011); Caetano, Fish Creek Mountains, and Stillwater Range complex caldera locations are modified from John et al. (2008). (B) Geologic map of study area and surrounding region. Base map was generated in GeoMapApp v.3.3.9 (Haxby et al., 2010) using the GMRT (Global Multi-Resolution Topography) base map (Ryan et al., 2009). Geologic unit boundaries are simplified from Crafford (2007), Colgan et al. (2010), and this study. MM—Mary's Mountain; ES—Emigrant Spring; WF—White Flats; DF—Dixie Flats; RS—Red Spring; CC—Cissillini Canyon; HR—Hackwood Ranch; CR—Cedar Ridge; SM—Squaw Mountain; RM—Robinson Mountain; HP—Harrison Pass.

Geosphere, published online on 5 February 2016 as doi:10.1130/GES01198.1

2012; Long, 2012). Some argue that, near the Ruby Mountains–East Humboldt Range (RMEH), motion on the west-dipping MCC detachment fault (Fig. 1) began at or before the Eocene or Oligocene (e.g., Dallmeyer et al., 1986; Dokka et al., 1986; McGrew and Snee, 1994; Howard, 2003), and the accumulation of Paleogene or older strata next to the Ruby Mountains has been used as evidence for significant pre-Miocene normal faulting (e.g., Solomon et al., 1979; Vandervoort and Schmitt, 1990; Mueller and Snoke, 1993; Brooks et al., 1995; Satarugsa and Johnson, 2000; Rahl et al., 2002). However, Henry (2008), Colgan et al. (2010), and Henry et al. (2012) provided evidence that RMEH MCC uplift happened almost entirely in the Miocene with negligible faulting prior to this time (see discussion in Henry et al., 2011), a discovery compatible with the Miocene uplift histories of other core complexes of the northern BRP (e.g., Miller et al., 1999; Konstantinou et al., 2012, 2013; Ruksznis, 2015).

This study directly addresses these problems and questions by documenting in detail the evolution of the upper crust across a broad region flanking the RMEH (Figs. 1B, 2, and 3) to investigate which events are recorded by its rich and long-lived Late Cretaceous and Cenozoic sedimentary and volcanic history, and how this evolution compares to the coeval history of the deeper crust represented by the igneous and metamorphic rocks of the RMEH. Our contribution is based on 1:24,000 scale geologic mapping of sedimentary and volcanic rocks present within central Huntington Valley and the eastern Piñon Range (Fig. 2) west of the southern and central RMEH. This region is underlain by a remarkably complete and well-exposed Cenozoic succession (Fig. 1B). Previous work (Smith and Ketner, 1976, 1978; Horton et al., 2004) reported thick accumulations of Late Cretaceous–Quaternary rocks, some of which have been previously interpreted to represent pre-Miocene synextensional sedimentation and volcanism associated with evolution and exhumation of the RMEH (Satarugsa and Johnson, 2000; Haynes, 2003; Howard, 2003; discussion in Henry et al., 2011). Our study of this same stratigraphy incorporates extensive detrital zircon U-Pb geochronology, $^{40}Ar/^{39}Ar$ ages of sanidine from tuffs, and U-Pb zircon geochronology and whole-rock geochemistry of volcanic rocks in order to better constrain depositional ages and improve lithologic correlations within this succession. Our new data allow us to more carefully assess the supracrustal history and compare it to the magmatic, metamorphic, and deformational history detailed for the RMEH MCC. The data also significantly improve our understanding of regionally important Cenozoic time-stratigraphic sections, some of which have been targeted for Cenozoic paleoclimate and paleoelevation studies (e.g., Horton et al., 2004; Mix et al., 2011; Chamberlain et al., 2012; Feng et al., 2013; Mulch et al., 2015).

GEOLOGIC SETTING

The RMEH exposes Precambrian basement, Neoproterozoic–Paleozoic metamorphosed shelf margin sediments, and Mesozoic–Cenozoic plutonic rocks (e.g., Snoke, 1980; Stewart, 1980; Wright and Snoke, 1993; MacCready et al., 1997; McGrew et al., 2000; Premo et al., 2008, 2014; Colgan et al., 2010; Lund et al., 2010; McGrew and Snoke, 2010, 2015; Howard et al., 2011). These rocks were exhumed by Cenozoic normal slip on a (now) shallowly west-dipping (~20°) brittle fault system mapped along the western side of the RMEH that cuts a subparallel mylonite shear zone (e.g., Mueller and Snoke, 1993; Sullivan and Snoke, 2007; Colgan et al., 2010). Continued uplift of the range occurred along steeply west- and east-dipping normal faults bounding the west and east sides of the range (Colgan et al., 2010; Fig. 1B).

Most of the pre-Cenozoic strata exposed in the Carlin-Piñon Range and surrounding region (Fig. 1) consist of ocean basin and continental slope sedimentary and volcanic rocks of the Roberts Mountains allochthon, emplaced over shelfal rocks during the earliest Mississippian Antler orogeny (Burchfiel and Davis, 1975; Johnson and Pendergast, 1981; Turner et al., 1989; Trexler and Nitchman, 1990; Burchfiel et al., 1992; Johnson and Visconti, 1992; Miller et al., 1992; Trexler et al., 2004). The study area (Fig. 1B) contains foreland basin strata deposited east of the Antler thrust front, including the Chainman Shale and Diamond Peak Formation sandstone and conglomerate (Smith and Ketner, 1978; Trexler and Nitchman, 1990; Longo et al., 2002; Colgan and Henry, 2009). Pennsylvanian–Permian terrestrial and shallow-marine carbonates of the Antler overlap sequence were subsequently deposited across the eroded Roberts Mountains allochthon, foreland basin succession, and lower plate autochthonous rocks (Smith and Ketner, 1975, 1978; Stewart, 1980; Johnson and Pendergast, 1981; Johnson and Visconti, 1992; Ketner, 1998; Cook and Corboy, 2004; Colgan and Henry, 2009). Specific lithologies in the map area include quartzite and chert pebble conglomerates of the Mississippian–Pennsylvanian Diamond Peak Formation, shale and sandstone of the Mississippian Chainman Shale, silty, cliff-forming, cherty limestones of the Pennsylvanian Moleen Formation, and undivided platy siltstones and sandstones of Pennsylvanian–Permian age (Smith and Ketner, 1975, 1978; Stewart, 1980; Coats, 1987).

Regional pre-Cenozoic subcrop maps constructed across the northern Great Basin west of the Sevier fold and thrust belt indicate that mostly Pennsylvanian, Permian, and Triassic age strata were exposed at the surface prior to the eruption of Eocene–Oligocene volcanic rocks (Gans and Miller, 1983; Van Buer et al., 2009; Konstantinou et al., 2012; Long, 2012). Minor exposures of Cretaceous to Eocene strata occur beneath the volcanic section in isolated localities across eastern Nevada (e.g., Fouch et al., 1979; Vandervoort and Schmitt, 1990; Rahl et al., 2002; Druschke et al., 2009, 2011), but the Elko Basin (including the study area; Figs. 1 and 2) is one of the few places that has significant exposures of strata in this age range (Smith and Ketner, 1976; Solomon et al., 1979; Server and Solomon, 1983; Ketner and Alpha, 1992; Haynes, 2003; Henrici and Haynes, 2006; Henry, 2008; Colgan and Henry, 2009; Colgan et al., 2010; this study). The generally low temperatures of diagenesis for strata beneath the unconformity, based on organic maturation and conodont alteration indices (Gans et al., 1990; Crafford, 2005; Long, 2012) and low-temperature thermochronology (e.g., Colgan et al., 2010), indicate that they were never buried beneath substantial accumulations of sediment or tectonic overburden that might have been subsequently eroded away.

Geosphere, published online on 5 February 2016 as doi:10.1130/GES01198.1

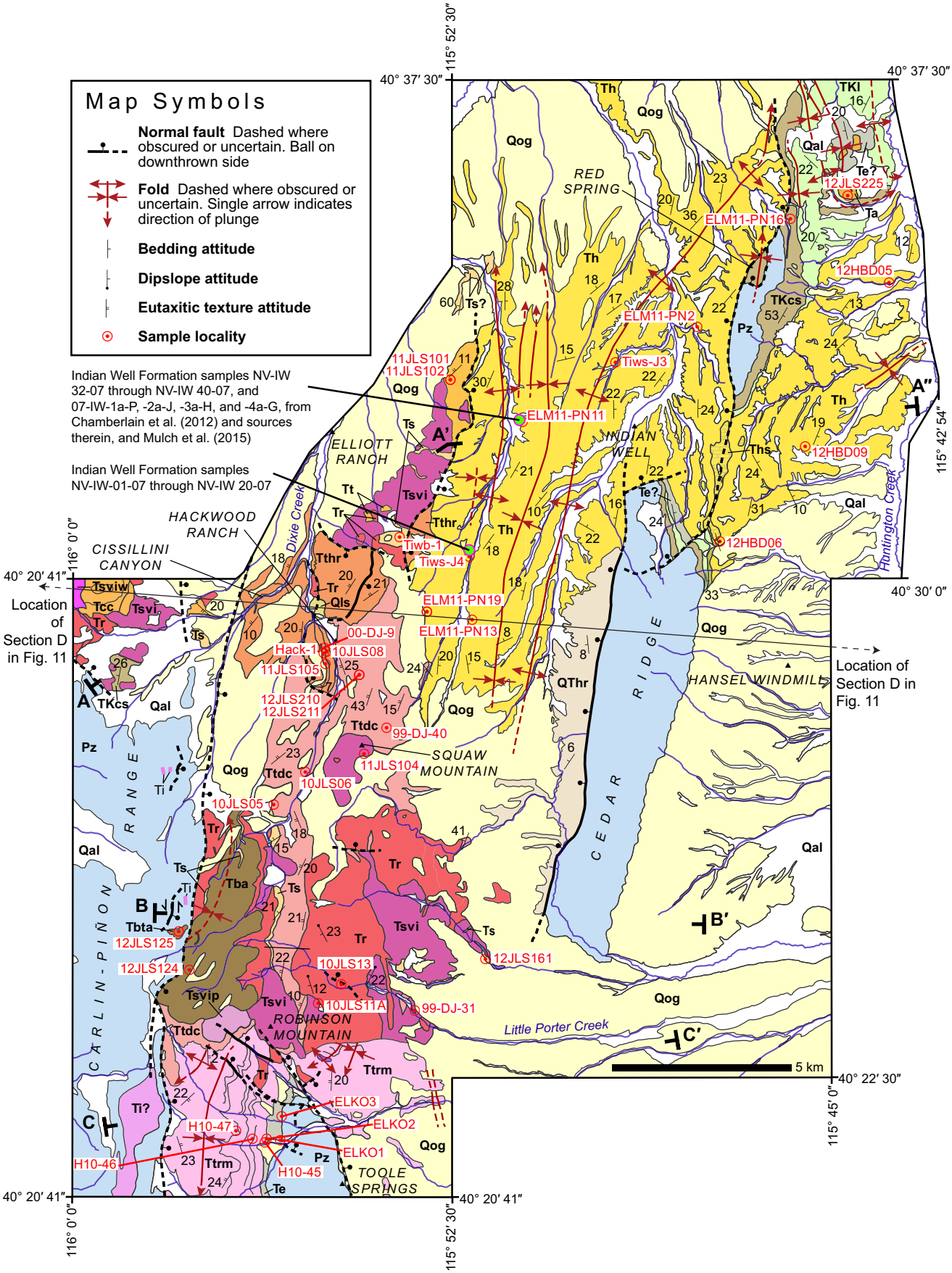

Figure 2 (*on this and following page*). Geologic map and cross sections of the study area, simplified from Lund Snee (2013) and Lund Snee and Miller (2015).

Geosphere, published online on 5 February 2016 as doi:10.1130/GES01198.1

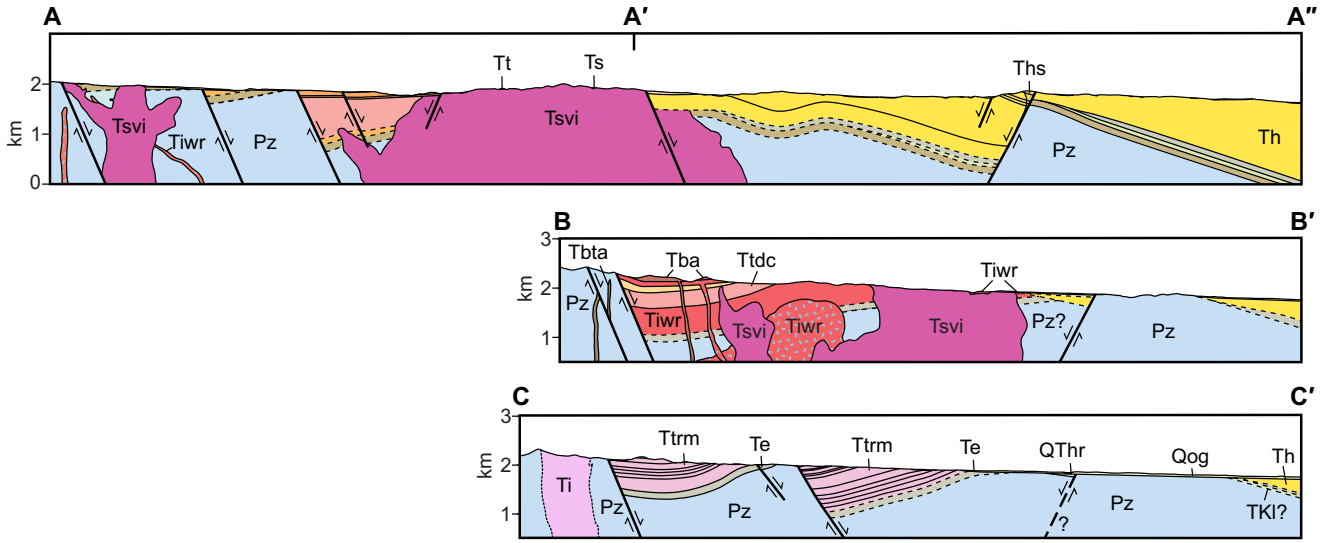

Qal Quaternary alluvium
Qls Quaternary landslide deposits
Qog Older Quaternary gravels
QThr Latest Neogene–Quaternary Hay Ranch Formation

MIOCENE HUMBOLDT FORMATION AND ASSOCIATED UNITS

Ta Miocene(?) andesite volcanic rocks
Ths Silicified sedimentary rocks
Th Humboldt Formation

EOCENE–OLIGOCENE(?) FELSIC TO MAFIC IGNEOUS ROCKS

Tthr Oligocene tuff of Hackwood Ranch and underlying sedimentary rocks
Tbta Eocene(?) basaltic trachyandesite
Tba Eocene(?) basaltic andesite

EOCENE ROBINSON MOUNTAIN VOLCANIC FIELD

Ts Eocene or Oligocene sedimentary rocks
Tsvi Undifferentiated subvolcanic intrusions
Tsvip Light gray–pink, flow-banded, biotite and smoky quartz-bearing subvolcanic intrusions
Tsviw White, flow-banded, tabular subvolcanic intrusions
Ti Light-colored, flow-banded silicic subvolcanic intrusions and dikes (Eocene?; mapped by Smith & Ketner, 1978)
Tr Rhyolite flows and domes, patterned on cross sections where intrusive equivalent is inferred
Tt Undifferentiated tuffs
Ttdc tuff of Dixie Creek
Ttrm tuff of Robinson Mountain
Tcc tuff of Cissillini Canyon

Te Eocene Elko Formation
TKl Late Cretaceous or Eocene(?) limestone
TKcs Late Cretaceous or Eocene(?) conglomerate, sandstone, siltstone, and limestone “redbeds”

Pz Undifferentiated Mississippian to Permian sedimentary and metasedimentary rocks (mapped by Smith & Ketner, 1978)

Figure 2 (*continued*).

Geosphere, published online on 5 February 2016 as doi:10.1130/GES01198.1

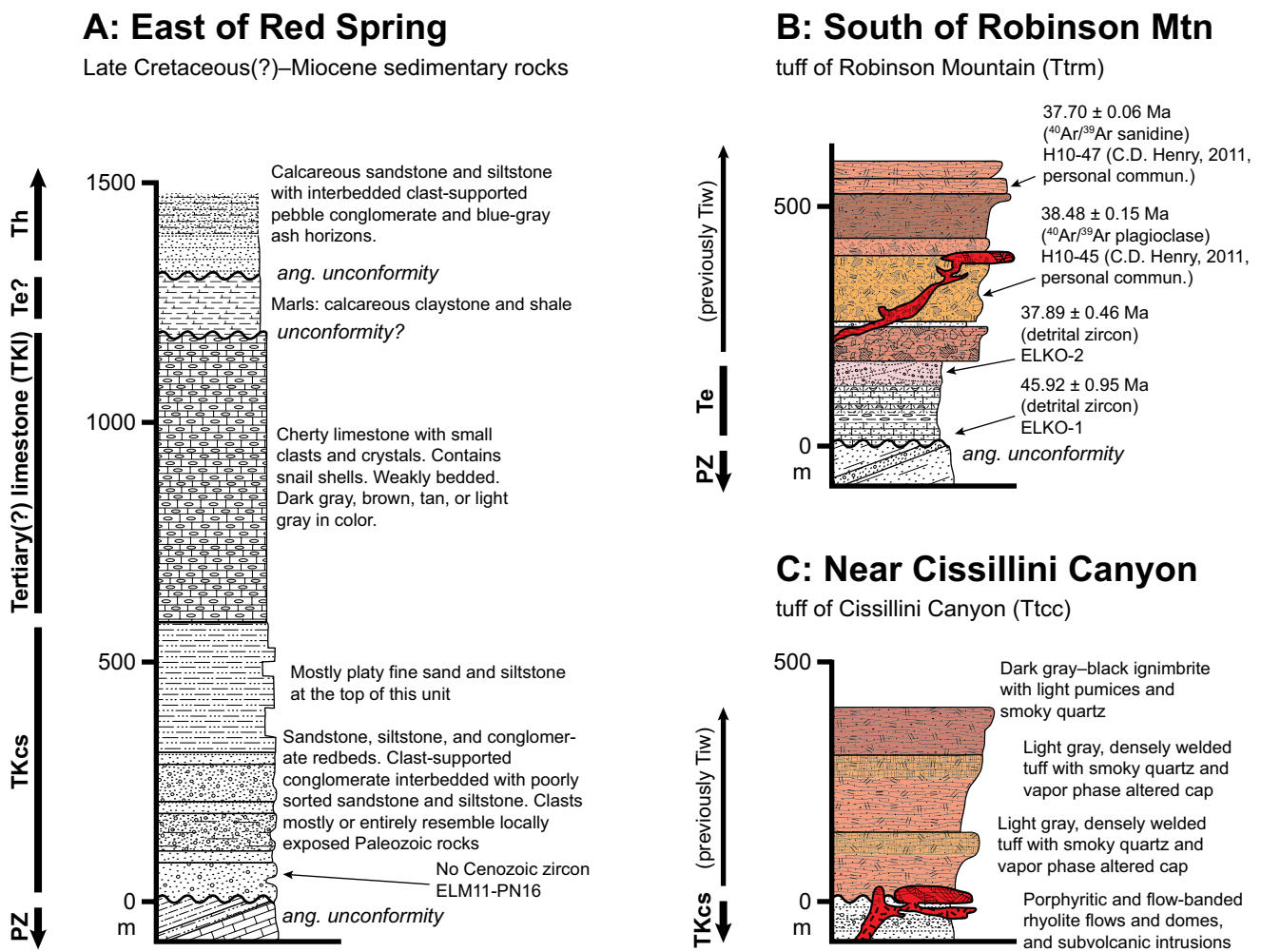

Figure 3 (*on this and following page*). (A–E) Generalized stratigraphic columns for the study area labeled by geographic names with locations shown in Figures 1B and 2. Where feasible, unit thicknesses were measured in the field or from map contacts where exposure is poor. Detrital zircon ages represent maximum depositional ages as discussed in the text. Th—Humboldt Formation; Te—Elko Formation; TKcs—conglomerate, sandstone, siltstone, and limestone; Tba—mafic–intermediate lavas; Tthr—tuff of Hackwood Ranch; Tiw—Indian Well Formation (name questioned); ang—angular.

However, one area, which includes the East Humboldt Range, Wood Hills, and Pequop Range, exposes strata exhibiting high metamorphic grades and yielding high geobarometric estimates (e.g., Camilleri, 1996; Camilleri and Chamberlain, 1997; McGrew et al., 2000; Hallett and Spear, 2014, 2015; Willis, 2014). It has been proposed that the Paleozoic rocks exposed in this area were buried during Jurassic–Cretaceous time beneath a thrust sheet, so this area would thus represent a proposed exception to the lack of tectonic burial elsewhere (Camilleri and Chamberlain, 1997; discussion in Long, 2012).

Volcanic activity began in the RMEH area of northeast Nevada ca. 42–40 Ma as part of the southward-sweeping volcanic front across Nevada (e.g., Armstrong, 1970; McKee et al., 1970, 1971; Armstrong and Ward, 1991; Best and Christiansen, 1991; Brooks et al., 1995; Humphreys, 1995; Ressel

Geosphere, published online on 5 February 2016 as doi:10.1130/GES01198.1

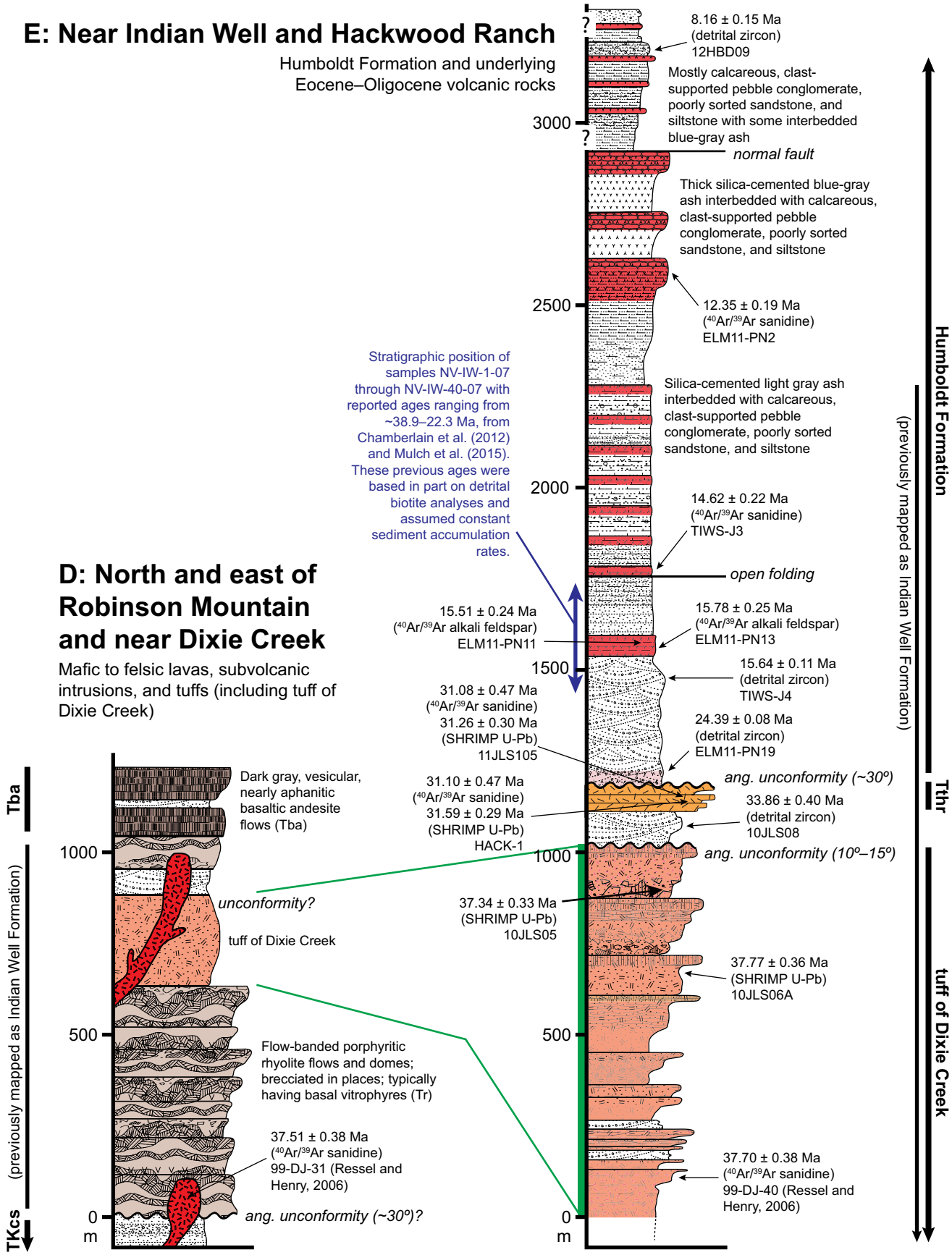

Figure 3 (*continued*).

Geosphere, published online on 5 February 2016 as doi:10.1130/GES01198.1

and Henry, 2006; Howard et al., 2011; Konstantinou et al., 2012). Voluminous volcanic and subvolcanic rocks in the study area (Fig. 2) record the arrival of the volcanic front ca. 38 Ma (Palmer et al., 1991; Gordee et al., 2000; Ressel and Henry, 2006; this study). The volcanic rocks are overlain by a thick succession of post-volcanic Miocene sedimentary rocks (Figs. 1–3) deposited in a fluviolacustrine setting with intercalated vitric tuffs derived from silicic eruptions in the Snake River Plain (Sharp, 1939; Perkins et al., 1998; Wallace et al., 2008; Colgan et al., 2010; Ellis et al., 2010; this study).

METHODS

Geologic mapping of Cenozoic rocks in the central Huntington Valley and the eastern Piñon Range was carried out at 1:24,000 scale (Lund Snee and Miller, 2015), and a simplified geologic map is included here (Fig. 2). Photographs, photomicrographs, and detailed lithologic descriptions are also presented in Lund Snee (2013) and summarized in Table 1. Within the Eocene Robinson Mountain volcanic field, we differentiated igneous rock types and, where possible, mapped individual cooling units. In most cases we retained the geologic unit names for sedimentary rocks used in previous studies (Smith and Howard, 1977; Smith and Ketner, 1978), but we consolidated some units and eliminated the Smith and Ketner (1978) Indian Well Formation, much of which, based on this study, now forms part of the mostly Miocene Humboldt Formation.

The U-Pb and $^{40}Ar/^{39}Ar$ geochronology was carried out on 24 samples to better constrain depositional ages. The results of these analyses are summarized in Table 2, together with ages for parts of the section obtained from previous studies. Ion microprobe analyses were undertaken at the Stanford–U.S. Geological Survey Microanalysis Center to acquire trace element and U-Pb data from volcanic and subvolcanic units. Crystallization ages were determined from Tera-Wasserburg concordia intercept ages defined by the youngest zircon population (Fig. 4). Single crystal fusion $^{40}Ar/^{39}Ar$ results from alkali feldspar were obtained at the Stanford Noble Gas Laboratory, and weighted mean ages were used to calculate eruptive ages (Fig. 5). Inverse isochron ages for these samples generally agree with the weighted mean ages within 95% confidence (Supplemental File[1]). Errors for $^{40}Ar/^{39}Ar$ ages quoted in the text and Table 2 are 2σ total errors that facilitate comparison with U-Pb ages. These total errors take into account the systematic errors in flux monitor $^{40}Ar^*/^{40}K$ (Phillips and Matchan, 2013) and ^{40}K decay constants (Renne et al., 2010), in addition to the analytical errors. We used laser ablation–inductively coupled plasma–mass spectrometry (LA-ICP-MS) methods to acquire detrital zircon age distributions at laboratories at the University of California, Santa Cruz and the University of Arizona LaserChron Center. Detrital zircon depositional ages were determined by taking the weighted mean of the youngest grains whose ages were indistinguishable at 95% confidence (Fig. 6). Detrital zircon age distributions are shown in Figure 7. Whole-rock geochemical analyses of 15 igneous samples were carried out at Macalester College (Minnesota) and Washington State University. A complete description of analytical details is included with data tables and supplementary plots of results in the Supplemental File.

CENOZOIC STRATIGRAPHY OF CENTRAL HUNTINGTON VALLEY AND THE EASTERN PIÑON RANGE, AND CONSTRAINTS UPON DEPOSITIONAL AGES

Late Cretaceous(?)–Eocene(?) Sedimentary Rocks

Conglomerate, sandstone, siltstone, and limestone are the oldest strata deposited above the Cenozoic unconformity developed across late Paleozoic strata. Pebble conglomerate and redbed sandstone occur at the base of the section (unit TKcs; Figs. 2 and 3A; Table 1). The redbeds are overlain by dense, brownish-purple, light orange, or white, massive to bedded limestone that commonly contains chert nodules (unit TKl; Fig. 3A). Although some (Smith and Ketner, 1976, 1978) differentiated the redbeds and overlying limestones into four map units, we follow Solomon et al. (1979), who grouped these strata into two units near the Elko Hills (Fig. 1B), TKcs and TKl (Fig. 2). TKcs and TKl have maximum thicknesses of ~580 m and ~600 m, respectively, and are stratigraphically below the Eocene Elko Formation (Fig. 2). Neither of these older units is present near Robinson Mountain, on the west side of the map area, where the younger Elko Formation directly overlies Mississippian- and Pennsylvanian-age rocks beneath the Cenozoic unconformity (Smith and Ketner, 1978; Figs. 1B and 2).

Conglomerates in the redbed succession (TKcs) have pebbles and cobbles of carbonate derived from underlying Paleozoic strata. Fine sandstones and siltstones are more common upward in the stratigraphic section, suggesting a transition from alluvial fan or fluvial to shallow lacustrine settings. A sample of pebbly sandstone (ELM11-PN16) collected from the redbeds (unit TKcs; Figs. 2 and 3A) yielded dominant U-Pb detrital zircon age peaks of 240 Ma, 380 Ma, 456 Ma, 629 Ma, 993 Ma, and 1.39 Ga, with minor maxima at 420 Ma, ca. 1.10 Ga, and 1.74 Ga (Fig. 7). The lack of Cenozoic zircons is striking compared to their abundance in younger strata (Fig. 7), and this supports Smith and Ketner's (1976) decision to differentiate this unit from overlying strata such as the Elko Formation based on the lack of Cenozoic volcanic detritus in the redbeds. Although the lack of zircon younger than Triassic in this sample prevented us from calculating a maximum depositional age, we conclude that the redbeds and overlying limestones were most likely deposited before late Eocene (ca. 46 Ma or later) volcanic detritus was deposited in the area. Limited fossil evidence suggests that TKcs is probably not older than Cretaceous (Smith and Ketner, 1976). Based upon lithologic comparisons with other basal Cenozoic or Late Cretaceous clastic sedimentary rocks and carbonates described across the region, such as the Sheep Pass Formation (Fouch et al., 1979; Moore et al., 1983; Ketner and Alpha, 1992; Druschke et al., 2009, 2011), we provisionally assign a Late Cretaceous to Eocene (pre–46 Ma) age for deposition of both the redbeds (TKcs) and limestones (TKl).

Lund Snee, J.-E., Miller, E.L., Grove, M., Hourigan, J.K., and Konstantinou, A., 2016, Cenozoic paleogeographic evolution of the Elko Basin and surrounding region, northeast Nevada: Geosphere, v. 12, doi:10.1130/GES01198.1.

SUPPLEMENTAL FILE. ANALYTICAL METHODS AND RESULTS

Overview

This section describes analytical and sample preparation methods for geochronology conducted in this study to obtain maximum depositional ages and detrital provenance information on Cenozoic rocks in the eastern Piñon Range and central Huntington Valley, Nevada. Methods for $^{40}Ar/^{39}Ar$ geochronology of sanidine are detailed in Section A.2, and analytical results are given in Tables A1 and A2 and shown in Figure 5. Inverse isochron and weighted mean model ages, as well as Ca/K plots, are shown for each sample in Figure A1. Methods for ion probe U-Pb geochronology and trace element analysis of zircon using SHRIMP-RG are described in Section A.3, and analytical results are tabulated in Tables A3 and A7 and shown in Figure 4. Methods for U-Pb geochronology of zircon using LA-ICP-MS are described in Section A.4, and results are tabulated in Tables A4 and A5 and plotted in Figures 6 and 7. Concordia plots for some U-Pb detrital zircon samples are shown in Figure A2. Methods for whole-rock geochemical analysis are described in Section A.4, and results are tabulated in Table A6 and shown in Figures A3 and A4. Geologic units are summarized in Table 1 and geochronologic results from this study and others near the study area are summarized in Table 2. Sample localities from this study are shown on the simplified geologic map of the study area (Figure 2) and their relative stratigraphic positions are indicated on Figure 3. Additional details of analytical procedures and results are in Lund Snee (2013).

$^{40}Ar/^{39}Ar$ sanidine geochronology

Six samples of sanidine-bearing ignimbrites and air-fall tuffs were selected for $^{40}Ar/^{39}Ar$ age analysis. The freshest available samples were extracted from outcrop with care taken to remove weathered rinds. The small dimensions and indurated nature of pumice present within the two ignimbrites analyzed from the tuff of Hackwood Ranch prevented extraction of sanidine directly from pumice. Samples were conventionally crushed and sieved to obtain the size fraction containing the largest proportions of sanidine. Recovered crystals were typically 250–500 μm. Sanidine was concentrated using a Frantz magnetic separator operated up to 2.1 A, ultrasonically cleaned in deionized water, hand selected with the aid of a binocular microscope, packed in Cu foil, and sealed under vacuum together with flux monitors in Cd-shielded quartz tubes. Taylor Creek sanidine flux monitors (28.34 ± 0.28 Ma; Renne et al., 1998) spaced at 5 mm were used to monitor the $^{39}K(n,p)^{39}Ar$ reaction in the central thimble of the U.S. Geological Survey TRIGA reactor in Lakewood, Colorado (Dalrymple et al., 1981). The 28.34 Ma age of Taylor Creek sanidine is equivalent to a Fish Canyon sanidine standard age of 28.02 ± 0.28 Ma based on intercalibration by Renne et al. (1998). J-factors calculated for the 6 samples using methods outlined in McDougall and Harrison (1999) varied from 0.001708-0.001713. Correction factors for K- and Ca-derived argon determined from kalsilite glass and CaF_2 included in the irradiation were: $^{40}Ar/^{39}Ar_K = 1.0x10^{-2} \pm 7.0x10^{-4}$, $^{38}Ar/^{39}ArK = 1.268x10^{-2} \pm 1x10^{-5}$, $^{36}Ar/^{37}Ar_{Ca} = 2.89x10^{-4} \pm 8x10^{-6}$, and $^{39}Ar/^{37}Ar_{Ca} = 6.70x10^{-4} \pm 3x10^{-6}$.

The $^{40}Ar/^{39}Ar$ measurements were undertaken at the Stanford University Noble Gas Laboratory. All measurements were performed 60 days after irradiation between 3–6 November, 2012. Single sanidine crystals were arranged in a Cu tray and baked in a double-pumped Cleartran laser chamber under vacuum at 120°C overnight prior to analysis. Argon release was

[1]Supplemental File. Analytical methods and results. The zipped Supplemental File includes one text file, four figures, and seven tables. Please visit http://dx.doi.org/10.1130/GES01198.S1 or the full-text article on www.gsapubs.org to view the Supplemental File.

Geosphere, published online on 5 February 2016 as doi:10.1130/GES01198.1

TABLE 1. SUMMARY OF GEOLOGIC UNITS IN THE MAPPED AREA

Relative age	Formation name	Subunit name	Map symbol (Figure 2)	Depositional age constraints* (Ma)	Description	Maximum thickness in study area (m)
Quaternary		Alluvium	Qal		Sedimentary deposits, usually in stream valleys	
Quaternary		Older gravels	Qog		Poorly sorted gravels with clasts as large as boulder size that appear to have formed a pediment surface, typically cap hills, and are cut by streams	
Pliocene–Pleistocene(?)	Hay Ranch Formation		QThr		Generally shallowly dipping conglomerate, sandstone, and siltstone with clasts eroded from nearby fault-exposed rocks	
Miocene	Humboldt Formation		Th	ca. 24.4–8.2†	Fluviolacustrine conglomerate, sandstone, siltstone, claystone, marl, and limestone, and characterized by vitric air-fall tuff horizons	~2130 (continues to thicken to the east)
Miocene(?)		Andesite	Ta		Red-weathering, dark gray, dense andesite that forms large hills	
Oligocene		tuff of Hackwood Ranch	Tthr	ca. 31.1	Thin, silicified, cliff-forming ash-fall ignimbrites	~85
Eocene(?)	Basaltic trachyandesite intrusion		Tbta		Hydrothermally altered intrusion	Intrusive
Eocene(?)	Basaltic andesite lavas		Tba		Dark gray, vesicular, and nearly aphanitic lavas containing resorbed felsic and mafic phenocrysts	At least 150
Eocene	Robinson Mountain volcanic field	Rhyolite flows and domes	Tr		Rhyolitic, flow-banded domes and flows that are transitional with subvolcanic intrusions and usually mantled by vitrophyres	Varies
		Minor sedimentary rocks	Ts	Varies	Thin (usually <50 m) beds between volcanic rocks, with clasts mostly resembling locally exposed Eocene volcanic rocks or Paleozoic metasedimentary rocks	Varies
		Subvolcanic intrusions	Tsvi	ca. 37.6–36.8	Rhyolitic porphyries with large plagioclase and sanidine phenocrysts	Intrusive
		tuff of Dixie Creek	Ttdc	ca. 37.8–37.3	Relatively homogeneous, light gray crystal vitric ignimbrites with complexly clustered and zoned plagioclase phenocrysts	At least 1000
		tuff of Robinson Mountain	Ttrm	ca. 38.5–37.7	Diverse felsic ignimbrites with simply zoned plagioclase phenocrysts	At least 600
		tuff of Cissilini Canyon	Ttcc	ca. 38–37?	Felsic ignimbrites	At least 400
Eocene	Elko Formation		Te	ca. 45.9–37.9†	Fluviolacustrine conglomerate, sandstone, siltstone, and limestone containing tuffaceous horizons and oil shale	~180
Late Cretaceous(?)–Eocene(?)		Limestone	TKl	Pre-46 and post-240	Dense limestone in places containing chert nodules; no Cenozoic volcanic material	~600
Late Cretaceous(?)–Eocene(?)		Conglomerate, sandstone, siltstone, and limestone	TKcs	Pre-46 and post-240	Redbeds lacking Cenozoic volcanic material	~580

*See the text and Table 2 for analytical details and citations.
†Maximum depositional ages.

Geosphere, published online on 5 February 2016 as doi:10.1130/GES01198.1

TABLE 2. NEW RADIOMETRIC AGES OBTAINED FOR THIS STUDY AND RELEVANT RADIOMETRIC AGES BASED ON PRIOR WORK WITH REFERENCES

Sample	Age	Unit (names from this study)	Other name	Description	In map area?	Coordinates		Maximum depositional age (Ma)	Absolute error (± 2s)	Number of analyses used for age	Mineral	Method	Technique	K-Ar decay constant	Primary standard	Laboratory	Reference	Reference notes
						WGS84 lat	WGS84 long											
12HBD09	Miocene	Humboldt Formation		pebbly sandstone	yes	40.533198	–115.759219	8.16	0.15	6 of 94	zircon (detrital)	weighted mean	U-Pb LA-ICP-MS		R33 at 419.26 ± 0.39 Ma	UC Santa Cruz LA-ICP-MS	this study	
ELM11-PN2	Miocene	Humboldt Formation		uppermost vitric tuff west of Cedar Ridge	yes	40.563141	–115.794887	12.35	0.19	13 of 13	sanidine	weighted mean	Ar/Ar	Steiger and Jäger (1977)	Taylor Creek sanidine at 28.34 ± 0.28 Ma	Stanford Noble Gas Lab	this study	
12HBD05	Miocene	Humboldt Formation		pebbly sandstone	yes	40.573984	–115.731693	14.15	0.21	9 of 92	zircon (detrital)	weighted mean	U-Pb LA-ICP-MS		R33 at 419.26 ± 0.39 Ma	UC Santa Cruz LA-ICP-MS	this study	
12HBD06	Miocene?	Humboldt Formation?		pebble conglomerate near Cedar Ridge	yes	40.509487	–115.787536	N/A	N/A		zircon (detrital)		U-Pb LA-ICP-MS		R33 at 419.26 ± 0.39 Ma	UC Santa Cruz LA-ICP-MS	this study	
Tiws-J3	Miocene	Humboldt Formation		vitric tuff west of Cedar Ridge	yes	40.554758	–115.822480	14.62	0.22	7 of 20	sanidine	weighted mean	Ar/Ar	Steiger and Jäger (1977)	Taylor Creek sanidine at 28.34 ± 0.28 Ma	Stanford Noble Gas Lab	this study	
ELM11-PN11	Miocene	Humboldt Formation		lowest vitric tuff	yes	40.539585	–115.852641	15.51	0.24	8 of 11	alkali feldspar	weighted mean	Ar/Ar	Steiger and Jäger (1977)	Taylor Creek sanidine at 28.34 ± 0.28 Ma	Stanford Noble Gas Lab	this study	
Tiws-J4	Miocene	Humboldt Formation		pebbly sandstone near base	yes	40.505785	–115.870215	15.64	0.11	42 of 91	zircon (detrital)	weighted mean	U-Pb LA-ICP-MS		R33 at 419.26 ± 0.39 Ma	UC Santa Cruz LA-ICP-MS	this study	
ELM11-PN13	Miocene	Humboldt Formation		lowest vitric tuff	yes	40.489965	–115.869293	15.78	0.25	10 of 11	alkali feldspar	weighted mean	Ar/Ar	Steiger and Jäger (1977)	Taylor Creek sanidine at 28.34 ± 0.28 Ma	Stanford Noble Gas Lab	this study	
ELM11-PN19	Miocene	Humboldt Formation		base of Humboldt Formation (tuffaceous sediments)	yes	40.492061	–115.883977	24.39	0.08	90 of 98	zircon (detrital)	weighted mean	U-Pb LA-ICP-MS		R33 at 419.26 ± 0.39 Ma	UC Santa Cruz LA-ICP-MS	this study	
11JLS105	Oligocene	Robinson Mountain volcanic field	Indian Well Formation	tuff of Hackwood Ranch	yes	40.478812	–115.917670	31.08	0.47	10 of 13	sanidine	weighted mean	Ar/Ar	Steiger and Jäger (1977)	Taylor Creek sanidine at 28.34 ± 0.28 Ma	Stanford Noble Gas Lab	this study	
HACK-1	Oligocene	Robinson Mountain volcanic field	Indian Well Formation	tuff of Hackwood Ranch	yes	40.481749	–115.918102	31.10	0.47	12 of 14	sanidine	weighted mean	Ar/Ar	Steiger and Jäger (1977)	Taylor Creek sanidine at 28.34 ± 0.28 Ma	Stanford Noble Gas Lab	this study	
11JLS105	Oligocene	Robinson Mountain volcanic field	Indian Well Formation	tuff of Hackwood Ranch	yes	40.478812	–115.917670	31.26	0.30	8 of 16	zircon (igneous)	concordia intercept	U-Pb SHRIMP		R33 at 419.26 ± 0.39 Ma	SUMAC SHRIMP-RG	this study	
HACK-1	Oligocene	Robinson Mountain volcanic field	Indian Well Formation	tuff of Hackwood Ranch	yes	40.481749	–115.918102	31.59	0.29	12 of 16	zircon (igneous)	concordia intercept	U-Pb SHRIMP		R33 at 419.26 ± 0.39 Ma	SUMAC SHRIMP-RG	this study	
10JLS08	Eocene–Oligocene	Robinson Mountain volcanic field	Indian Well Formation	sediments	yes	40.481948	–115.917267	33.86	0.40	18 of 28	zircon (detrital)	weighted mean	U-Pb LA-ICP-MS		Sri Lanka (SL) at 563.5 ± 3.2 Ma	Arizona LaserChron Center (Tucson) LA-ICP-MS	this study	
10JLS11A	Eocene	Robinson Mountain volcanic field	Indian Well Formation	subvolcanic intrusion	yes	40.393860	–115.919954	36.84	0.34	4 of 14	zircon (igneous)	concordia intercept	U-Pb SHRIMP		R33 at 419.26 ± 0.39 Ma	SUMAC SHRIMP-RG	this study	

(*continued*)

Geosphere, published online on 5 February 2016 as doi:10.1130/GES01198.1

TABLE 2. NEW RADIOMETRIC AGES OBTAINED FOR THIS STUDY AND RELEVANT RADIOMETRIC AGES BASED ON PRIOR WORK WITH REFERENCES (*continued*)

Sample	Age	Unit (names from this study)	Other name	Description	In map area?	Coordinates		Maximum depositional age (Ma)	Absolute error (± 2s)	Number of analyses used for age	Mineral	Method	Technique	K-Ar decay constant	Primary standard	Laboratory	Reference	Reference notes
						WGS84 lat	WGS84 long											
Tiwb-1	Eocene–Oligocene(?)	Robinson Mountain volcanic field	Indian Well Formation	sediments	yes	40.510668	–115.893101	37.33	0.14	67 of 94	zircon (detrital)	weighted mean	U-Pb LA-ICP-MS		R33 at 419.26 ± 0.39 Ma	UC Santa Cruz LA-ICP-MS	this study	
10JLS05	Eocene	Robinson Mountain volcanic field	Indian Well Formation	tuff of Dixie Creek	yes	40.443491	–115.935207	37.34	0.33	5 of 12	zircon (igneous)	concordia intercept	U-Pb SHRIMP		R33 at 419.26 ± 0.39 Ma	SUMAC SHRIMP-RG	this study	
11JLS104	Eocene	Robinson Mountain volcanic field	Indian Well Formation	subvolcanic intrusion	yes	40.456488	–115.905190	37.64	0.74	4 of 16	zircon (igneous)	concordia intercept	U-Pb SHRIMP		R33 at 419.26 ± 0.39 Ma	SUMAC SHRIMP-RG	this study	
12JLS161	Eocene	Robinson Mountain volcanic field	Indian Well Formation	reworked tuff	yes	40.404960	–115.864885	37.67	0.27	22 of 83	zircon (detrital)	weighted mean	U-Pb LA-ICP-MS		R33 at 419.26 ± 0.39 Ma	UC Santa Cruz LA-ICP-MS	this study	
10JLS06A	Eocene	Robinson Mountain volcanic field	Indian Well Formation	tuff of Dixie Creek	yes	40.451901	–115.924212	37.77	0.36	5 of 12	zircon (igneous)	concordia intercept	U-Pb SHRIMP		R33 at 419.26 ± 0.39 Ma	SUMAC SHRIMP-RG	this study	
ELKO-2	Eocene	Elko Formation		tuffaceous sandstone near top of section	yes	40.360219	–115.935313	37.89	0.46	30 of 34	zircon (detrital)	weighted mean	U-Pb LA-ICP-MS		Sri Lanka (SL) at 563.5 ± 3.2 Ma	Arizona LaserChron Center (Tucson) LA-ICP-MS	this study	
ELKO-3	Eocene	Elko Formation		sandstone near base	yes	40.365606	–115.932034	45.00	0.48	32 of 37	zircon (detrital)	weighted mean	U-Pb LA-ICP-MS		Sri Lanka (SL) at 563.5 ± 3.2 Ma	Arizona LaserChron Center (Tucson) LA-ICP-MS	this study	
ELKO-1	Eocene	Elko Formation		sandstone near base	yes	40.359420	–115.930448	45.92	0.95	20 of 100	zircon (detrital)	weighted mean	U-Pb LA-ICP-MS		Sri Lanka (SL) at 563.5 ± 3.2 Ma	Arizona LaserChron Center (Tucson) LA-ICP-MS	this study	
ELM11-PN16	Eocene?	conglomeratic sandstone		sandstone redbeds	yes	40.590217	–115.764024	NA	NA		zircon (detrital)		U-Pb LA-ICP-MS		R33 at 419.26 ± 0.39 Ma	UC Santa Cruz LA-ICP-MS	this study	
	Miocene	Humboldt Formation		tephra	no	40.581300	–115.712167	9.91			tephra		tephra correlation				Wallace et al. (2008)	Perkins et al. (1998)
	Miocene	Humboldt Formation		tephra	no	40.581300	–115.712167	11.92			tephra		tephra correlation				Wallace et al. (2008)	Perkins et al. (1998)
	Miocene	Humboldt Formation		tephra	no	40.581300	–115.712167	12.03			tephra		tephra correlation				Wallace et al. (2008)	Perkins et al. (1998)
	Miocene	Humboldt Formation		tephra	no	40.581300	–115.712167	12.12			tephra		tephra correlation				Wallace et al. (2008)	Perkins et al. (1998)
	Miocene	Humboldt Formation		tephra	no	40.581300	–115.712167	12.17			tephra		tephra correlation				Wallace et al. (2008)	Perkins et al. (1998)
	Miocene	Humboldt Formation		tephra	no	40.581300	–115.712167	14			tephra		tephra correlation				Wallace et al. (2008)	Perkins et al. (1998)
	Miocene	Humboldt Formation		tephra	no	40.581300	–115.712167	14.67	0.05		sanidine	laser fusion; weighted mean	Ar/Ar				Wallace et al. (2008)	

(*continued*)

Geosphere, published online on 5 February 2016 as doi:10.1130/GES01198.1

TABLE 2. NEW RADIOMETRIC AGES OBTAINED FOR THIS STUDY AND RELEVANT RADIOMETRIC AGES BASED ON PRIOR WORK WITH REFERENCES (*continued*)

Sample	Age	Unit (names from this study)	Other name	Description	In map area?	Coordinates		Maximum depositional age (Ma)	Absolute error (± 2s)	Number of analyses used for age	Mineral	Method	Technique	K-Ar decay constant	Primary standard	Laboratory	Reference	Reference notes
						WGS84 lat	WGS84 long											
	Miocene	Humboldt Formation		tephra	no	40.581300	–115.712167	14.78			tephra		tephra correlation				Wallace et al. (2008)	Perkins et al. (1998)
	Miocene	Humboldt Formation		tephra	no	40.581300	–115.712167	15.28			tephra		tephra correlation				Wallace et al. (2008)	Perkins et al. (1998)
	Miocene	Humboldt Formation		tephra	no	40.581300	–115.712167	15.35	0.06		sanidine	laser fusion; weighted mean	Ar/Ar				Wallace et al. (2008)	
	Miocene	Humboldt Formation		tephra	no	40.581300	–115.712167	15.31			tephra		tephra correlation				Wallace et al. (2008)	Perkins et al. (1998)
JC06-HP110	Miocene	Humboldt Formation		tephra	no	40.344068	–115.608749	11.582	0.048		sanidine	laser fusion; weighted mean	Ar/Ar	Steiger and Jäger (1977)			Colgan et al. (2010)	
JC06-HP110	Miocene	Humboldt Formation		tephra	no	40.344068	–115.608749	11.608	0.054		sanidine	laser fusion; weighted mean	Ar/Ar	Steiger and Jäger (1977)			Colgan et al. (2010)	
JC07-MC42	Miocene	Humboldt Formation		tephra	no	40.153818	–115.639774	15.234	0.07		sanidine	laser fusion; weighted mean	Ar/Ar	Steiger and Jäger (1977)			Colgan et al. (2010)	
JC07-MC42	Miocene	Humboldt Formation		tephra	no	40.153818	–115.639774	15.229	0.061		sanidine	laser fusion; weighted mean	Ar/Ar	Steiger and Jäger (1977)			Colgan et al. (2010)	
JC06-RW118	Miocene	Humboldt Formation		tephra	no	40.212985	–115.307542	13.922	0.65		sanidine	laser fusion; weighted mean	Ar/Ar	Steiger and Jäger (1977)			Colgan et al. (2010)	
JC07-MR116	Miocene	Humboldt Formation		tephra	no	40.243541	–115.272542	13.819	0.71		sanidine	laser fusion; weighted mean	Ar/Ar	Steiger and Jäger (1977)			Colgan et al. (2010)	
HC-04	Miocene	Humboldt Formation			yes	NR	NR	14.99	0.98		zircon		U-Pb SHRIMP			SUMAC SHRIMP-RG	Horton et al. (2004)	
HC-08	Miocene	Humboldt Formation			yes	NR	NR	15.18	0.74		zircon		U-Pb SHRIMP			SUMAC SHRIMP-RG	Horton et al. (2004)	
9	Miocene	Humboldt Formation		vitric tuff; air fall	yes	40.559814	–115.793299	9.5	*1.9*		zircon		Fission-track				Smith and Ketner (1976)	
67	Oligocene	tuff of Hackwood Ranch	tuff of Hackwood		yes	~40.492958	~–115.911683	30.5	NR		biotite		K-Ar	Steiger and Jäger (1977)		University of Western Ontario (London, Canada)	Palmer et al. (1991)	
67	Oligocene	tuff of Hackwood Ranch	tuff of Hackwood		yes	~40.492958	~–115.911683	30.3	NR		biotite-free		K-Ar	Steiger and Jäger (1977)		University of Western Ontario (London, Canada)	Palmer et al. (1991)	
79	Oligocene	tuff of Hackwood Ranch	tuff of Hackwood		yes	~40.492958	~–115.911683	29.2	NR		whole rock		K-Ar	Steiger and Jäger (1977)		University of Western Ontario (London, Canada)	Palmer et al. (1991)	
79	Oligocene	tuff of Hackwood Ranch	tuff of Hackwood		yes	~40.492958	~–115.911683	28.1	NR		whole rock		K-Ar	Steiger and Jäger (1977)		University of Western Ontario (London, Canada)	Palmer et al. (1991)	

(*continued*)

Geosphere, published online on 5 February 2016 as doi:10.1130/GES01198.1

TABLE 2. NEW RADIOMETRIC AGES OBTAINED FOR THIS STUDY AND RELEVANT RADIOMETRIC AGES BASED ON PRIOR WORK WITH REFERENCES (*continued*)

Sample	Age	Unit (names from this study)	Other name	Description	In map area?	Coordinates		Maximum depositional age (Ma)	Absolute error (± 2s)	Number of analyses used for age	Mineral	Method	Technique	K-Ar decay constant	Primary standard	Laboratory	Reference	Reference notes
						WGS84 lat	WGS84 long											
67 and 79?	Oligocene	tuff of Hackwood Ranch	tuff of Hackwood		yes	-	-	30.8	0.1		whole rock?	isochron	K-Ar	Steiger and Jäger (1977)		University of Western Ontario (London, Canada)	Palmer et al. (1991)	
?	Oligocene	tuff of Hackwood Ranch	tuff of Hackwood		yes	NR	NR	30.5	NR		biotite		K-Ar				Gordee et al. (2000)	
00-DJ-9	Oligocene	tuff of Hackwood Ranch			yes	40.48282	–115.91739	31.37	0.16		sanidine	single crystal weighted mean	Ar/Ar	Steiger and Jäger (1977)		New Mexico Geochronological Research Laboratory (Socorro)	C.D. Henry and D.A. John (2011, personal commun.)	
99-DJ-40	Eocene	tuff of Dixie Creek	tuff of Jiggs		yes	40.46288	–115.89749	37.70	0.38		sanidine	single crystal weighted mean	Ar/Ar	Steiger and Jäger (1977)		Nevada Isotope Geochronology Laboratory (University of Nevada, Las Vegas)	Ressel and Henry (2006)	
23	Eocene	tuff of Dixie Creek	tuff of Jiggs	silicic ignimbrite	yes	~40.481274	~–115.912417	35.7	NR		biotite		K-Ar	Steiger and Jäger (1977)		University of Western Ontario (London, Canada)	Palmer et al. (1991)	
21	Eocene	tuff of Dixie Creek	tuff of Jiggs	silicic ignimbrite	yes	NR	NR	35.8	NR		biotite	recalculated age	K-Ar	Steiger and Jäger (1977)		University of Western Ontario (London, Canada)	Palmer et al. (1991)	Smith and Ketner (1976)
21	Eocene	tuff of Dixie Creek	tuff of Jiggs	silicic ignimbrite	yes	NR	NR	34	NR		sanidine	recalculated age	K-Ar	Steiger and Jäger (1977)		University of Western Ontario (London, Canada)	Palmer et al. (1991)	Smith and Ketner (1976)
76	Oligocene?	tuff of Dixie Creek	tuff in Humboldt Formation		yes	40.433333	–115.926389	33.2	*1.4*		sanidine		K-Ar				McKee et al. (1971)	
76	Eocene	tuff of Dixie Creek	tuff in Humboldt Formation		yes	40.433333	–115.926389	34.9	*1.4*		biotite		K-Ar				McKee et al. (1971)	
99-DJ-31	Eocene	subvolcanic intrusion (Tsvi)		rhyolite intrusion	yes	40.39215	–115.88812	37.51	0.38		sanidine	single crystal weighted mean	Ar/Ar	Steiger and Jäger (1977)		Nevada Isotope Geochronology Laboratory (University of Nevada, Las Vegas)	Ressel and Henry (2006)	
NEP-14	Eocene	Robinson Mountain volcanic field tuff	Rhyodacite	white biotite-rich tuff; rhyodacite	no	40.569417	–116.006378	37.47	0.11		biotite		Ar/Ar	Steiger and Jäger (1977)?		U.S. Geological Survey	R. Fleck, *in* Haynes (2003)	
NEP-14	Eocene	Robinson Mountain volcanic field tuff	Rhyodacite	white biotite-rich tuff; rhyodacite	no	40.569417	–116.006378	38.00	0.30		hornblende		Ar/Ar	Steiger and Jäger (1977)?		U.S. Geological Survey	R. Fleck, *in* Haynes (2003)	
95	Eocene	tuff of Cissilini Canyon	tuff of Jiggs	silicic ignimbrite	no	40.522222	–115.990278	37	NR		biotite	recalculated age	K-Ar	Steiger and Jäger (1977)		University of Western Ontario (London, Canada)	Palmer et al. (1991)	Smith and Ketner (1976)
109	Eocene			biotite ademellite	no	40.519444	–116.023611	35.3	*1.4*		whole rock		K-Ar				Armstrong (1970)	

(*continued*)

Geosphere, published online on 5 February 2016 as doi:10.1130/GES01198.1

TABLE 2. NEW RADIOMETRIC AGES OBTAINED FOR THIS STUDY AND RELEVANT RADIOMETRIC AGES BASED ON PRIOR WORK WITH REFERENCES (*continued*)

Sample	Age	Unit (names from this study)	Other name	Description	In map area?	Coordinates		Maximum depositional age (Ma)	Absolute error (± 2s)	Number of analyses used for age	Mineral	Method	Technique	K-Ar decay constant	Primary standard	Laboratory	Reference	Reference notes
						WGS84 lat	WGS84 long											
111	Eocene	tuff of Cissilini Canyon		biotite quartz latite crystal vitric tuff	no	40.522222	–115.990278	36.2	*1.4*		biotite		K-Ar	Smith (1964)		Yale University (New Haven, Connecticut)	Armstrong (1970)	
110	Eocene	tuff of Cissilini Canyon		rhyolite porphyry	no	40.519444	–116.023611	36	*2.8*		whole rock		K-Ar			Yale University (New Haven, Connecticut)	Armstrong (1970)	
99-468	Miocene			rhyolite lava	no	40.711667	–116.268333	15.32	0.08		sanidine	single crystal weighted mean	Ar/Ar	Steiger and Jäger (1977)	Fish Canyon sanidine at 28.02 Ma	New Mexico Geochronological Research Laboratory (Socorro)	Ressel and Henry (2006)	
NEP-44	Eocene			biotite quartz-feldspar intrusion	no	40.5091	–116.00855	37.38	0.16		sanidine	single crystal weighted mean	Ar/Ar	Steiger and Jäger (1977)	Fish Canyon sanidine at 28.02 Ma	New Mexico Geochronological Research Laboratory (Socorro)	Ressel and Henry (2006)	
RCR-62-2151	Eocene			basaltic andesite dike	no	40.640000	116.040000	37.80	2.40		Matrix	step heating Isochron	Ar/Ar	Steiger and Jäger (1977)	Fish Canyon sanidine at 28.02 Ma	Nevada Isotope Geochronology Laboratory (University of Nevada, Las Vegas)	Ressel and Henry (2006)	
RCR-61-2092	Eocene			porphyritic diorite dike	no	40.640000	116.040000	39.13	0.36		biotite	step heating Isochron	Ar/Ar	Steiger and Jäger (1977)	Fish Canyon sanidine at 28.02 Ma	Nevada Isotope Geochronology Laboratory (University of Nevada, Las Vegas)	Ressel and Henry (2006)	
RCR-9-676	Eocene			Monazite porphyry dike	no	40.618	–115.975	37.50	1.60		zircon		U-Pb SHRIMP				Longo et al. (2002)	S. Garwin (2001)
73	Eocene	Robinson Mountain volcanic field tuff	tuff in Humboldt Formation	tuff	no	40.577778	–115.995833	38.6	*1.6*		biotite		K-Ar			U.S. Geological Survey	McKee et al. (1971)	
3	Eocene			silicic intrusive rocks (stock)	no	~40.5204262	~–116.0235817	36.8	*1*		biotite		K-Ar			U.S. Geological Survey	Smith and Ketner (1976)	
3	Eocene			silicic intrusive rocks (stock)	no	~40.5204262	~–116.0235817	35.4	*1.1*		sanidine		K-Ar			U.S. Geological Survey	Smith and Ketner (1976)	
H10-47	Eocene	tuff of Robinson Mountain			yes	40.362005	–115.946683	37.70	0.06		sanidine	single crystal weighted mean	Ar/Ar	Steiger and Jäger (1977)	Fish Canyon sanidine at 28.201 Ma	New Mexico Geochronological Research Laboratory (Socorro)	C.D. Henry (2011, personal commun.)	
H10-45	Eocene	tuff of Robinson Mountain			yes	40.35914133	–115.93660264	38.48	0.15		plagioclase	step heating plateau	Ar/Ar	Steiger and Jäger (1977)	Fish Canyon sanidine at 28.201 Ma	New Mexico Geochronological Research Laboratory (Socorro)	C.D. Henry (2011, personal commun.)	

(*continued*)

Geosphere, published online on 5 February 2016 as doi:10.1130/GES01198.1

TABLE 2. NEW RADIOMETRIC AGES OBTAINED FOR THIS STUDY AND RELEVANT RADIOMETRIC AGES BASED ON PRIOR WORK WITH REFERENCES (*continued*)

Sample	Age	Unit (names from this study)	Other name	Description	In map area?	Coordinates		Maximum depositional age (Ma)	Absolute error (± 2s)	Number of analyses used for age	Mineral	Method	Technique	K-Ar decay constant	Primary standard	Laboratory	Reference	Reference notes
						WGS84 lat	WGS84 long											
8	Oligocene?		Diamond Hills	dark gray lava flows	no	~40.190159	~–115.923396	32.5	NR		whole rock		K-Ar	Steiger and Jäger (1977)		University of Western Ontario (London, Canada)	Palmer et al. (1991)	
10	Oligocene?		Diamond Hills	dark gray lava flows	no	~40.113362	~–115.814142	32.6	NR		whole rock		K-Ar	Steiger and Jäger (1977)		University of Western Ontario (London, Canada)	Palmer et al. (1991)	
88	Oligocene?		Diamond Hills	dark gray lava flows	no	~40.203843	~–115.916680	32.3	NR		whole rock		K-Ar	Steiger and Jäger (1977)		University of Western Ontario (London, Canada)	Palmer et al. (1991)	
6	Eocene		tuff of Jiggs	silicic ignimbrite	no	~40.225759	~–115.961281	35.8	NR		biotite		K-Ar	Steiger and Jäger (1977)		University of Western Ontario (London, Canada)	Palmer et al. (1991)	
H05-RM104	Eocene	Harrison Pass Pluton		Toyn Creek phase	no	40.328291	–115.516245	37.3	0.3		zircon		U-Pb SHRIMP			SUMAC SHRIMP-RG	Colgan et al. (2010)	
JC06-HP105	Eocene	Harrison Pass Pluton		Corral Creek phase	no	40.294263	–115.511022	36.5	0.2		zircon		U-Pb SHRIMP			SUMAC SHRIMP-RG	Colgan et al. (2010)	
JC05-HP3	Eocene	Harrison Pass Pluton		Toyn Creek phase?	no	40.330235	–115.575664	36.3	0.4		zircon		U-Pb SHRIMP			SUMAC SHRIMP-RG	Colgan et al. (2010)	
112	Miocene			rhyolite	no	40.615278	–116.197222	15.0	*2.0*		whole rock		K-Ar	Smith (1964)		Yale University (New Haven, Connecticut)	Armstrong (1970)	
7	Oligocene?			mafic to intermediate plugs and dikes	no	~40.5033369	~–116.1805841	31.9	*1.1*		whole rock		K-Ar			U.S. Geological Survey	Smith and Ketner (1976)	
2	Eocene		Indian Well Formation	Indian Well Formation volcanics	no	40.5909319	–116.1652036	37.6	*1.3*		biotite		K-Ar			U.S. Geological Survey	Smith and Ketner (1976)	
03JA122	Miocene			rhyolite tephra	no	NR	NR	14.00	0.30		zircon	weighted mean	U-Pb LA-ICP-MS			WSU GeoAnalytical Lab	Ryskamp et al. (2008)	
04EB123	Oligocene			andesite (Ta)	no	40.118634	–115.983209	31.40	+1.3 / –0.5		zircon	"TuffZirc" routine of Isoplot (Ludwig, 2003)	U-Pb LA-ICP-MS			WSU GeoAnalytical Lab	Ryskamp et al. (2008)	
04EB044	Eocene			dacite domes (Tpd)	no	40.146413	–116.011605	35.10	0.50		zircon	weighted mean	U-Pb LA-ICP-MS			WSU GeoAnalytical Lab	Ryskamp et al. (2008)	
04EB041	Eocene			biotite dacite tuff (Tbd)	no	40.154092	–116.017341	35.50	0.40		zircon	weighted mean	U-Pb LA-ICP-MS			WSU GeoAnalytical Lab	Ryskamp et al. (2008)	
04EB86	Eocene			biotite porphyry intrusion (Tbp)	no	40.155586	–116.027758	35.90	0.50		zircon	weighted mean	U-Pb LA-ICP-MS			WSU GeoAnalytical Lab	Ryskamp et al. (2008)	
04JA156	Jurassic			square quartz porphyry (Jsqp)	no	NR	NR	157.10	1.80		zircon	weighted mean	U-Pb LA-ICP-MS			WSU GeoAnalytical Lab	Ryskamp et al. (2008)	

(*continued*)

Geosphere, published online on 5 February 2016 as doi:10.1130/GES01198.1

TABLE 2. NEW RADIOMETRIC AGES OBTAINED FOR THIS STUDY AND RELEVANT RADIOMETRIC AGES BASED ON PRIOR WORK WITH REFERENCES (*continued*)

Sample	Age	Unit (names from this study)	Other name	Description	In map area?	Coordinates		Maximum depositional age (Ma)	Absolute error (± 2s)	Number of analyses used for age	Mineral	Method	Technique	K-Ar decay constant	Primary standard	Laboratory	Reference	Reference notes
						WGS84 lat	WGS84 long											
00-187GS	Eocene	Elko Formation?		tuff in upper shale	no	40.578559	–115.883695	36.60	0.50		sanidine		Ar/Ar	Steiger and Jäger (1977)		Queen's University (Kingston, Ontario, Canada)	Haynes (2003)	
77	Eocene?	Elko Formation	tuff in Humboldt Formation	tuff	yes	40.616111	–115.748056	33.9	*1.8*		biotite		K-Ar				McKee et al. (1971)	
78	Eocene	Elko Formation	tuff in Humboldt Formation	tuff	yes	40.610000	–115.747778	39.2	*1.6*		biotite		K-Ar				McKee et al. (1971)	
TE-22	Eocene	Elko Formation			yes	NR	NR	39.9	1.5		zircon		U-Pb SHRIMP				Horton et al. (2004)	
TE-17	Eocene	Elko Formation			yes	NR	NR	42.5	1.5		zircon		U-Pb SHRIMP				Horton et al. (2004)	
BJS-10	Eocene			andesite overlying Elko Formation	no	40.766240	–115.767563	35.2	*2.2*		whole rock		K-Ar				Solomon et al. (1979)	
BJS-5	Oligocene?			andesite overlying Elko Formation	no	40.775000	–115.775000	30.9	*2.0*		whole rock		K-Ar				Solomon et al. (1979)	
1410B	Eocene			andesite	no	40.784257	–115.728535	38.07	2.48		plagioclase		Ar/Ar	Steiger and Jäger (1977)		Queen's University (Kingston, Ontario, Canada)	Haynes (2003)	
00-177GS	Eocene			intrusive rhyolite of Elko Mountain	no	40.891246	–115.618148	38.60	0.10		zircon		U-Pb SHRIMP			University of British Columbia (Vancouver, Canada)	Haynes (2003)	
BJS-6	Eocene	Elko Formation		white biotite-rich tuff in shale	no	40.774961	–115.759225	37.1	*2.0*		biotite		K-Ar				Solomon et al. (1979)	
BJS-3	Eocene	Elko Formation		white biotite-rich tuff in shale	no	40.813815	–115.736982	38.9	*0.6*		biotite		K-Ar				Solomon et al. (1979)	
00-035GS	Eocene	Elko Formation?		white biotite-rich tuff in shale	no	40.816119	–115.721287	38.90	0.30		zircon		U-Pb SHRIMP			University of British Columbia (Vancouver, Canada)	Haynes (2003)	
BJS-1	Eocene	Elko Formation		pink air-fall tuff	no	40.805476	–115.717579	43.3	*0.8*		biotite		K-Ar				Solomon et al. (1979)	same locality as sample 00-188GS
00-188GS	Eocene	Elko Formation	basal conglomerate	pink air-fall tuff in basal conglomerate	no	40.804930	–115.717957	46.10	0.20		zircon		U-Pb SHRIMP			University of British Columbia (Vancouver, Canada)	Haynes (2003)	same locality as sample BJS-1

Note: Italics indicate ages converted to 2-sigma errors. WGS84—World Geodetic System 1984; NR—no data; NA—not applicable; SHRIMP—sensitive high-resolution ion microprobe; LA-ICP-MS—laser ablation–inductively coupled plasma–mass spectrometry; UC—University of California; SUMAC—Stanford-U.S. Geological Survey Micro Analysis Center (Stanford, California); WSU—Washington State University.

Geosphere, published online on 5 February 2016 as doi:10.1130/GES01198.1

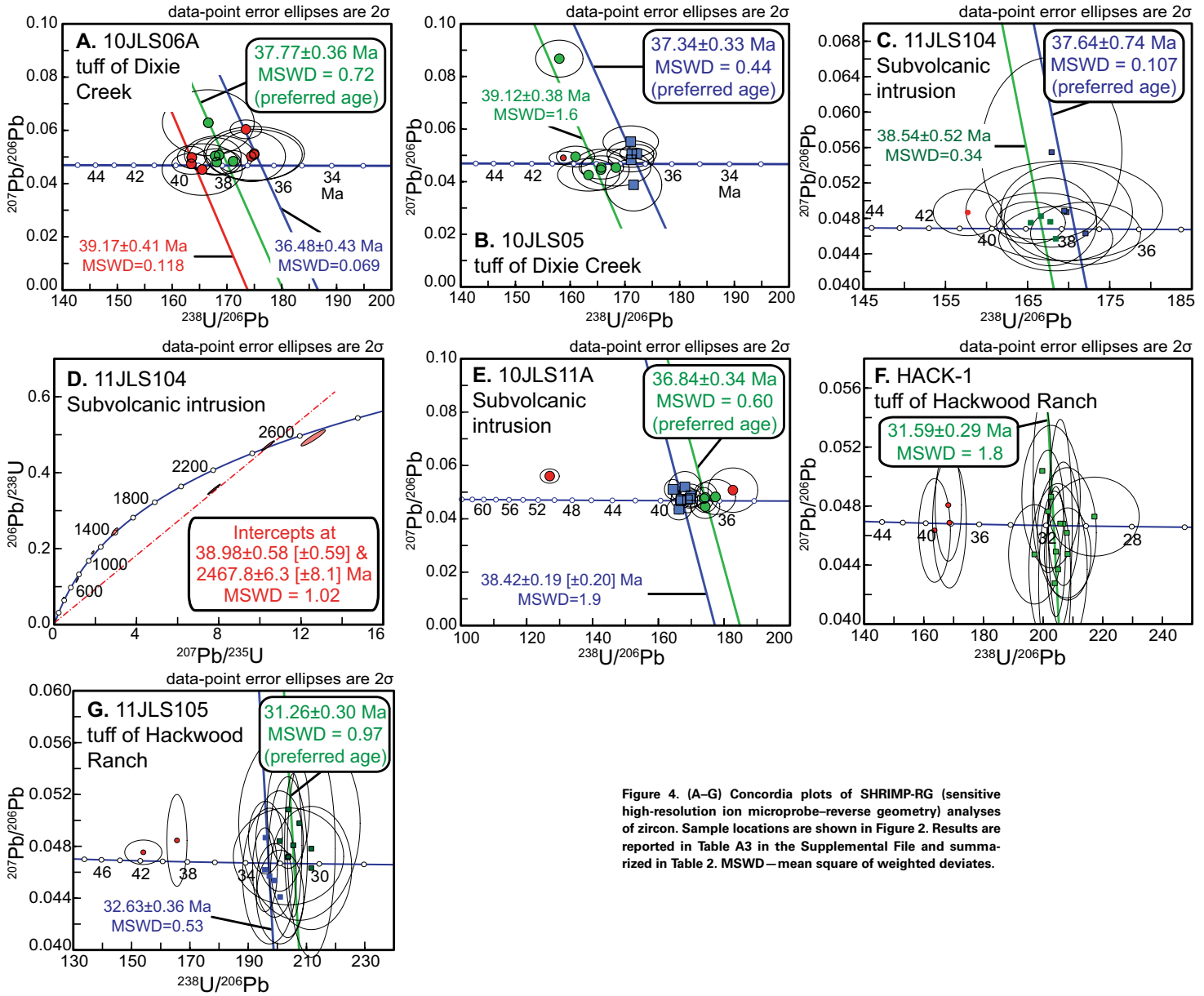

Figure 4. (A–G) Concordia plots of SHRIMP-RG (sensitive high-resolution ion microprobe–reverse geometry) analyses of zircon. Sample locations are shown in Figure 2. Results are reported in Table A3 in the Supplemental File and summarized in Table 2. MSWD—mean square of weighted deviates.

Geosphere, published online on 5 February 2016 as doi:10.1130/GES01198.1

Sample ELM11-PN16 has a detrital zircon signature (Fig. 7) most strongly resembling that of Mesozoic and late Paleozoic strata of northern Nevada and Utah. Detrital zircon age maxima exhibited by sample ELM11-PN16 are similar to those exhibited by the Chinle Formation, including peaks ca. 240 Ma, 456 Ma, 1.15–0.95 Ga, 1.5–1.35 Ga, and 1.8–1.6 Ga (Dickinson and Gehrels, 2008; Gehrels and Pecha, 2014; Figs. 7 and 8). The zircon signature of ELM11-PN16 thus likely represents recycling of zircons from the erosion of Triassic miogeoclinal strata that were exposed in the greater Elko Basin region at the end of the Mesozoic and beginning of the Cenozoic (Konstantinou et al., 2012; Long, 2012). Many of the observed age peaks in ELM11-PN16 are, in addition, shared with those in older Permian sedimentary rocks (e.g., samples PER-SS and DC-1 of Konstantinou et al., 2012) collected northeast of the study area (Figs. 1A and 8). The detrital zircon signature of Late Cretaceous(?)–Eocene(?) redbeds represented by sample ELM11-PN16 also appears to match the detrital zircon signature of the Pennsylvanian Spray Lakes Group and Permian Kindle Formation of British Columbia, particularly because these northern strata share a strong peak between 490 and 400 Ma (Gehrels and Pecha, 2014; Fig. 8). The lack of Mesozoic zircon in the Late Cretaceous(?)–Eocene(?) redbeds indicates no contribution from the Jurassic to Cretaceous Sierra Nevada batholith, which was undergoing uplift and erosion at this time (Van Buer et al., 2009), or from more proximal Mesozoic plutons (du Bray, 2007). This suggests that river systems draining Mesozoic granitic basement to the west flowed elsewhere and that local Mesozoic plutons, intruded at depth in the stratigraphic succession, were not yet sufficiently uplifted to be exposed at the surface.

A number of ages determined for strata within the overlying Elko Formation may have mistakenly been ascribed to the TKcs redbed conglomerates, which lack Cenozoic volcanic detritus (Horton et al., 2004; Mulch et al., 2015). These include a 46.1 ± 0.1 Ma U-Pb zircon age (sample 00-188GS in Table 2) obtained by Haynes et al. (2002) and Haynes (2003) on an air fall tuff from the Elko Formation in the Elko Hills (Fig. 1B). A ca. 43 Ma K-Ar age was also obtained from the same tuff (cf. Solomon et al., 1979; Haynes, 2003; Henrici and Haynes, 2006; sample BJS-1 in Table 2) as the 46 Ma zircon sample. Mulch et al. (2015, p. 322–324) mistakenly used these ages from the Elko Formation together with their new $^{40}Ar/^{39}Ar$ ages to extrapolate a 46.1–42.5 Ma depositional age range for portions of the underlying "cherty limestone" unit (our TKl). Horton et al. (2004, p. 868, 880, 882) cited an age range of 54.5–42.1 Ma for "limestone and limestone clast conglomerate," "cherty limestone," and "conglomerate, sandstone, siltstone" units. Both of the Horton et al. (2004) limestone units appear to be part of our mapped TKl, and their clastic unit is probably our TKcs. All of these units underlie the Elko Formation. In summary, the stratigraphic position of the limestones (TKl) and redbeds (TKcs) below the Elko Formation, together with their lack of volcanic material, suggests that they are older than 46 Ma, the oldest age determined on the Elko Formation, but how much older is unclear. Implications posed to stable isotope studies by this misclassification of ages for TKcs and TKl are discussed herein.

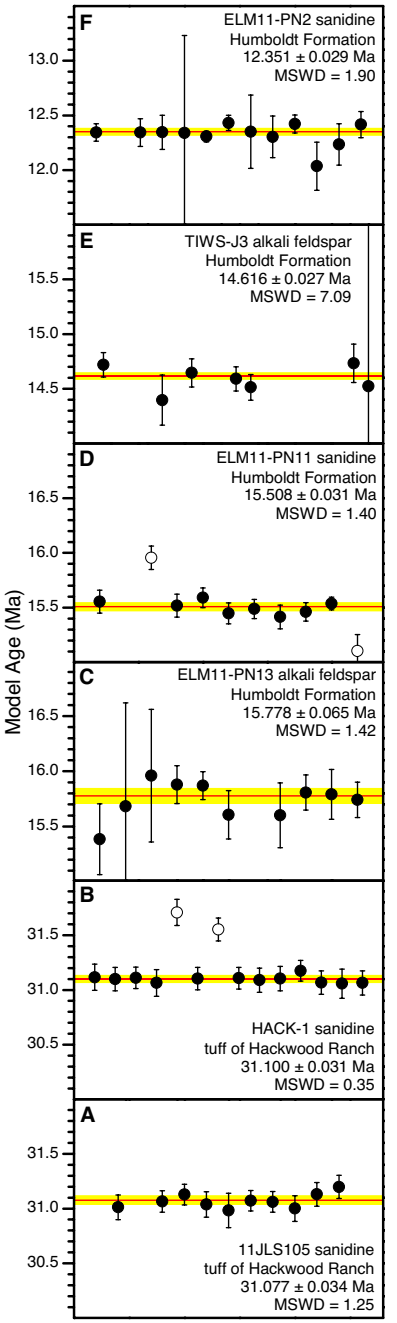

Figure 5. (A–F) Weighted mean age plots of sanidine $^{40}Ar/^{39}Ar$ analyses. Sample locations are shown in Figure 2. Results are reported in Tables A1 and A2 in the Supplemental File and summarized in Table 2. Inverse isochron and Ca/K plots for these samples are shown in Figure A1 in the Supplemental File. Only analytical uncertainties (2σ) are shown in the figures; total 2σ errors are reported in the text and Table 2. MSWD—mean square of weighted deviates.

Eocene Elko Formation

The Eocene Elko Formation (unit Te) is stratigraphically above the Late Cretaceous(?)–Eocene(?) limestone (TKl) but directly overlies Paleozoic rocks across an angular unconformity in other parts of the mapped area (Figs. 2 and 3). The Elko Formation is a generally fining-upward succession of boulder to pebble conglomerate, sandstone, siltstone, limestone (commonly with chert nodules), laminated paper shale, and claystone with tuffaceous horizons and oil shale deposited within a generally fluvial-lacustrine environment (Smith and Ketner, 1976; Solomon et al., 1979; Moore et al., 1983;

Geosphere, published online on 5 February 2016 as doi:10.1130/GES01198.1

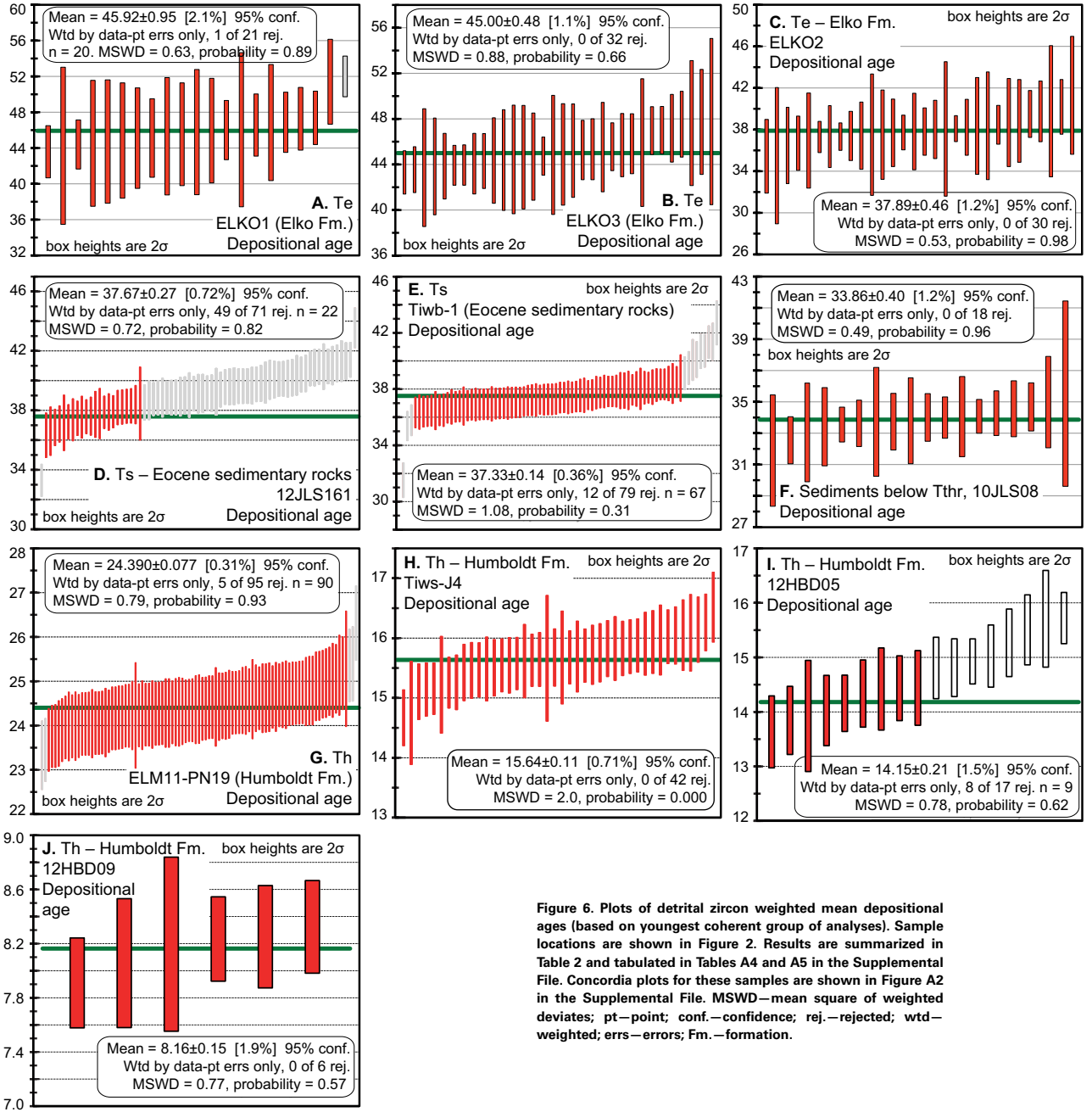

Figure 6. Plots of detrital zircon weighted mean depositional ages (based on youngest coherent group of analyses). Sample locations are shown in Figure 2. Results are summarized in Table 2 and tabulated in Tables A4 and A5 in the Supplemental File. Concordia plots for these samples are shown in Figure A2 in the Supplemental File. MSWD—mean square of weighted deviates; pt—point; conf.—confidence; rej.—rejected; wtd—weighted; errs—errors; Fm.—formation.

Geosphere, published online on 5 February 2016 as doi:10.1130/GES01198.1

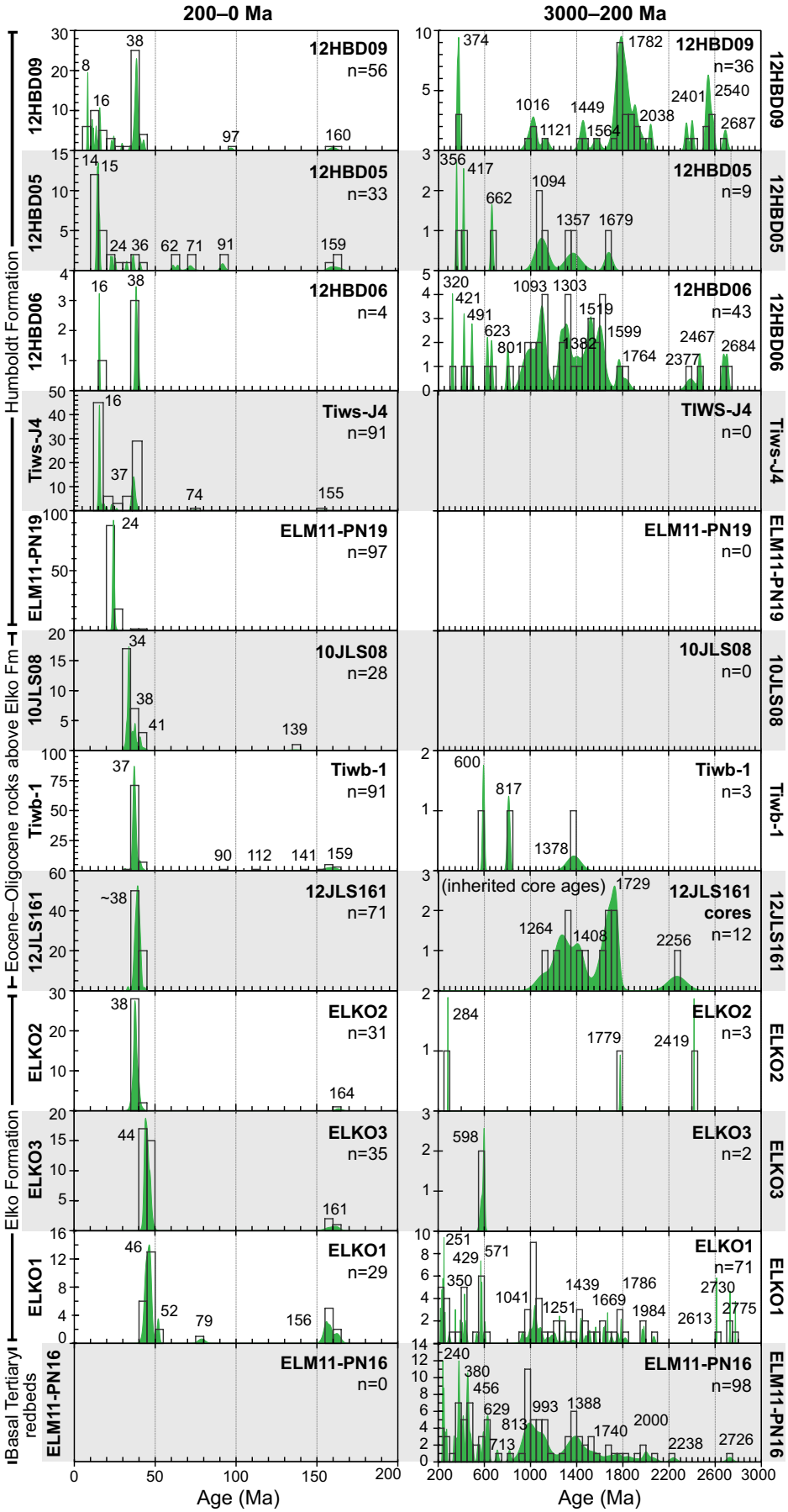

Figure 7. Probability density plots with age histograms for detrital zircon samples, displayed from youngest sample (top) to oldest sample (bottom), based on maximum depositional ages indicated by youngest zircon populations. Each row represents a single sample. Columns highlight age results for different time scales (200–0 Ma and 3000–200 Ma). Sample locations are shown in Figure 2. Results are summarized in Table 2 and tabulated in Tables A4 and A5 in the Supplemental File.

Geosphere, published online on 5 February 2016 as doi:10.1130/GES01198.1

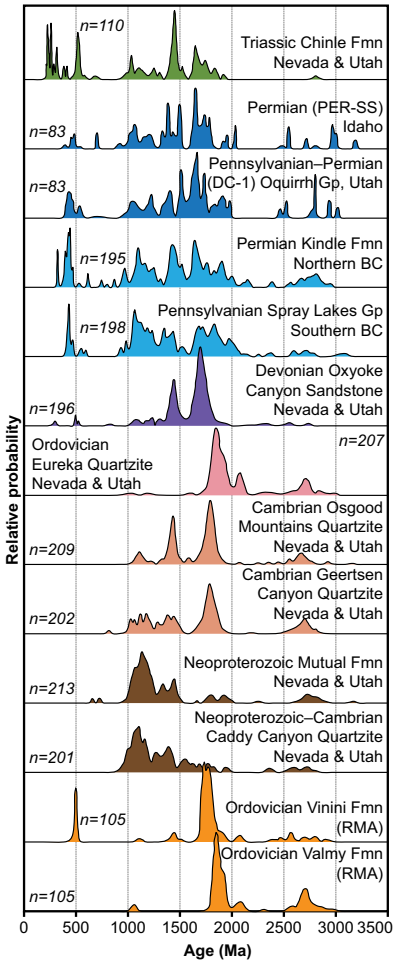

Figure 8. Detrital zircon probability density plots from reference sections of the Cordilleran passive margin. Plots from the Late Triassic Chinle Formation (Fmn), Permian Kindle Formation (BC—British Columbia), Pennsylvanian Spray Lakes Group (Gp), Middle Devonian Oxyoke Canyon Sandstone, Middle Ordovician Eureka Quartzite, early Cambrian Osgood Mountain Quartzite, Neoproterozoic to early Cambrian Geertsen Canyon Quartzite, Neoproterozoic Mutual Formation, and Neoproterozoic Caddy Canyon Quartzite are from Gehrels and Pecha (2014). Plots from the Ordovician Vinini and Valmy Formations, which are part of the Roberts Mountains allochthon, are also from Gehrels and Pecha (2014). Early Permian silty limestone (sample PER-SS) from the Black Pine Range, Idaho, and Early Pennsylvanian–Permian Oquirrh Group calcareous sandstone (sample DC-1) from Dove Creek Pass, Utah, are from Konstantinou et al. (2012).

Server and Solomon, 1983; Ketner and Alpha, 1992; Haynes, 2003; Cline et al., 2005; Henrici and Haynes, 2006). In the mapped area, the Elko Formation is ~180 m thick (Fig. 3B). Pebble conglomerate is exposed only immediately above the basal unconformity with Paleozoic rocks at one location (Figs. 2 and 3B), and paper shale and mudstone are interbedded with coarse clastic strata in the lower part of the section. Overall, the basal pebble conglomerate, sandstone, siltstone, and limestone fine upward to shale and interbedded tuff.

Sample ELKO-1 was selected from near the mapped base of the Elko Formation (Figs. 2 and 3B). It yielded a maximum depositional age of 45.92 ± 0.95 Ma, calculated from 20 of 100 detrital zircon grains (Fig. 6A; Table 2). Major age peaks occur at 156 Ma, 251 Ma, 429 Ma, 571 Ma, and 1.04 Ga and smaller peaks are at 1.44 Ga and 1.79 Ga (Fig. 7). Sandstone (sample ELKO-3) collected slightly higher in the Elko Formation (Figs. 2 and 3B) yielded a maximum depositional age of 45.00 ± 0.48 Ma on the basis of 32 of 37 analyses (Fig. 6B; Table 2). Additional minor age maxima occur at 161 and 598 Ma (Fig. 7). Tuffaceous sandstone sampled near the contact with overlying Eocene tuffs (ELKO-2; Fig. 2) yielded a maximum depositional age of 37.89 ± 0.46 Ma based upon inclusion of most measured grains in the sample (Fig. 6D). Only four older zircons were present in the sample (Fig. 7). Our new maximum depositional age constraints for the Elko Formation show that its deposition ranged from ca. 45.9 to 37.9 Ma (Table 2), in excellent agreement with prior work showing that the Elko Formation was deposited between ca. 46.1 and 38.9 Ma (Haynes, 2003). These results show that deposition of the Elko Formation spans a greater age range than assumed by Horton et al. (2004; 42–39.4 Ma), Mix et al. (2011; 42.6–39.4[?] Ma), and Mulch et al. (2015; 42.5–38.6[?] Ma), and the studies that cited these values (Chamberlain et al., 2012; Feng et al., 2013).

The lower part of the Eocene Elko Formation (sample ELKO-1; Fig. 2) records an abrupt shift in provenance (Fig. 7) expressed by the appearance of Eocene zircon. The oldest strata contain abundant ca. 46 Ma zircons (Figs. 6A and 7) whose age overlaps tightly with the age of volcanism within the Challis volcanic field (Sanford, 2005, and references therein), located north of the Snake River Plain in Idaho (Fig. 1A). The presence of Eocene volcanic material, including a tuff dated as ca. 46 Ma in the lower conglomerate member of the Elko Formation (Haynes, 2003; Table 2), differentiates the conglomerates of the Elko Formation from conglomerates in the older redbeds (TKcs) (Fig. 3B). Previous work throughout the northern Great Basin has documented reworking of Challis-derived volcanic detritus into local sedimentary basins (Haynes, 2003; Henry, 2008). Results from sample ELKO-3 exhibit a slightly younger ca. 45–44 Ma age peak (Figs. 6B and 7) at the young end of ages reported for Challis volcanism (Janecke and Snee, 1993; Janecke et al., 1999; Gaschnig et al., 2009; Chetel et al., 2011; Fig. 1A). Volcanism in the more proximal northeast Nevada volcanic field occurred between 42.6 and 39.0 Ma (Brooks et al., 1995; Fig. 1A). It is interesting that detrital material in this younger age range is absent in the Elko Formation, except in an area significantly to the northwest of the mapped area (Haynes, 2003). Detrital zircon peaks ca. 38 Ma are present at the very top of the Elko Formation within the mapped area (sample ELKO-2; Figs. 6C and 7), where they generally overwhelm other detrital zircon populations. These populations are interpreted as locally derived and to represent the onset of volcanism in the Robinson Mountain volcanic field ca. 38.5 Ma, continuing until 36.8 Ma (Table 2). Two zircons analyzed ca. 52 Ma in the lowermost Elko Formation (sample ELKO-1; Fig. 7) are slightly older than the Challis volcanic field of Idaho and southwest Montana, but are similar in age to the Lowland Creek volcanics and the early Dillon volcanic rocks of southwest Montana (Fritz et al., 2007; Gaschnig et al., 2009; Dudás et al., 2010; Chetel et al., 2011).

The age distributions of pre-Cenozoic zircons in the Elko Formation are broadly similar to those of the underlying Late Cretaceous(?)–Eocene(?) redbeds (Fig. 7). Lower Elko Formation deposits probably contain recycled zircons from the older redbeds and/or received recycled zircons from underlying Triassic and/or late Paleozoic passive margin sediments (Fig. 8). Unlike the older redbeds, Elko Formation samples ELKO-1, ELKO-3, and ELKO-2 all

Geosphere, published online on 5 February 2016 as doi:10.1130/GES01198.1

exhibit a Jurassic peak ca. 164–155 Ma (Fig. 7). Although Jurassic plutons are mapped in the RMEH and could represent a source for Jurassic detritus (e.g., du Bray, 2007), the Elko Formation lacks associated detrital muscovite or metamorphic lithics and other lithic fragments that would likely be derived from the uplift of deep-seated rocks in the RMEH. Based on these observations, it is unlikely that the RMEH was a source of sediment for the Elko Basin during the Eocene. It is most likely that the Jurassic zircon contained within the Elko Formation originated from the erosion of Jurassic volcanic and high-level intrusive rocks exposed in the nearby Cortez Mountains to the west of the Piñon Range and/or the more distant Delcer Buttes and Medicine Range east of the RMEH (e.g., Smith and Ketner, 1976, 1978; Ressel and Henry, 2006; Crafford, 2007; du Bray, 2007; Colgan and Henry, 2009). Smith and Ketner (1978) mapped a volcanic unit of possible Jurassic age (the Frenchie Creek Rhyolite) in the southeastern Piñon Range, southwest of the mapped area (Fig. 1B), but the eruption age of this unit is very uncertain (Smith and Ketner, 1976). The age of the oldest volcanic rocks erupted across the region of deposition of the Elko Formation provides a well-defined upper age bracket for the formation. Sample H10–45, collected from the lowest exposed cooling unit in the tuff of Robinson Mountain, yielded a $^{40}Ar/^{39}Ar$ age of 38.48 ± 0.15 Ma (C.D. Henry, 2011, personal commun.; Figs. 2 and 3B; Table 2).

Eocene Robinson Mountain Volcanic Field and Associated Sedimentary Rocks

Eocene volcanic, subvolcanic, and associated sedimentary rocks of the Robinson Mountain volcanic field were previously mapped as part of the Eocene–Oligocene Indian Well Formation (Smith and Ketner, 1976, 1978). However, new geochronology, together with geologic mapping, demonstrates that most sedimentary rocks in the map area originally assigned to the Indian Well Formation are instead part of the Miocene Humboldt Formation. We therefore suggest discontinuing the name Indian Well Formation, and simply refer to the Eocene igneous rocks on the basis of their presence within the Robinson Mountain volcanic field (Ressel and Henry, 2006). The stratigraphy of the Robinson Mountain volcanic field and its minor associated sedimentary rocks is described in the following.

Tuff of Cissilini Canyon and Associated Igneous and Sedimentary Rocks

The tuff of Cissilini Canyon (Ttcc) appears to have been deposited unconformably above the basal redbeds (TKcs) in the northwest part of the mapped area (Figs. 2 and 3). This tuff consists of smoky quartz–bearing felsic ignimbrites ranging from distinctive dark gray lithic-crystal tuffs with light gray pumice to biotite-rich light gray–pink crystal-vitric tuffs containing light gray–pink pumice. North of the map area, near Emigrant Spring (Fig. 1B), a possibly correlative white, biotite-rich rhyodacite tuff has yielded biotite and hornblende $^{40}Ar/^{39}Ar$ ages of 37.47 ± 0.11 and 38.0 ± 0.3 Ma, respectively (sample NEP-14 of R. Fleck, *in* Haynes, 2003; Table 2). Subvolcanic intrusions and flow-banded rhyolite flows and domes are exposed nearby (Fig. 2). Eocene intrusions in the vicinity of Emigrant Spring and the Railroad mining district (Fig. 1B) are dated between ca. 39.1 and 37.4 Ma (Ressel and Henry, 2006; Table 2).

Tuff of Robinson Mountain and Associated Igneous Rocks

The silicic tuff of Robinson Mountain (Ttrm) conformably overlies the Elko Formation (Fig. 2). It consists of heterogeneous, mostly moderately to densely welded lithic to crystal ignimbrites best exposed south of Robinson Mountain (Figs. 1B, 2, and 3C). This tuff is differentiated by tabular zoned plagioclase phenocrysts that are distinct from the clumped and concentrically zoned plagioclase observed in other Robinson Mountain volcanic rocks. A sanidine $^{40}Ar/^{39}Ar$ age of 38.48 ± 0.15 Ma (sample H10–45) was previously obtained from the lowermost flow, and another sanidine $^{40}Ar/^{39}Ar$ age of 37.70 ± 0.06 Ma (sample H10–47) was obtained from an upper flow (C.D. Henry, 2014, personal commun.). These ages both closely overlap with our maximum depositional age constraints for the underlying uppermost Elko Formation (Fig. 3B; Table 2).

Tuff of Dixie Creek and Associated Igneous and Sedimentary Rocks

The light gray crystal-vitric tuff of Dixie Creek (Ttdc) records at least 12 eruptive events that produced a poorly to moderately welded stack of calc-alkaline trachydacite ignimbrites (Figs. 2, 3D, and 3E). Although these and other nearby tuffs have been referred to as the "tuff of Jiggs" (Palmer et al., 1991; Gordee et al., 2000), their proximity to Dixie Creek, not the town of Jiggs (Fig. 1B), was the reason we informally renamed them. Weathering of the tuff below its more resistant upper part forms distinctive light gray rounded boulders.

Ion probe U-Pb zircon results indicate that the tuff of Dixie Creek was erupted between ca. 37.8 ± 0.4 and 37.3 ± 0.3 Ma (Table 2). Sample 10JLS06A consists of pumice collected from the third-highest exposed cooling event (Figs. 2 and 3). Of 12 zircons, 5 yield a maximum concordia intercept age of 37.7 ± 0.4 Ma (Fig. 4A); 4 additional grains constrain a slightly younger concordia intercept age of 36.5 ± 0.4 Ma, but this is less robust due to the relatively large uncertainties of the results used to constrain the intercept age (Fig. 4A). Sample 10JLS05 is pumice from the uppermost exposed cooling event (Figs. 2 and 3), and 5 of 12 zircons yield an intercept age of 37.34 ± 0.33 Ma (Table 2; Fig. 4B). These ages are consistent with a previously obtained sanidine $^{40}Ar/^{39}Ar$ age of 37.70 ± 0.38 Ma collected by D.A. John from one of the lowest flows exposed (sample 99-DJ-40; Ressel and Henry, 2006; Table 2).

Despite their similar appearance and age, there is evidence that the chemistry of the magma chamber these tuffs erupted from was heterogeneous or that it evolved during its eruptive history (Supplemental File). While the dominant white–light gray–pink pumice represented by samples 10JLS205

Geosphere, published online on 5 February 2016 as doi:10.1130/GES01198.1

and 10JLS206A is dacite in composition, less common dacite with a papery texture (12JLS211) and more mafic trachydacite to trachyandesite pumice (12JLS210) are also present (Figs. A3 and A4 in the Supplemental File). The strong resorption textures exhibited by pumice with different geochemistries in single eruption units (Supplemental File) suggests mixing of more mafic magma with the dominant dacitic composition magma at the time of eruption.

Based on the geochemistry of vitrophyres, nearby lava flows and domes consist of both peraluminous and calc-alkaline rhyolite (unit Tr, Figs. 2 and 3; Figs. A3 and A4 in the Supplemental File) that were probably erupted in multiple stages because they both locally underlie and overlie the tuff of Dixie Creek. Rhyolites range from glassy and crystal poor to phenocryst rich, and are transitional in some places to subvolcanic intrusions (see following discussion). Most flows are mantled above and/or below by vitrophyres and breccias, allowing them to be separated into individual cooling units. The rhyolite flows and domes share numerous petrological characteristics with flow-banded 35.1 ± 0.5 Ma dacite lava domes exposed in the Sulphur Spring Range (unit Tpd of Ryskamp et al., 2008; Fig. 1B), including similar large plagioclase phenocrysts.

Subvolcanic Intrusions and Associated Sedimentary Deposits

Weakly calc-alkaline rhyolite porphyries form the tall edifices of Robinson Mountain and Squaw Mountain, which were probably large volcanic necks that intruded local ignimbrites (Figs. 1B and 2; Supplemental File). This most common type of subvolcanic intrusion (Tsvi) typically contains complex clusters of large plagioclase phenocrysts that are commonly concentrically zoned and closely resemble those in the rhyolite flows and domes and the tuff of Dixie Creek. These and other petrologic similarities suggest a shared magmatic source that differs somewhat from the otherwise compositionally similar tuff of Robinson Mountain, which shows simply zoned, monocrystalline plagioclase phenocrysts. Subvolcanic intrusions having different mineralogy or appearance from the dominant type are exposed locally in parts of the map area (Tsviw and Tsvip, Fig. 2).

Subvolcanic intrusions mostly postdate and intrude the Eocene volcanic rocks, including the ignimbrites and rhyolite domes (Fig. 2). However, in one location west of the southern part of Cedar Ridge, a tabular subvolcanic intrusion may represent a partially exhumed conduit that fed eruption of nearby rhyolite flows and domes (Fig. 2). A sanidine $^{40}Ar/^{39}Ar$ age of 37.51 ± 0.38 Ma was previously obtained from this intrusion (sample 99-DJ-31; Ressel and Henry, 2006; Table 2). This result is similar to our new ion microprobe U-Pb zircon crystallization age of 37.64 ± 0.74 Ma (sample 11JLS104) for an exposure of the Tsvi unit elsewhere in the mapped area (Fig. 2; Table 2). The crystallization age for sample 11JLS104 is based on results obtained from 4 of 16 grains (Figs. 2 and 4C). We interpret older grains detected in 11JLS104 as inherited from the source region. We obtained a younger ion microprobe U-Pb zircon crystallization age of 36.84 ± 0.34 Ma for an additional sample (10JLS11A). We used 4 of 14 zircon results to constrain the age for sample 11JLS11A, excluding a single, discordant measurement with a high error (Fig. 4E). A concordia upper intercept age of 2467.8 ± 6.3 Ma was obtained for this sample (Fig. 4D).

Thin sandstone, siltstone, and shale (unit Ts) layers are commonly exposed adjacent to subvolcanic intrusions or rhyolite flows and domes (Fig. 2), which could represent detrital sources for the sedimentary layers. These sedimentary deposits typically contain clasts of felsic volcanic rocks resembling Robinson Mountain volcanic rocks. A U-Pb detrital zircon sample, 12JLS161, was collected from a possibly reworked or mass-wasted volcanic rock in one such exposure; this established a maximum depositional age of 37.67 ± 0.27 Ma (Fig. 7; Table 2), based on 22 of 83 measurements (Fig. 6D). One younger zircon analysis (ca. 33.3 ± 1.1 Ma; Table A5 in the Supplemental File) was not considered because a single analysis is not sufficient to establish a maximum depositional age, but it is possible that the depositional age of sample 12JLS161 is younger than ca. 33 Ma (Fig. 6D). The large population of ca. 37.7 Ma detrital zircon grains (Fig. 6D) in sample 12JLS161 was likely derived from the contemporaneous (Table 2) tuff of Dixie Creek or the nearby subvolcanic intrusions (Fig. 2). Although 12 analyses yielded Proterozoic ages with peaks at 1.73 Ga, 1.41 Ga, and 1.26 Ga, cathodoluminescence imaging of these grains reveals that most analyses were obtained from the cores of igneous zircons (Figs. 7 and 9). The core ages match age maxima prevalent in Devonian, Cambrian, and Neoproterozoic strata of the Great Basin region (Gehrels and Pecha, 2014). We thus interpret the zircon cores to represent material inherited from either Precambrian basement and/or Neoproterozoic to early Paleozoic strata in the source region of late Eocene magma genesis deep in the crust.

A second sedimentary sample in contact with Eocene volcanic and subvolcanic rocks (TIWB-1) is characterized by bedded, biotite-rich, white sandstones, and yielded an Eocene maximum depositional age (Fig. 6E) of 37.33 ± 0.14 Ma (on the basis of 67 of 94 analyses), nearly identical to ages obtained for nearby subvolcanic intrusions (Table 2). There is also a small age maximum ca. 159 Ma (Fig. 7). Applying the same conservative approach that was used with 12JLS161, we neglected 3 slightly younger U-Pb ages in specimen TIWB-1 that could be geologically meaningful. Based upon the youngest of these ages, the depositional age of TIWB-1 could be younger than ca. 35 Ma (Fig. 6E). A Jurassic peak at 159 Ma indicates either continued detrital zircon input from nearby Jurassic high-level volcanic and intrusive rocks or recycling of older Cenozoic strata containing material of Jurassic age (Fig. 7).

Oligocene(?) Volcanic and Associated Sedimentary Rocks

Mafic to Intermediate Composition Volcanic Rocks

At least two flows of platy, vesicular, dark gray, and nearly aphanitic basaltic andesite (Tba) with a total thickness of >150 m overlie rhyolite flows

Geosphere, published online on 5 February 2016 as doi:10.1130/GES01198.1

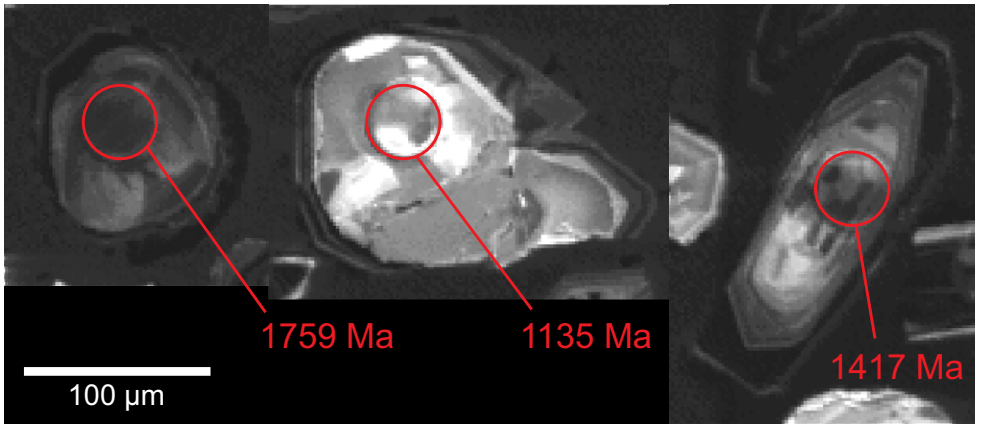

Figure 9. Cathodoluminescence scanning electron microscope images of representative zircons from sample 12JLS161 (reworked, rafted, or mass wasted Eocene tuff of the Robinson Mountain volcanic field) that yielded pre-Cenozoic ages. Most pre-Cenozoic ages were obtained on what are interpreted as inherited cores within Cenozoic zircons.

of the Eocene Robinson Mountain volcanic field (Figs. 2 and 3D). In addition, a small (≤0.2 km^2 map area), black, isolated basaltic trachyandesite intrusion (sample 12JLS125, Supplemental File) is exposed to the west of an east-dipping normal fault system that bounds the east side of the Piñon Range (Figs. 2 and 3D, unit Tbta). For discussions of additional unit descriptions and speculative age constraints, see Lund Snee (2013) and Lund Snee and Miller (2015).

Sedimentary Rocks and the Oligocene Tuff of Hackwood Ranch

Shallowly west dipping, thin (~35 m), poorly consolidated, cross-bedded, silty sandstone and pebble conglomerate were deposited above the tuff of Dixie Creek, across a 10°–15° angular unconformity that dips to the west (Palmer et al., 1991; Gordee et al., 2000). Mapped in Figure 2 as the stratigraphically lowest part of unit Tthr, these rocks have the same dip angle as the overlying Oligocene tuff of Hackwood Ranch (unit Tthr) and demonstrate that underlying Eocene volcanic rocks were tilted before deposition of the Oligocene sediments. Additional westward tilting occurred after eruption and deposition of the tuff of Hackwood Ranch.

Detrital zircon results from a sample near the stratigraphic middle of this sedimentary deposit indicate a maximum depositional age of 33.86 ± 0.40 Ma (sample 10JLS08, Fig. 6F; Table 2), based on 18 of 28 grains. Most of the older zircon in this sample (ca. 41–36 Ma) is similar in age to the Robinson Mountain volcanic rocks, and a single Cretaceous zircon is also present. No igneous rocks with ages close to the main 33.9 Ma zircon population in sample 10JLS08 are present in the map area (Table 2). Possible sources for these zircons include the ca. 33.8 Ma Caetano Tuff or the older and less widespread 34.2 Ma tuff of Cove Mine, which also erupted from the Caetano caldera to the southwest (John et al., 2008; Fig. 1A).

The tuff of Hackwood Ranch consists of three cliff-forming, poorly welded eruptive units (Figs. 2 and 3E). On the basis of phenocryst content, the tuff of Hackwood Ranch is transitional between a quartz latite and latite; however, resorption textures in some phenocrysts suggest that they are xenocrystic. Whole-rock (11JLS105) and pumice-only (HACK-1) geochemical analyses indicate that the tuff is a high-silica rhyolite (Supplemental File). Outcrop and thin section evidence for posteruptive silicification suggests that its high silica (and low alkali) content is due to secondary alteration. The age of the tuff of Hackwood Ranch places constraints on the minimum depositional age of the underlying sedimentary deposits. Ion probe U-Pb ages of zircon and $^{40}Ar/^{39}Ar$ sanidine ages for samples of the tuff of Hackwood Ranch range from 31.59 to 31.08 Ma (Table 2), with 31.08 Ma representing our interpretation of the best age for its eruption. Zircon extracted from pumice in sample HACK-1 yielded a maximum eruptive age of 31.59 ± 0.29 Ma (12 of 16 grains; Fig. 4F). Single crystal, total fusion $^{40}Ar/^{39}Ar$ ages of sanidine from sample HACK-1 yielded a weighted mean age of 31.10 ± 0.47 Ma (2σ total error; mean square of weighted deviates, MSWD = 0.35). Of 14 grains, 2 were rejected as detrital contamination. Zircon recovered from pumice and ash matrix from the second sample (11JLS105) yielded a maximum eruptive age of 31.26 ± 0.30 Ma (8 of 16 grains; Fig. 4G). The second sample (11JLS105) yielded a $^{40}Ar/^{39}Ar$ weighted mean age of 31.08 ± 0.47 Ma (10 of 13 grains; Figs. 3E and 5A; Table 2). The agreement of the $^{40}Ar/^{39}Ar$ and U-Pb age results within 95% confidence from 2 samples of the tuff of Hackwood Ranch strengthens our conclusion that the eruptive age of the tuff of Hackwood Ranch was 31.08 Ma.

Although the age of the Hackwood Ranch tuff overlaps with zircon and monazite ages from metamorphic and igneous rocks in the northern RMEH (as young as 29 Ma; Wright and Snoke, 1993; MacCready et al., 1997; Howard et al., 2011; Fig. 10), this tuff is not thought to have been erupted locally, but most likely erupted from a caldera near the Desatoya and Clan Alpine Mountains in central Nevada (Fig. 1A). Some tuffs traveled hundreds of kilometers from their eruptive centers, and the 31.2 Ma tuff of Rattlesnake Canyon is closest in age to the tuff of Hackwood Ranch (Faulds et al., 2005; Henry et al., 2012; Henry and John, 2013). A similar age of 31.40 +1.3/–0.5 Ma was also obtained from U-Pb LA-ICP-MS analysis of zircon from an andesite in the Sulphur Spring Range to the southwest (sample 04EB123, Ryskamp et al., 2008; Table 2). Otherwise, this is an unusual age for volcanic rocks in northern Nevada, which erupted across a very narrow time interval (Fig. 10).

Geosphere, published online on 5 February 2016 as doi:10.1130/GES01198.1

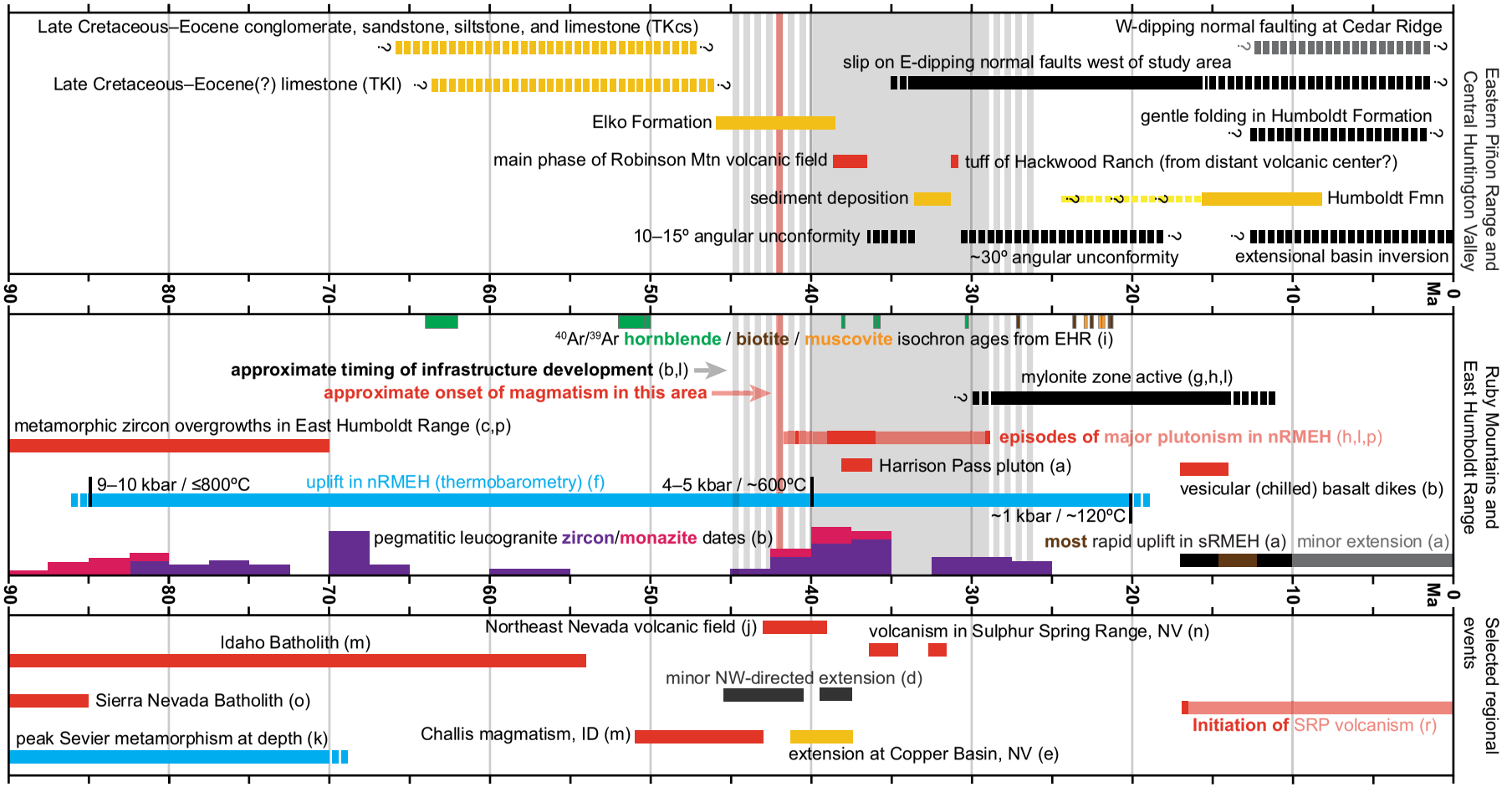

Figure 10. Summary of geologic events in the study area and surrounding region. (A) Events recorded in the study area in Huntington Valley and the eastern Piñon Range. (B) Ruby Mountains–East Humboldt Range (RMEH) metamorphic core complex. (C) Basin and Range Province (BRP) and nearby regions. Abbreviations: s—southern; n—northern; EHR—East Humboldt Range; MCC—metamorphic core complex; ID—Idaho; NV—Nevada; SRP—Snake River Plain. References: a—Colgan et al. (2010); b—Howard et al. (2011); c—McGrew and Snoke (2015); d—Henry (2008); e—Rahl et al. (2002); f—McGrew et al. (2000); g—Haines and van der Pluijm (2010); h—Wright and Snoke (1993); i—McGrew and Snee (1994); j—Brooks et al. (1995); k—Miller and Gans (1989); l—Maccready et al. (1997); m—Gaschnig et al. (2011); n—Ryskamp et al. (2008); o—Van Buer et al. (2009); p—Premo et al. (2014).

Geosphere, published online on 5 February 2016 as doi:10.1130/GES01198.1

Miocene Humboldt Formation

The name Humboldt Formation (Th) has been applied to diverse sedimentary rocks of Miocene age deposited in basins in northeastern Nevada (Sharp, 1939; Smith and Ketner, 1976, 1978; Smith and Howard, 1977; Solomon et al., 1979; Stewart, 1980; Wallace et al., 2008; Fig. 1B). Sharp (1939) initially measured ~1800 m of Humboldt Formation along the eastern flanks of Huntington Creek, west of the RMEH (Fig. 1B). Smith and Ketner (1978) restricted the name Humboldt Formation to the middle and part of the upper members of the Sharp (1939) section, measuring >560 m thick and consisting of upper Miocene conglomerate, sandstone, siltstone, and claystone with beds of limestone, tuff, and ash. West of these deposits, Smith and Ketner (1978) mapped a large portion of the present study area as latest Oligocene–Eocene (time scale of Walker et al., 2012) Indian Well Formation (Fig. 1B), and subsequent workers also used this name (Solomon et al., 1979; Satarugsa and Johnson, 2000; Haynes, 2003; Horton et al., 2004; Chamberlain et al., 2012; Mulch et al., 2015).

Geologic mapping with supplemental geochronology (this study) has determined that most of the sediments previously mapped as Indian Well Formation west of Cedar Ridge and Red Spring and near Indian Well (including the type section of Smith and Ketner, 1976), are significantly younger strata belonging to the mostly Miocene (and possibly as old as latest Oligocene) Humboldt Formation (Figs. 1B and 2). If we include these strata in the Humboldt Formation, its total thickness is ~2130 m in the mapped area alone (Figs. 2 and 3E).

Tephra is present within Miocene sections in northeast Nevada beginning ca. 16 Ma, derived from the explosive rhyolitic volcanic centers of the Snake River Plain–Yellowstone hotspot track (Perkins et al., 1998; Perkins and Nash, 2002; Wallace et al., 2008; Colgan et al., 2010; Fig. 1A). The rhyolites were anhydrous and erupted at high temperature, and they contain little or no biotite (Honjo et al., 1992; Perkins and Nash, 2002; Cathey and Nash, 2009; Ellis et al., 2010; Konstantinou et al., 2012). Snake River Plain tephra thus provide a good means for establishing maximum depositional ages and the stratigraphic age range of the Humboldt Formation. Samples analyzed from the Humboldt Formation reveal at least 5 Miocene age populations: ca. 15.6 Ma, ca. 14.2 Ma, ca. 12.4 Ma, ca. 10.9 Ma, and ca. 8.2 Ma (Figs. 5–7). The 15.6 Ma peak could be derived from several Snake River Plain volcanic sources in Oregon and Nevada, including the High Rock and McDermitt caldera complexes or the Lake Owyhee volcanic field, and the ca. 14.2 Ma tephra could be sourced from the Owyhee-Humboldt volcanic field on the Idaho-Utah-Nevada border (Perkins et al., 1998; Perkins and Nash, 2002; Coble and Mahood, 2012; Fig. 1A). Zircons that are 12.4 Ma in age could be derived from eruptions at the Bruneau-Jarbridge volcanic field of southern Idaho, and ca. 10.9 Ma and ca. 8.2 Ma zircon ages may represent air fall from the Bruneau-Jarbridge, Twin Falls, or Picabo volcanic fields (Perkins and Nash, 2002; Cathey and Nash, 2009; Ellis et al., 2010; Konstantinou et al., 2012). Rare zircons of ca. 32–31 Ma age are also present in Miocene sedimentary rocks and might be derived from the erosion of the underlying tuff of Hackwood Ranch.

Based on map relationships (Fig. 2) and the above ages, the exposures of the Humboldt Formation are youngest eastward toward Huntington Valley (Colgan et al., 2010; this study). The oldest strata of the Humboldt Formation yield detrital zircon age distributions dominated by latest Oligocene to middle Miocene zircon with essentially no zircon older than 200 Ma (see samples ELM11-PN19 and Tiws-J4 in Fig. 7). The Humboldt Formation has been repeated by gentle folds and a west-dipping normal fault system with at least 700 m of throw near Cedar Ridge and Red Spring (herein called the Cedar Ridge fault system) (Wallace et al., 2008; Figs. 1B, 2, and 3E). West of the Cedar Ridge fault system, strata of the Humboldt Formation become finer and more carbonate rich upsection, suggesting a transition from fluvial to lacustrine depositional environments. However, east of the fault system the percentage and thickness of pebble conglomerate horizons increases stratigraphically upward, suggesting a depositional environment increasingly dominated by fluvial activity, consistent with the interpretation of Sharp (1939). Dense, dark blue-gray chert exposed near the normal fault system (unit Ths, Fig. 2) is interpreted to be silicified Humboldt Formation related to hydrothermal activity surrounding the fault system or to silicification in a lacustrine setting. East of the fault system, the upper parts of the mostly Miocene Humboldt Formation (samples 12HBD05 and 12HBD09) appear to represent an unroofing sequence in which previously deeply buried strata of the RMEH were eroded as they were exhumed by middle Miocene faulting (e.g., Colgan et al., 2010).

The basal beds of the Humboldt Formation overlie the Oligocene tuff of Hackwood Ranch across a ≥30° angular unconformity that is mapped in float but is not directly exposed (Figs. 2 and 3E). These lowest deposits include poorly sorted, cross-bedded pebble conglomerate, sandstone, and siltstone with interbedded volcanic ash and clasts resembling Eocene igneous rocks and Paleozoic metasedimentary rocks exposed nearby (Figs. 2 and 3E). Sample ELM11-PN19 is sandstone that was sampled from close to the stratigraphically lowest exposures of the Humboldt Formation (Figs. 2 and 3E). It is volcanogenic and yielded a U-Pb detrital zircon maximum depositional age of 24.39 ± 0.08 Ma on the basis of 90 of 98 grains (Fig. 6G). In calculating this result, we excluded 2 slightly younger ages of 23.3 ± 0.8 Ma and 23.5 ± 0.7 Ma. Possible sources for this mostly ca. 24.4 Ma detrital zircon population include the Fish Creek Mountains Tuff from the Fish Creek Mountains caldera west of the Shoshone Range, that erupted ca. 24.7 Ma (John et al., 2008), or 25–24 Ma eruptions at the Elevenmile Canyon and Poco Canyon calderas of the Stillwater Range to the west (John, 1995; Fig. 1A).

Detrital zircon sample TIWS-J4 was collected from ~250 m above the exposed base of the section (Fig. 3E) and represents the sandstone matrix of volcanic ash–rich, cross-bedded, pebble conglomerate within the Humboldt Formation. This sample yielded a significantly younger U-Pb detrital zircon maximum depositional age of 15.64 ± 0.11 Ma (Fig. 6H; Table 2), based on 42 of 91 analyses. No younger grains were excluded. This upper bound for the depositional age is in good agreement with the $^{40}Ar/^{39}Ar$ sanidine constraints (Table 2) obtained from the lowest air fall tuff exposed in the Hum-

Geosphere, published online on 5 February 2016 as doi:10.1130/GES01198.1

boldt Formation (see following). Sample TIWS-J4 also contains older Cenozoic and a few Cretaceous zircons (Fig. 7). Our sample TIWS-J4 was collected near the locality where several samples collected by Chamberlain et al. (2012) and Mulch et al. (2015) have depositional ages spanning 38.9–38.0 Ma based on $^{40}Ar/^{39}Ar$ dating of biotite and assumed sedimentation rates (NV-IW 01–07 through NV-IW 20–07; ages and sample numbers slightly different in Mulch et al., 2015; Figs. 2 and 3E). Because our geochronologic analyses yielded many zircon grains with significantly younger (Miocene) ages in the same part of the stratigraphic section dated by them, we interpret their ages as dating detrital biotites eroded from the underlying Eocene Robinson Mountain volcanic field, which is exposed nearby, is extremely rich in biotite, and is of the same (ca. 38 Ma) age range (discussed in preceding). In contrast, high-temperature, anhydrous eruptions from the Snake River Plain produced very biotite-poor tephra that was deposited in some of the same strata during Miocene time (Perkins et al., 1998; Wallace et al., 2008; Colgan et al., 2010; Ellis et al., 2010). As the Humboldt basin formed, the Robinson Mountain volcanic rocks were tilted to the east and debris from their erosion was delivered into the basin from its western side (Fig. 2). Boulder to cobble horizons derived almost exclusively from these volcanic rocks are common in the western exposures of the Humboldt Formation.

Above its lowest exposures of conglomeratic sandstone, the Humboldt Formation is characterized by marl with local limestone and calcite-cemented conglomerate beds and horizons of poorly consolidated, ~5–20-m-thick, light tan to blue-gray Snake River Plain volcanic ash (Smith and Ketner, 1976; this study; Figs. 2 and 3E). Alkali feldspar $^{40}Ar/^{39}Ar$ ages obtained from samples of air fall tuffs within the lower parts of the Humboldt Formation place additional bounds on the maximum depositional ages (Fig. 5). However, because these air fall tuffs may have been in part or entirely reworked, the ages obtained from them could be somewhat older than their true depositional age. Sample ELM11-PN13, collected from the lowest Snake River Plain air fall tuff exposed in the Humboldt Formation (Figs. 2 and 3E), yielded an alkali feldspar $^{40}Ar/^{39}Ar$ maximum eruptive age of 15.78 ± 0.25 Ma (10 of 11 grains; Fig. 5C). Sample ELM11-PN11 (Figs. 2 and 3E), collected from an along-strike exposure of the same air fall tuff as ELM11-PN13, yielded an alkali feldspar $^{40}Ar/^{39}Ar$ maximum eruptive age of 15.51 ± 0.24 Ma (8 of 11 grains; Fig. 5D). Although $^{40}Ar/^{39}Ar$ ages of ELM11-PN13 and ELM11-PN11 overlap at ± 2σ total error, it is problematic that their ages fail to overlap at ± 2σ analytical error because these samples were coirradiated and collected from the same air fall tuff (15.78 ± 0.07 Ma; MSWD = 1.42 for ELM11-PN13 versus 15.51 ± 0.03; MSWD = 1.40 for ELM11-PN11; Table A1 in the Supplemental File). Variability in Ca/K ratios and age expressed by high MSWD values (Figs. A1C and A1D in the Supplemental File) suggests that our results may have been affected by detrital contamination that occurred during reworking of the ash deposits by surficial processes. Sample ELM11-PN11 was collected at roughly the same locality as Indian Well Formation samples NV-IW 32–07 through NV-IW 40–07 of Chamberlain et al. (2012) and Mulch et al. (2015); their reported ages span the Eocene to earliest Miocene (38.0–22.3 Ma) and are based on $^{40}Ar/^{39}Ar$ and K-Ar of biotite and sanidine, as well as assumed sedimentation rates between dated samples. As discussed herein, our new data clearly indicate a middle Miocene age for this part of the Humboldt Formation, based on multiple U-Pb and $^{40}Ar/^{39}Ar$ data sets. We interpret the results of Chamberlain et al. (2012) and Mulch et al. (2015) as ages obtained on detrital biotite derived from the underlying Robinson Mountain volcanic field, as this biotite-rich debris is extremely common in this part of the Humboldt Formation (Fig. 3E).

Sample TIWS-J3 was collected from a stratigraphically higher air fall tuff in the Humboldt Formation (Fig. 2). We calculated a weighted mean age of 14.62 ± 0.22 Ma from the youngest 7 of 20 grains in this sample (Figs. 3E and 5E). However, the high MSWD (7.1) associated with this result indicates that our selection is unlikely to define a homogeneous age distribution. We thus regard the TIWS-J3 result as a maximum bound upon the depositional age of the strata that overlie the tuff.

Horton et al. (2004) and Chamberlain et al. (2012) assigned pre-Miocene ages to the section of the Miocene Humboldt Formation that is below the locality of sample TIWS-J3 (Figs. 1B, 2, and 3E), which was previously mapped as the Indian Well Formation. Using the assumption of constant sediment accumulation rates between (and extrapolated beyond) their samples dated by the $^{40}Ar/^{39}Ar$ method on detrital biotite, the Indian Well Formation was believed by Horton et al. (2004) and Chamberlain et al. (2012) to span ca. 38.9–22.3 Ma; our reassignment of these strata to the mostly Miocene Humboldt Formation is significant because they reported a major isotopic shift (~6‰ $\delta^{18}O$ decrease) near the contact between the Elko Formation and the overlying Indian Well Formation, which they reported was constrained between ca. 40 and 38 Ma (Horton et al., 2004; Mix et al., 2011; Chamberlain et al., 2012; Feng et al., 2013; Mulch et al., 2015). This shift is cited as evidence for a rapid elevation gain (~2.5 km in <2 m.y.) (Horton et al., 2004; Mix et al., 2011; Chamberlain et al., 2012; Feng et al., 2013) related to volcanism reaching this latitude at 38 Ma. Previous workers (Chamberlain et al., 2012) inferred middle Eocene topographic relief of as much as 2.2 km in northeast Nevada by subtracting lower and upper bound elevation estimates determined within this general region. The lower bound elevation estimates of 2.0 ± 0.2 km in the late-middle Eocene (ca. 42–39 Ma) were determined using leaf physiognomic methods for strata collected in Copper Basin, Nevada (Wolfe et al., 1998). The upper bound elevation estimates of as much as ~4.2 km hypsometric mean (Mix et al., 2011; Chamberlain et al., 2012) were obtained by stable isotope methods for strata from Huntington Valley, ~130 km south of Copper Basin (Fig. 1A), since the strata in question were originally thought to be of similar age. Because all samples collected and dated from Huntington Valley that were originally thought to span ca. 38.9–22.3 Ma are now known to be ca. 16–15 Ma, the upper bound paleoelevation postulated for northeast Nevada across this time span instead probably represents conditions in the middle Miocene (ca. 16–15 Ma), not the Eocene.

Sample ELM11-PN2 was collected from the stratigraphically highest air fall tuff exposed in the section of the Humboldt Formation exposed west of the Cedar Ridge fault system (Figs. 2 and 3E).

Geosphere, published online on 5 February 2016 as doi:10.1130/GES01198.1

The sample yielded sanidines having a weighted mean age of 12.35 ± 0.19 Ma and a MSWD of 1.90 for 13 of 13 grains (Fig. 5F). The Humboldt Formation is partially repeated east of the Cedar Ridge normal fault system (Wallace et al., 2008; Figs. 2 and 3E). The lowest mapped stratigraphic levels on the east side of the fault system unconformably overlie an undated unit resembling the Eocene Elko Formation (Figs. 1B and 2). A single detrital zircon grain from pebble conglomerate interpreted to represent low stratigraphic levels of the Humboldt Formation east of the Cedar Ridge fault system (sample 12HBD06; Fig. 2) yielded a poorly constrained maximum depositional age of 15.7 ± 0.5 Ma. However, unlike samples ELM11-PN19 and TIWS-J4, this sample is volcanic-fragment poor, yielding only one post-Eocene zircon analysis (15.7 ± 0.5 Ma) and three significantly older analyses forming a small maximum ca. 38 Ma (Fig. 7). The majority of zircon in this sample defines age peaks at 1.09 Ga, 1.30 Ga, 1.52 Ga, and 1.60 Ga, with a smaller maximum at 421 Ma (Fig. 7). It is interesting that a large proportion (>40%) of grains analyzed in 12HBD06 have high ^{204}Pb (>400 counts per second; many are >1000 counts per second; Table A5 in the Supplemental File). This might be related to hydrothermal fluid circulation around the Cedar Ridge fault system, which could have introduced common Pb into older, radiation damaged zircon.

Sample 12HBD06 marks the transition from sediments with volcanic-dominated zircon to recycled zircon from sedimentary sources, as also evidenced by the high proportion of Paleozoic clasts in this sample. The age distribution of pre–200 Ma zircon extracted from 12HBD06 is similar to that from the Late Cretaceous(?)–Eocene(?) redbeds (TKcs) and the Eocene Elko Formation. This includes one 421 Ma analysis and populations at 1.15–0.90 Ga and 1.60–1.25 Ga. The similar age distributions (Fig. 7) of sample 12HBD06 and the Late Cretaceous–Eocene redbeds (TKcs) suggest that sediment contained within both was derived from erosion of Mesozoic and late Paleozoic strata exposed throughout the northern Great Basin or recycled from sediments eroded from these formations.

Uppermost strata of the Humboldt Formation in the mapped area (Figs. 2 and 3E) are light tan, poorly consolidated marls, siltstones, sandstones, and pebbly sandstones with interbedded vitric tuffs. In contrast to 12HBD06, samples collected from the youngest portion of the Humboldt Formation (12HBD05 and 12HBD09) contain clastic material that can be more confidently inferred to have been derived from the erosion of metamorphic rocks in the RMEH. Detrital muscovite, epidote, and lithic fragments of strained quartzite are observed in some of the stratigraphically high samples of the Humboldt Formation (12HBD05; Fig. 2), suggesting input from the erosion of the RMEH. Sample 12HBD05 is Humboldt Formation sandstone that yielded sufficient young zircon (9 of 92 grains) to define a maximum depositional age of 14.15 ± 0.21 Ma (Fig. 6I). This result is similar to ^{40}Ar/^{39}Ar results from volcanic tuff sample TIWS-J3 (Table 2), west of the Cedar Ridge fault system, suggesting that it may be stratigraphically equivalent. Well-defined U-Pb age maxima span the Paleoproterozoic through Paleozoic, and minor populations are detected at 159 Ma and between 91 and 55 Ma, with minor maxima at 71 and 61 Ma, and between 37 and 23 Ma (Fig. 7).

The presence of Jurassic and minor early Cenozoic to Late Cretaceous detrital zircon in this sandstone is consistent with derivation from eroded granites and pegmatites in the RMEH (Fig. 10; Howard et al., 2011). We consider it significant that Late Cretaceous detrital zircon was, in general, not detected in older samples of the Humboldt Formation that we have studied. Rare Late Cretaceous ages of ca. 74 Ma, ca. 90 Ma, and ca. 79 Ma were found in samples of Eocene strata (TIWS-J4, TIWB-1, and ELKO-1, respectively; Fig. 7), but those are solitary ages and are not accompanied by the presence of metamorphic clasts and muscovite. Therefore, we consider it highly unlikely that the rare Late Cretaceous ages in the underlying Eocene strata represent an influx of detrital material from the RMEH. Instead, the signal that we can confidently tie to the RMEH is detected only in the uppermost Humboldt Formation strata exposed in the mapped area. This finding is consistent with ^{87}Sr/^{86}Sr values that increase from lower values of 0.7076–0.7085 in Miocene Humboldt Formation strata within the study area that are now known to be ca. 15 Ma or older (Fig. 3E), and 0.7092 at the base of a section measured <5 km east of the mapped area (Fig. 1B), to 0.7106 stratigraphically higher within the Humboldt Formation (Mulch et al., 2015). This trend of increasing ^{87}Sr/^{86}Sr values upward in the Miocene Humboldt Formation supports our interpretation that previously deeply buried rocks of the RMEH were first exposed midway through Humboldt Formation deposition (ca. 14.2 Ma), thereafter providing a new basement-derived sediment source to the evolving basin.

The youngest maximum depositional age for the Humboldt Formation was obtained from sandstone sample 12HBD09 (Figs. 2 and 3E) using U-Pb detrital zircon geochronology. An age of 8.16 ± 0.15 Ma was obtained from 6 of 94 grains (Fig. 6J; Table 2). This result is the youngest depositional age constraint reported for the Humboldt Formation in Huntington Valley by >1 m.y. (Perkins et al., 1998; Wallace et al., 2008; Colgan et al., 2010). Like samples 12HBD05 and 12HBD06, sample 12HBD09 is poor in Cenozoic zircon. Age populations for this sample range from Miocene to Neoarchean, with major maxima at 374 Ma, 1.02 Ga, 1.45 Ga, 1.78 Ga, and 2.54 Ga (Fig. 7). Additional maxima in sample 12HBD09 are at 16 Ma, ca. 40–38 Ma, 42–41 Ma, and 160 Ma with sparse intervening ages, including 2 grains analyzed near 24 Ma and a single grain analyzed ca. 97 Ma (Fig. 7).

The presence of metamorphic clasts that include fragments of quartz mylonite, and the detrital zircon age maxima in sample 12HBD09, supports derivation of sediment from the RMEH. While the 42–38 Ma populations in this sample closely match similar populations in the Eocene Elko Formation, zircon of this age would also be explained by erosion of the RMEH because these ages partly overlap with plutonic ages in the RMEH, such as the 38 Ma Harrison Pass pluton (Colgan et al., 2010). Older quartz diorite and quartz dioritic orthogneisses in the RMEH range from ca. 40 to 29 Ma (Wright and Snoke, 1993). Another important feature of the detrital zircon age distribution of sample 12HBD09 from the uppermost Humboldt Formation is the nature of its Proterozoic age distribution. Detrital zircon populations at 1.12 Ga, 1.45 Ga, 1.70–2.04 Ga, and 2.69 Ga in this youngest Humboldt

Geosphere, published online on 5 February 2016 as doi:10.1130/GES01198.1

Formation sample (Fig. 7) match similar peaks in the Neoproterozoic–early Cambrian Geertsen Canyon Quartzite, early Cambrian Osgood Mountain Quartzite, and Middle Ordovician Eureka Quartzite (Gehrels and Pecha, 2014; Fig. 8), and indicate that erosion of early Paleozoic and late Neoproterozoic strata in the RMEH may have contributed debris to the upper Humboldt Formation. Note that the abundant 1.4 Ga and 1.7 Ga zircon prevalent in 12HBD09 (Fig. 7) does not closely match the Grenville-dominated Proterozoic detrital zircon age distributions that would be contributed by Permian and Triassic strata in the upper part of the passive margin succession (Fig. 8). We thus interpret the Mesoproterozoic zircon in sample 12HBD09 as recycled from the erosion of the structurally deepest, Neoproterozoic and early Paleozoic part of the miogeoclinal succession exposed in the RMEH. The results from sample 12HBD09 are consistent with the interpretation that Neoproterozoic and early Paleozoic rocks in the RMEH were not exposed until extensional faulting began in the middle Miocene (Colgan et al., 2010).

In summary, the Humboldt Formation documents an unroofing sequence produced by the progressive fault-related exhumation and erosion of the RMEH. Humboldt Formation strata recycled zircons eroded from late Paleozoic and Mesozoic sedimentary rocks exposed at the paleosurface beneath the Tertiary unconformity until ca. 14.2 Ma or earlier. A detrital zircon signature that suggests derivation from RMEH plutonic rocks is first detected in sample 12HBD05 (Figs. 2, 3E, and 7), collected from beds that also contain abundant detrital muscovite and metamorphic clasts, which yielded a maximum depositional age of 14.15 ± 0.21 Ma (Table 2). This was followed by the arrival, at 8.2 Ma or earlier (sample 12HBD09; Table 2), of Precambrian and Cambrian sediment sources, which are the lowest stratigraphic levels currently exposed in the southern RMEH (Willden and Kistler, 1979; Crafford, 2007). This documented sequence of events suggests that the faulting that brought these rocks to the surface occurred in the Miocene, consistent with recent work showing that rapid fault slip unroofed the southern RMEH between ca. 17–16 Ma and ca. 12–10 Ma (Colgan et al., 2010).

Post-Miocene Sedimentary Rocks

The Hay Ranch Formation (Regnier, 1960; Smith and Ketner, 1976) consists of poorly consolidated conglomerate, sandstone, and siltstone. Fossil and zircon fission-track dating indicate a maximum depositional age of middle Pliocene–middle Pleistocene (Smith and Ketner, 1976). In addition, Quaternary gravel deposits commonly cap hilltops and slopes, indicating that broad alluvial surfaces were once developed across the map area and have since been eroded, cut by streams, and filled with younger Quaternary deposits (Fig. 2). For more detailed descriptions of these units, see Lund Snee (2013) and Lund Snee and Miller (2015).

DISCUSSION

Upper Crustal Perspective on the Evolution of the RMEH MCC

This study utilizes geologic mapping, geochronology, and geochemistry to understand the Late Cretaceous through Cenozoic upper crustal geologic history adjacent to the southern and central parts of the developing RMEH MCC in order to address some of the controversies about the evolution of the core complex and its age and mechanism of exhumation. Our geochronologic data from supracrustal sections enable high-temporal-resolution comparison between events documented at the surface of the Earth to those occurring in the deeper crust, as represented by igneous and metamorphic rocks of the RMEH MCC (Fig. 10).

Throughout the well-documented history of Late Cretaceous to Oligocene metamorphism, partial melting, and lower crustal flow within the developing RMEH MCC (e.g., Wright and Snoke, 1993; McGrew and Snee, 1994; MacCready et al., 1997; McGrew et al., 2000; Howard et al., 2011), events at the Earth's surface represent relative quiescence (Figs. 10 and 11). The oldest deposits in the mapped area are above a regional late Mesozoic or basal Cenozoic unconformity and include redbeds, conglomerate, sandstone, siltstone, and limestone of Late Cretaceous(?)–Eocene(?) age representing nonmarine continental and lacustrine depositional settings. Their detrital zircon signature indicates recycling from local underlying bedrock units and/or their regional correlatives. It remains unclear whether deposition was continuous between these basal Cenozoic strata and the overlying Eocene Elko Formation, because the contact between the two units is not well exposed in the study area, but others have suggested that the Elko Formation may unconformably overlie the underlying TKl limestones and that there may be slight angular discordance within TKl and TKcs (Smith and Ketner, 1976). Deposition of the Elko Formation began ca. 46 Ma (Figs. 10 and 11), as recorded by the presence of a 45.9 ± 1.0 Ma tuff near its base (Haynes, 2003; this study; Table 2). This tuff, and another dated as 45.0 ± 0.5 Ma (Table 2), were likely erupted from the Challis volcanic field, the closest region with eruptive units of that age (e.g., Gaschnig et al., 2009; Fig. 1A). The onset of Eocene volcanism in Idaho and Montana was coeval with MCC development north of the Snake River Plain and involved the development of topographically elevated regions that fed major river systems that delivered sediment to the Pacific coast (Dumitru et al., 2013). Thus it is possible that rivers could also have drained southward from Idaho and Montana at this time, transporting material into the Elko Basin. This would suggest higher topography to the north than to the south during the Eocene. Gans (1990), Mix et al. (2011), and Chamberlain et al. (2012) suggested that a southward-propagating, thermally driven topographic high or bulge could have accompanied the well-documented southward-sweeping onset of volcanism. If so, the Elko Basin could have developed as a topographic low relative to areas further north that were elevated by the onset of volcanism at 42–38 Ma (Brooks et al., 1995; Ressel and Henry, 2006; Konstantinou et al., 2012; this study). However, the present-day extent of the Elko Basin is elongated in the north-south direction (Haynes, 2003), and this is particularly true after removal of Cenozoic extension, so relating its development to topographic effects associated with southward-sweeping volcanism is speculative. Although the Elko Formation is more spatially continuous than the underlying TKcs and TKl units, it is <180 m

Geosphere, published online on 5 February 2016 as doi:10.1130/GES01198.1

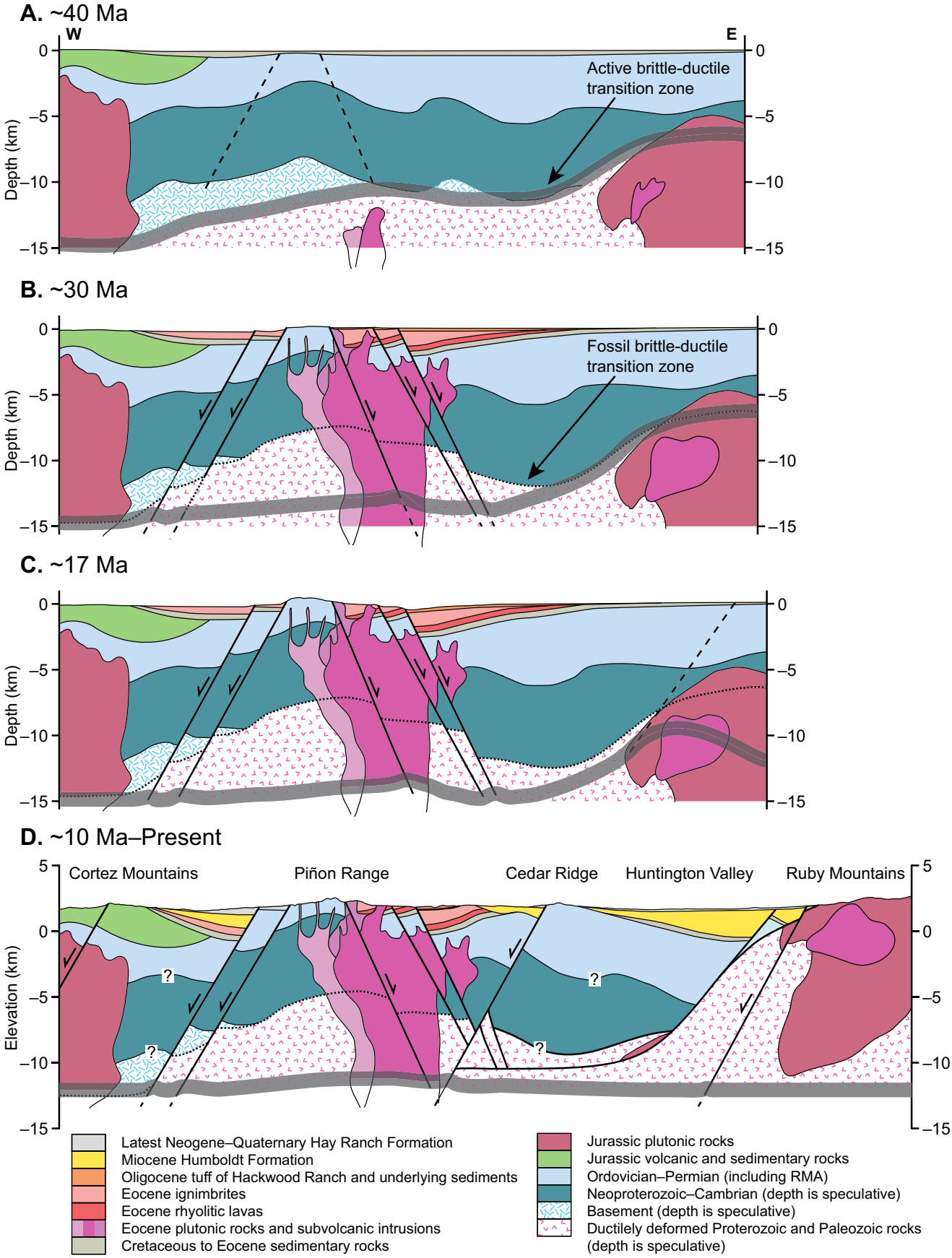

Figure 11. (A–D) Generalized Cenozoic tectonic history of the Carlin-Piñon–Ruby Mountains–East Humboldt Range region. Section location is shown in Figures 1B and 2. Fault, pluton, and stratigraphic geometries are based on those of Smith and Ketner (1978), Wannamaker and Doerner (2002), Colgan et al. (2010), and this study. The depths of the brittle-ductile transition, basement, and Neoproterozoic–lower Paleozoic succession are speculative. RMA—Roberts Mountains allochthon.

Geosphere, published online on 5 February 2016 as doi:10.1130/GES01198.1

thick in the mapped area (Figs. 2, 3A, and 3B), but a thickness of ~850 m has been measured in the Elko Hills (Haynes, 2003; Fig. 1B). There is no evidence from this study or from the interpretation of seismic reflection data in Huntington Valley that the Elko Formation and other pre-Miocene sedimentary rocks thicken significantly eastward into the west-dipping RMEH detachment fault (Satarugsa and Johnson, 2000; Haynes, 2003; Colgan et al., 2010). Interpretations based on the existing seismic lines (Satarugsa and Johnson, 2000) are challenging due to the data quality.

Southward-migrating volcanism reached northern Nevada ca. 42.6 Ma (Brooks et al., 1995), and coincided with the beginning of a Cenozoic phase of crustal melting (ca. 42–29 Ma) deep in the MCC infrastructure now exposed in the northern RMEH (e.g., Wright and Snoke, 1993; McGrew and Snee, 1994; MacCready et al., 1997; Howard et al., 2011; Drew, 2013; Fig. 10). Volcanism reached the mapped area ca. 38 Ma (Ressel and Henry, 2006; this study). A tuff dated as 37.9 ± 0.5 Ma (Table 2) near the top of the Elko Formation dates the end of deposition of the Elko Formation ca. 38 Ma. Because the ages of ash flow tuffs in the basal overlying volcanic package overlap this age within error, the uppermost dated tuff in the Elko Formation may have erupted from the Robinson Mountain volcanic field or from slightly to the north, near Emigrant Pass (Ressel and Henry, 2006; Figs. 1B and 3B; Table 2). No unconformity is observed between strata assigned to the Elko Formation and the overlying Eocene volcanic rocks of the Robinson Mountain volcanic field (Fig. 2), formerly mapped as the Indian Well Formation by Smith and Ketner (1978).

Ignimbrites of the Robinson Mountain volcanic field were erupted between ca. 38.5 and 37.3 Ma (Table 2) in a subaerial or shallow lacustrine environment, and are >1000 m thick in parts of the mapped area (Fig. 3E). The ignimbrites were likely erupted from vents in the Robinson Mountain area, as suggested by the presence of voluminous Eocene rhyolite domes of similar mineralogy and geochemistry (Supplemental File) and the lack of mapped calderas of this age (Henry and John, 2013). Eocene rocks of the Robinson Mountain volcanic field may have been deposited as far west as the eastern flanks of the present Cortez Mountains (Figs. 1B and 11), where patches of strata previously mapped as Indian Well Formation include basalt flows and white Paleogene lapilli tuffs exposed beneath Quaternary and late Cenozoic sedimentary cover (Smith and Ketner, 1976, 1978). The slightly younger ages of the crosscutting subvolcanic intrusions in the mapped area (ca. 37.6–36.8 Ma; Fig. 2; Table 2) document magmatism continuing to this time. Once erupted, the resistant volcanic rocks protected underlying sedimentary strata from subsequent erosion. Westward tilting (10°–15°) occurred after the eruption of 37.3 ± 0.3 Ma ignimbrites. Following tilting, Eocene volcanic rocks were covered with cross-bedded sandstone with a maximum depositional age of 33.9 ± 0.4 Ma (Figs. 2 and 11; Table 2).

Despite evidence that metamorphism, partial melting of the crust, and intrusion of magmas continued at depth in the developing RMEH until at least 29 Ma (e.g., Wright and Snoke, 1993; McGrew and Snee, 1994; MacCready et al., 1997; Howard et al., 2011; Fig. 10), volcanic activity at the surface ended ca. 36 Ma (Ressel and Henry, 2006; Walker et al., 2006; du Bray, 2007; this study; Fig. 10; Table 2). The thin tuff of Hackwood Ranch was erupted across the sediments overlying the Robinson Mountain volcanic rocks at 31.1 ± 0.3 Ma (Figs. 10 and 11), but, as discussed, it is likely that it was erupted from a distant caldera, probably near the Desatoya or Clan Alpine Mountains (Faulds et al., 2005; Henry et al., 2012; Henry and John, 2013). Based on these relationships, it is clear that magmatism at depth in the crust did not result in surface eruptions between 36 and 29 Ma. The tuff of Hackwood Ranch was subsequently tilted gently westward (Figs. 2 and 11). Because exposures of Eocene and Oligocene volcanic rocks are absent east of Cedar Ridge and Red Spring (Figs. 2 and 3A), they may have been deposited thinly or not at all (Fig. 11). If appreciable thicknesses of volcanic rocks had been deposited east of Cedar Ridge, they must have been eroded away before middle Miocene time.

The gently east dipping, mostly Miocene Humboldt Formation overlies the gently west dipping Oligocene tuff of Hackwood Ranch with ~30° of angular discordance (Fig. 2). This angular discordance probably developed as a result of westward tilting between ca. 31.1 and 24.4 Ma. This early phase of westward tilting could have resulted from slip on east-dipping faults west of the exposures of the tuff of Hackwood Ranch, and/or from differential uplift of the region that was to become the RMEH MCC relative to surrounding areas due to crustal flow and/or diapiric rise of rocks at depth beneath what was to become the Ruby Mountains (Figs. 1B, 2, 10, and 11). Basin development along the west side of the RMEH (Fig. 1B) is heralded by deposition of the Humboldt Formation perhaps as early as 24.4 Ma. The basin filled mostly between ca. 16 and 12 Ma, and the youngest deposits are dated as 8.2 Ma (Colgan et al., 2010; this study). The youngest biotites previously dated within the RMEH, along the western side of the range, yielded early Miocene (ca. 24–21 Ma; Fig. 10) $^{40}Ar/^{39}Ar$ ages (McGrew and Snee, 1994). These ages are compatible with stratigraphic evidence for the onset of uplift by faulting in the Miocene and, because they may represent ages set within the partial retention zone for argon in biotite, they would represent maximum ages for faulting.

Although extensional faulting may have begun as early as 24.4 Ma, it accelerated ca. 16–15 Ma, as recorded by the onset of rapid deposition in the study area. This conclusion is in close agreement with recent findings, based on several techniques, that rapid uplift of the southern RMEH began ca. 17–15 Ma (Colgan et al., 2010). More than 2100 m of sediment were deposited across just the mapped area during Miocene time. The Humboldt Formation thickens eastward toward the RMEH (Satarugsa and Johnson, 2000; Fig. 1B), from where its younger strata are now known to have been sourced (Colgan et al., 2010; this study). An unroofing signature is recorded in the Humboldt Formation with the arrival ca. 14.2 Ma or later of metamorphic clasts and a detrital zircon age spectrum consistent with derivation of sediment from Proterozoic and early Paleozoic rocks now exposed in the southern RMEH.

Thus, prior to ca. 16 Ma, the supracrustal history of the sedimentary basin on the western flank of the RMEH MCC provides evidence for only minor tilting near and within the Piñon Range, or

Geosphere, published online on 5 February 2016 as doi:10.1130/GES01198.1

the western flank of the future RMEH MCC. It is possible that these tilts are a result of east-dipping normal faults, or they might reflect adjustments in the upper crust related to Eocene and Oligocene flow at depth, and thus could represent the western side of a dome-like uplift.

Our results, which indicate only minor surface deformation in the time span from the Late Cretaceous to the Miocene, help to underscore the dilemma posed by the suggestion that large-magnitude thrusting followed by large-magnitude extension occurred across the region of the RMEH in the Late Cretaceous to early Cenozoic (e.g., Coney and Harms, 1984; Vandervoort and Schmitt, 1990; Hodges and Walker, 1992; Mueller and Snoke, 1993; Camilleri, 1996; Camilleri and Chamberlain, 1997; McGrew et al., 2000; Howard, 2003; Hallett and Spear, 2014, 2015). In particular, the growing detrital zircon record obtained from sandstones and conglomeratic units at the base of the Cenozoic unconformity across the northern BRP does not show evidence for recycling and thus uplift of the lower part of the shelf succession (late Precambrian to Cambrian) or widespread deposition related to high-angle faulting and half-graben formation prior to Eocene time (e.g., Druschke et al., 2009, 2011; Konstantinou et al., 2012; Ruksznis, 2015; this study). These findings in turn challenge proposals that large-magnitude extension in the hinterland of the Mesozoic Sevier fold and thrust belt was driven by the onset of melting and extensional collapse of structurally overthickened, gravitationally unstable crust (e.g., Molnar and Chen, 1983; Coney and Harms, 1984; Hodges and Walker, 1992). Instead, major extension near the RMEH and Piñon Range, as documented by the deposits studied here, probably began in middle Miocene time, more than 50 m.y. after Mesozoic crustal thickening, metamorphism, and magmatism peaked in the Sevier hinterland (Miller and Gans, 1989). Even allowing 20 m.y. for the relaxation of isotherms in thickened crust (e.g., Camilleri and Chamberlain, 1997; DeCelles, 2004; Mattinson et al., 2007), Miocene extension began more than 30 m.y. after attainment of these elevated temperatures.

In contrast to the view from the upper crust discussed here, pressure-temperature-time paths determined using metamorphic mineral assemblages and U-Pb monazite cooling ages yield evidence for uplift and cooling of originally deep-seated northern RMEH rocks beginning during the Late Cretaceous or even earlier (Dallmeyer et al., 1986; Hodges et al., 1992; Hallett and Spear, 2014, 2015; Fig. 10). Fission-track, U-Pb, and $^{40}Ar/^{39}Ar$ thermochronology data suggest that uplift of these rocks continued through Oligocene time (e.g., Dallmeyer et al., 1986; Dokka et al., 1986; Wright and Snoke, 1993; McGrew and Snee, 1994; MacCready et al., 1997; McGrew et al., 2000; Snoke et al., 2004; Premo et al., 2005; Fig. 10). Further work is needed to understand the nature and location of structures that accommodated uplift of these rocks and to reconcile these structures with what is now known about the surface geology and topography of the area near the RMEH during this time span. Our data from supracrustal rocks do not preclude uplift of the deeper parts of the crust by a process such as diapirism and/or crustal thinning, as modeled by Rey et al. (2009), who suggested that mechanical decoupling occurred between the brittle upper crust and the ductile crust below (see also MacCready et al., 1997). This could explain the relatively low degrees of brittle faulting and topographic changes prior to Miocene extension.

Implications for Estimates of Paleotopography, Paleoelevation, and Paleoclimate

Stable isotope studies that address the evolution of Paleocene to Holocene climate, elevation, and topographic relief across the Sevier hinterland utilize and are heavily influenced by data collected from the Elko Basin (Horton et al., 2004; Mix et al., 2011; Chamberlain et al., 2012; Feng et al., 2013; Mulch et al., 2015). These studies argue for a rapid elevation gain that swept southward through the latitude of the Elko Basin in the Eocene, tracking the southward migration of volcanism following the end of flat-slab subduction (Gans, 1990; Mix et al., 2011; Chamberlain et al., 2012). Chamberlain et al. (2012) and Mulch et al. (2015) suggested that the shift in stable isotope values documented in the Elko Basin for ca. 40–38 Ma also heralds the formation of rugged topography with peaks >4000 m across the region that affected climate and rainfall.

Our findings do not bear on absolute elevations, but call into question the suggestion that rugged topographic relief with peaks >4000 m formed here in the Eocene (Chamberlain et al., 2012; Mulch et al., 2015). Instead, geologic data suggest that the region had relatively low relief and was covered by volcanic rocks that underwent low magnitudes of erosion after volcanism ceased (Henry, 2008; Best et al., 2009; Van Buer et al., 2009; Henry et al., 2012; Konstantinou et al., 2012; Long, 2012; this study). A major implication of our remapping and more detailed dating of the section is that the measured isotopic shift reported by Horton et al. (2004), Mix et al. (2011), Chamberlain et al. (2012), and Mulch et al. (2015) is no longer constrained to have occurred in the Eocene, but could have taken place anytime between ca. 40 and 16 Ma. Thus the isotopic data (Horton et al., 2004; Mix et al., 2011; Chamberlain et al., 2012; Mulch et al., 2015), when tied to the revised stratigraphy presented here, are in general agreement with a low-relief Eocene volcanic tableland, followed much later in the Miocene by the development of higher mean elevations and mountain ranges (rugged topography) during Basin and Range faulting (e.g., Miller et al., 1999; Colgan et al., 2010; Konstantinou et al., 2012; this study).

CONCLUSIONS

Our detailed geological study of Huntington Valley and the eastern Piñon Range, together with supporting geochronology, reveals that the upper crust and supracrustal section exposed in this area experienced mostly tectonic quiescence from Late Cretaceous through Oligocene time. It is striking that this interval of surficial tectonic quiescence coincides with partial melting, metamorphism, and lower crustal flow at depth in the developing RMEH MCC (e.g., Wright and Snoke, 1993; McGrew and Snee, 1994; MacCready et al., 1997; Howard et al., 2011; Figs. 10 and 11).

Deposition was minor or absent in central Huntington Valley and the eastern Piñon Range

Geosphere, published online on 5 February 2016 as doi:10.1130/GES01198.1

during the time span of Mesozoic crustal shortening. Regional erosion followed, exposing gently folded late Paleozoic and Mesozoic (Triassic) strata that are now beneath the Tertiary unconformity. Redbeds and limestone were deposited unconformably and discontinuously over the older folded strata. The detrital zircon signatures of the redbeds and those of the overlying Eocene Elko Formation suggest recycling of zircons specifically from Permian and Triassic miogeoclinal strata. The Eocene Elko Formation is only ~180 m thick at its greatest in the mapped area, but is as much as ~850 m regionally (Haynes, 2003). The Elko Formation contains ca. 46–38 Ma detrital zircon populations that represent air fall derived from volcanic eruptions north of the Snake River Plain (46–42 Ma) and locally (39–38 Ma). Local eruption of rhyodacite ignimbrites, rhyolite domes and flows, and intrusion of subvolcanic rhyolite of the ca. 38.5–36.8 Ma Robinson Mountain volcanic field followed deposition of the Elko Formation.

Westward tilting of 10°–15° occurred before deposition of thin 33.9 Ma (or younger) sediments and eruption of the 31.08 ± 0.47 Ma rhyolitic tuff of Hackwood Ranch, which was probably derived from a distant caldera. This was followed by additional, apparently localized, westward tilting by ≥10°–15° that occurred before ca. 24.4 Ma. At least some of the westward tilting was probably caused by normal slip on east-dipping faults west of the study area, but it is also possible that tilting could be related to uplift of a developing RMEH gneiss dome at greater depth in the crust. If so, our data may suggest decoupling of events in the deep and shallow crust and may allow for earlier (diapiric) rise of metamorphic rocks, such as is now documented for the Albion–Raft River–Grouse Creek Mountains MCC (Strickland et al., 2011; Konstantinou et al., 2012, 2013). Rapid slip began ca. 16 Ma on a west-dipping normal fault bounding the west side of the RMEH (Colgan et al., 2010); this led to deposition of the Humboldt Formation from ca. 15.8 to 12 Ma, with minor deposition beginning perhaps as early as 24 Ma and continuing until ca. 8.2 Ma or later. More than 2000 m of Miocene Humboldt Formation strata were deposited across the study area, and deposits of this basin thicken eastward toward the RMEH. Detrital zircon populations and metamorphic clasts thought to demonstrate RMEH provenance are first detected in 14.2 Ma (or younger) Humboldt Formation deposits, which constrain the timing of RMEH unroofing. Our conclusions parallel earlier discoveries that the metamorphic rocks in MCCs of the northern BRP were uplifted in their final stage only in Miocene time (Miller et al., 1999; Colgan et al., 2010; Konstantinou et al., 2012, 2013; Ruksznis, 2015).

Our work also has implications for the paleogeographic evolution of the hinterland of the Sevier fold and thrust belt. We reassign a thick succession of sedimentary strata previously assigned to the Eocene–Oligocene Indian Well Formation to the lower part of the mostly Miocene Humboldt Formation on the basis of geologic mapping and extensive geochronologic constraints. The reassignment of these strata compels a reinterpretation of stable isotope–based paleoelevation estimates and raises the prospect that the proposed large and rapid elevation gain (~2.5 km in <2 m.y.) in the Eocene (e.g., Chamberlain et al., 2012) could have taken place over any time interval between the middle Eocene and middle Miocene. Although we cannot establish paleoelevations of this region based on our current work, the stratigraphic details of the Cretaceous(?) to Miocene section studied precludes the conclusion arising from stable isotope studies that rugged topography was established across this region in the Eocene (Horton et al., 2004; Mix et al., 2011; Chamberlain et al., 2012; Feng et al., 2013; Mulch et al., 2015). Instead, the region was topographically subdued and covered with volcanic rocks until the Miocene, when rugged topography first formed.

ACKNOWLEDGMENTS

This research was supported by Stanford University, U.S. Geological Survey EdMap award G12AC20189 to Lund Snee and Miller, and National Science Foundation Tectonics Program grant 1322084 to Miller. We thank Alan J. McGrew and an anonymous reviewer for constructive reviews, and Terry Pavlis for thoughtful and responsive editorial assistance. Our research benefitted from discussions with J.P. Colgan, D.A. John, C.D. Henry, T.A. Dumitru, and G.A. Thompson. We thank H. Dudley, M. Erviti, J. Knox, M. Raftrey, B. Girma, S. Xiao, and the students of Stanford Field Class GES 190 for their able assistance.

REFERENCES CITED

Armstrong, R.L., 1970, Geochronology of Tertiary igneous rocks, eastern Basin and Range Province, western Utah, eastern Nevada, and vicinity, USA: Geochimica et Cosmochimica Acta, v. 34, p. 203–232, doi:10.1016/0016-7037(70)90007-4.

Armstrong, R.L., 1982, Cordilleran metamorphic core complexes—From Arizona to southern Canada: Annual Review of Earth and Planetary Sciences, v. 10, p. 129–154, doi:10.1146/annurev.ea.10.050182.001021.

Armstrong, R.L., and Ward, P., 1991, Evolving geographic patterns of Cenozoic magmatism in the North American Cordillera: The temporal and spatial association of magmatism and metamorphic core complexes: Journal of Geophysical Research, v. 96, no. B8, p. 13,201–13,213, doi:10.1029/91JB00412.

Barnes, C.G., Burton, B.R., Burling, T.C., Wright, J.E., and Karlsson, H.R., 2001, Petrology and geochemistry of the late Eocene Harrison Pass pluton, Ruby Mountains core complex, northeastern Nevada: Journal of Petrology, v. 42, p. 901–929, doi:10.1093/petrology/42.5.901.

Best, M.G., and Christiansen, E.H., 1991, Limited extension during peak Tertiary volcanism, Great Basin of Nevada and Utah: Journal of Geophysical Research, v. 96, no. B8, p. 13,509–13,528, doi:10.1029/91JB00244.

Best, M.G., Barr, D.L., Christiansen, E.H., Gromme, S., Deino, A.L., and Tingey, D.G., 2009, The Great Basin Altiplano during the middle Cenozoic ignimbrite flareup: Insights from volcanic rocks: International Geology Review, v. 51, p. 589–633, doi:10.1080/00206810902867690.

Brooks, W.E., Thorman, C.H., and Snee, L.W., 1995, The $^{40}Ar/^{39}Ar$ ages and tectonic setting of the middle Eocene northeast Nevada volcanic field: Journal of Geophysical Research, v. 100, no. B7, p. 10,403–10,416, doi:10.1029/94JB03389.

Burchfiel, B.C., and Davis, G.A., 1975, Nature and controls of Cordilleran orogenesis, western United States: Extensions of an earlier synthesis: American Journal of Science, v. 275, p. 363–396.

Burchfiel, B.C., Cowan, D.S., and Davis, G.A., 1992, Tectonic overview of the Cordilleran orogen in the western United States, *in* Burchfiel, B., et al., eds., The Cordilleran orogen: Conterminous U.S.: Boulder, Colorado, Geological Society of America, Geology of North America, v. 3, p. 407–479.

Camilleri, P.A., 1996, Evidence for Late Cretaceous–early Tertiary(?) extension in the Pequop Mountains, Nevada: Implications for the nature of the early Tertiary unconformity, *in* Taylor, W.J., and Langrock, H., eds., Cenozoic structure and stratigraphy of central Nevada: Nevada Petroleum Society 1996 Field Conference Volume, p. 19–28.

Camilleri, P.A., and Chamberlain, K.R., 1997, Mesozoic tectonics and metamorphism in the Pequop Mountains and Wood Hills region, northeast Nevada: Implications for the architecture and evolution of the Sevier orogen: Geological Society of America Bulletin, v. 109, p. 74–94, doi:10.1130/0016-7606(1997)109<0074:MTAMIT>2.3.CO;2.

Camilleri, P.A., Yonkee, A., Coogan, J., DeCelles, P., McGrew, A., and Wells, M., 1997, Hinterland to foreland transect through the Sevier orogen, northeast Nevada to north central Utah; structural style, metamorphism, and kinematic history of a large contractional orogenic wedge: Brigham Young University Geology Studies, v. 42, p. 297–309.

Geosphere, published online on 5 February 2016 as doi:10.1130/GES01198.1

Cathey, H.E., and Nash, B.P., 2009, Pyroxene thermometry of rhyolite lavas of the Bruneau-Jarbidge eruptive center, central Snake River Plain: Journal of Volcanology and Geothermal Research, v. 188, p. 173–185, doi:10.1016/j.jvolgeores.2009.05.024.

Chamberlain, C.P., Mix, H.T., Mulch, A., Hren, M.T., Kent-Corson, M.L., Davis, S.J., Horton, T.W., and Graham, S.A., 2012, The Cenozoic climatic and topographic evolution of the western North American Cordillera: American Journal of Science, v. 312, p. 213–262, doi:10.2475/02.2012.05.

Chetel, L.M., Janecke, S.U., Carroll, A.R., Beard, B.L., Johnson, C.M., and Singer, B.S., 2011, Paleogeographic reconstruction of the Eocene Idaho River, North American Cordillera: Geological Society of America Bulletin, v. 123, p. 71–88, doi:10.1130/B30213.1.

Cline, J.S., Hofstra, A.H., Muntean, J.L., Tosdal, R.M., and Hickey, K.A., 2005, Carlin-type gold deposits in Nevada: Critical geologic characteristics and viable models: Economic Geology, 100th Anniversary Volume, p. 451–484.

Coats, R.R., 1987, Geology of Elko County, Nevada: Nevada Bureau of Mines and Geology Bulletin 101, 112 p.

Coble, M.A., and Mahood, G.A., 2012, Initial impingement of the Yellowstone plume located by widespread silicic volcanism contemporaneous with Columbia River flood basalts: Geology, v. 40, p. 655–658, doi:10.1130/G32692.1.

Colgan, J.P., 2013, Reappraisal of the relationship between the northern Nevada rift and Miocene extension in the northern Basin and Range province: Geology, v. 41, p. 211–214, doi:10.1130/G33512.1.

Colgan, J.P., and Henry, C.D., 2009, Rapid middle Miocene collapse of the Mesozoic orogenic plateau in north-central Nevada: International Geology Review, v. 51, p. 920–961, doi:10.1080/00206810903056731.

Colgan, J.P., Howard, K.A., Fleck, R.J., and Wooden, J.L., 2010, Rapid middle Miocene extension and unroofing of the southern Ruby Mountains, Nevada: Tectonics, v. 29, TC6022, 38 p., doi:10.1029/2009TC002655.

Coney, P.J., 1980, Cordilleran metamorphic core complexes: An overview, *in* Crittenden, M.D., et al., eds., Cordilleran metamorphic core complexes: Geological Society of America Memoir 153, p. 7–31, doi:10.1130/MEM153-p7.

Coney, P.J., and Harms, T.A., 1984, Cordilleran metamorphic core complexes: Cenozoic extensional relics of Mesozoic compression: Geology, v. 12, p. 550–554, doi:10.1130/0091-7613(1984)12<550:CMCCCE>2.0.CO;2.

Cook, H.E., and Corboy, J.J., 2004, Great Basin Paleozoic carbonate platform: Facies, facies transitions, depositional models, platform architecture, sequence stratigraphy, and predictive mineral host models: U.S. Geological Survey Open-File Report 2004-1078, 135 p.

Cooper, F.J., Platt, J.P., Anczkiewicz, R., and Whitehouse, M.J., 2010, Footwall dip of a core complex detachment fault: Thermobarometric constraints from the northern Snake Range (Basin and Range, USA): Journal of Metamorphic Petrology, v. 28, p. 997–1020, doi:10.1111/j.1525-1314.2010.00907.x.

Crafford, A.E.J., 2005, New digital conodont color alteration index (CAI) maps of Nevada: Geological Society of America Abstracts with Programs, v. 37, no. 7, p. 379.

Crafford, A.E.J., 2007, Geologic map of Nevada: U.S. Geological Survey Data Series 249, 46 p.

Dallmeyer, R.D., Snoke, A., and McKee, E.H., 1986, The Mesozoic–Cenozoic tectonothermal evolution of the Ruby Mountains, East Humboldt Range, Nevada: A Cordilleran metamorphic core complex: Tectonics, v. 5, p. 931–954, doi:10.1029/TC005i006p00931.

DeCelles, P.G., 2004, Late Jurassic to Eocene evolution of the Cordilleran thrust belt and foreland basin system, western U.S.A.: American Journal of Science, v. 304, p. 105–168, doi:10.2475/ajs.304.2.105.

DeCelles, P.G., and Coogan, J.C., 2006, Regional structure and kinematic history of the Sevier fold-and-thrust belt, central Utah: Geological Society of America Bulletin, v. 118, p. 841–864, doi:10.1130/B25759.1.

Dickinson, W.R., 2006, Geotectonic evolution of the Great Basin: Geosphere, v. 2, no. 7, p. 353–368, doi: 10.1130/GES00054.1.

Dickinson, W.R., 2013, Phanerozoic palinspastic reconstructions of Great Basin geotectonics (Nevada-Utah, USA): Geosphere, v. 9, no. 5, p. 1384–1396, doi:10.1130/GES00888.1.

Dickinson, W.R., and Gehrels, G.E., 2008, U-Pb ages of detrital zircons in relation to paleogeography: Triassic paleodrainage networks and sediment dispersal across southwest Laurentia: Journal of Sedimentary Research, v. 78, p. 745–764, doi:10.2110/jsr.2008.088.

Dokka, R.K., Mahaffie, M.J., and Snoke, A.W., 1986, Thermochronologic evidence of major tectonic denudation associated with detachment faulting, northern Ruby Mountains–East Humboldt Range, Nevada: Tectonics, v. 5, p. 995–1006, doi:10.1029/TC005i007p00995.

Drew, J., 2013, Cretaceous and Eocene U-Pb zircon migmatite ages from the East Humboldt Range metamorphic core complex, Nevada [M.S. thesis]: Las Vegas, University of Nevada Las Vegas, paper 1820, 73 p.

Druschke, P., Hanson, A.D., Wells, M.L., Rasbury, T., Stockli, D.F., and Gehrels, G., 2009, Synconvergent surface-breaking normal faults of Late Cretaceous age within the Sevier hinterland, east-central Nevada: Geology, v. 37, p. 447–450, doi:10.1130/G25546A.1.

Druschke, P., Hanson, A.D., Wells, M.L., Gehrels, G.E., and Stockli, D., 2011, Paleogeographic isolation of the Cretaceous to Eocene Sevier hinterland, east-central Nevada: Insights from U-Pb and (U-Th)/He detrital zircon ages of hinterland strata: Geological Society of America Bulletin, v. 123, p. 1141–1160, doi:10.1130/B30029.1.

du Bray, E.A., 2007, Time, space, and composition relations among northern Nevada intrusive rocks and their metallogenic implications: Geosphere, v. 3, p. 381–405, doi:10.1130/GES00109.1.

Dudás, F.Ö., Ispolatov, V.O., Harlan, S.S., and Snee, L.W., 2010, $^{40}Ar/^{39}Ar$ geochronology and geochemical reconnaissance of the Eocene Lowland Creek volcanic field, west-central Montana: Journal of Geology, v. 118, p. 295–304, doi:10.1086/651523.

Dumitru, T.A., Ernst, W.G., Wright, J.E., Wooden, J.L., Wells, R.E., Farmer, L.P., Kent, A.J.R., and Graham, S.A., 2013, Eocene extension in Idaho generated massive sediment floods into the Franciscan trench and into the Tyee, Great Valley, and Green River basins: Geology, v. 41, p. 187–190, doi:10.1130/G33746.1.

Ellis, B.S., Barry, T., Branney, M.J., Wolff, J.A., Bindeman, I., Wilson, R., and Bonnichsen, B., 2010, Petrologic constraints on the development of a large-volume, high temperature, silicic magma system: The Twin Falls eruptive centre, central Snake River Plain: Lithos, v. 120, p. 475–489, doi:10.1016/j.lithos.2010.09.008.

Ewart, A., 1982, The mineralogy and petrology of Tertiary–Recent orogenic volcanic rocks: With special reference to the andesitic–basaltic compositional range: Andesites: Orogenic Andesites and Related Rocks, v. 7, p. 25–98.

Faulds, J.E., Henry, C.D., and Hinz, N.H., 2005, Kinematics of the northern Walker Lane: An incipient transform fault along the Pacific–North American plate boundary: Geology, v. 33, p. 505–508, doi:10.1130/G21274.1.

Feng, R., Poulsen, C.J., Werner, M., Chamberlain, C.P., Mix, H.T., and Mulch, A., 2013, Early Cenozoic evolution of topography, climate, and stable isotopes in precipitation in the North American Cordillera: American Journal of Science, v. 313, p. 613–648, doi:10.2475/07.2013.01.

Fouch, T.D., Hanley, J.H., and Forester, R.M., 1979, Preliminary correlation of Cretaceous and Paleogene lacustrine and related nonmarine sedimentary and volcanic rocks in parts of the eastern Great Basin of Nevada and Utah, *in* Newman, G.W., and Cooke, H.D., eds., RMAG-UGA 1979 Basin and Range Symposium: Rocky Mountain Association of Geologists and Utah Geological Association, p. 305–312.

Fritz, W.J., Sears, J.W., McDowell, R.J., and Wampler, J.M., 2007, Cenozoic volcanic rocks of southwestern Montana: Northwest Geology, v. 36, p. 91–110.

Gans, P.B., 1990, Space-time patterns of Cenozoic N-S extension, N-S shortening, E-W extension, and magmatism in the Basin and Range Province: Evidence for active rifting. Geological Society of America Abstracts with Programs, v. 22, p. 24.

Gans, P.B., and Miller, E.L., 1983, Style of mid-Tertiary extension in east-central Nevada, *in* Gurgel, K.D., ed., Geologic excursions in the overthrust belt and metamorphic core complexes of the intermountain region: Guidebook, Part 1: Utah Geological and Mineral Survey Special Studies 59, p. 107–139.

Gans, P.B., Repetski, J.E., Harris, A.G., and Clark, D.H., 1990, Conodont geothermometry of Paleozoic supracrustal rocks in the eastern Great Basin: Geology and ore deposits of the Great Basin: Geological Society of Nevada Great Basin Symposium Program with Abstracts, p. 103.

Gaschnig, R.M., Vervoort, J.D., Lewis, R.S., and McClelland, W.C., 2009, Migrating magmatism in the northern US Cordillera: In situ U-Pb geochronology of the Idaho batholith: Contributions to Mineralogy and Petrology, v. 159, p. 863–883, doi:10.1007/s00410-009-0459-5.

Gaschnig, R.M., Vervoort, J.D., Lewis, R.S., and Tikoff, B., 2011, Isotopic evolution of the Idaho batholith and Challis intrusive province, northern US Cordillera: Journal of Petrology, v. 52, p. 2397–2429, doi:10.1093/petrology/egr050.

Gehrels, G.E., and Pecha, M., 2014, Detrital zircon U-Pb geochronology and Hf isotope geochemistry of Paleozoic and Triassic passive margin strata of western North America: Geosphere, v. 10, p. 49–65, doi:10.1130/GES00889.1.

Gordee, S.M., Dettloff, C.L., and Burton, B.R., 2000, Geologic and geochemical comparison of late Eocene–Oligocene volcanic and intrusive rocks, Carlin-Piñon Range and central Ruby Mountains, Elko County, Nevada: Geological Society of America Abstracts with Programs, v. 32, no. 7, p. 159.

Haines, S.H., and van der Pluijm, B.A., 2010, Dating the detachment fault system of the Ruby Mountains, Nevada: Significance for the kinematics of low-angle normal faults: Tectonics, v. 29, TC4028, doi:10.1029/2009TC002552.

Geosphere, published online on 5 February 2016 as doi:10.1130/GES01198.1

Hallett, B.W., and Spear, F.S., 2014, The P-T History of anatectic pelites of the northern East Humboldt Range, Nevada: Evidence for tectonic loading, decompression, and anatexis: Journal of Petrology, v. 55, p. 3–36, doi:10.1093/petrology/egt057.

Hallett, B.W., and Spear, F.S., 2015, Monazite, zircon, and garnet growth in migmatitic pelites as a record of metamorphism and partial melting in the East Humboldt Range, Nevada: American Mineralogist, v. 100, p. 951–972, doi:10.2138/am-2015-4839.

Haxby, W.F., Melkonian, A.K., Coplan, J., Chan, S.-M., and Ryan, W.B.F., 2010, GeoMapApp freeware software: Palisades, New York, Lamont-Doherty Earth Observatory.

Haynes, S.R., 2003, Development of the Eocene Elko basin, northeastern Nevada: Implications for paleogeography and regional tectonism [M.S. thesis]: Vancouver, University of British Columbia, 159 p.

Haynes, S.R., Hickey, K.A., Mortensen, J.K., and Tosdal, R., 2002, Onset of extension in the Basin and Range: Basin analysis of the Eocene Elko Formation, NE Nevada: Geological Society of America Abstracts with Programs, v. 34, no. 6, p. 83.

Henrici, A.C., and Haynes, S.R., 2006, Elkobatrachus brocki, a new pelobatid (Amphibia: anura) from the Eocene Elko Formation of Nevada: Annals of the Carnegie Museum, v. 75, p. 11–35, doi:10.2992/0097-4463(2006)75[11:EBANPA]2.0.CO;2.

Henry, C.D., 2008, Ash-flow tuffs and paleovalleys in northeastern Nevada: Implications for Eocene paleogeography and extension in the Sevier hinterland, northern Great Basin: Geosphere, v. 4, p. 1–35, doi:10.1130/GES00122.1.

Henry, C.D., and John, D.A., 2013, Magmatism, ash-flow tuffs, and calderas of the ignimbrite flareup in the western Nevada volcanic field: Geosphere, v. 9, p. 951–1008, doi:10.1130/GES00867.1.

Henry, C.D., McGrew, A.J., Colgan, J.P., Snoke, A.W., and Brueske, M.E., 2011, Timing, distribution, amount, and style of Cenozoic extension in the northern Great Basin, *in* Lee, J., and Evans, J.P., eds., Geologic field trips to the Basin and Range, Rocky Mountains, Snake River Plain, and terranes of the U.S. Cordillera: Geological Society of America Field Guide 21, p. 27–66, doi:10.1130/2011.0021(02).

Henry, C.D., Hinz, N.H., Faulds, J.E., Colgan, J.P., John, D.A., Brooks, E.R., Cassel, E.J., Garside, L.J., Davis, D.A., and Castor, S.B., 2012, Eocene–early Miocene paleotopography of the Sierra Nevada–Great Basin–Nevadaplano based on widespread ash-flow tuffs and paleovalleys: Geosphere, v. 8, p. 1–27, doi:10.1130/GES00727.1.

Hodges, K.V., and Walker, J.D., 1992, Extension in the Cretaceous Sevier orogen, North American Cordillera: Geological Society of America Bulletin, v. 104, p. 560–569, doi:10.1130/0016-7606(1992)104<0560:EITCSO>2.3.CO;2.

Hodges, K.V., Snoke, A.W., and Hurlow, H.A., 1992, Thermal evolution of a portion of the Sevier Hinterland: The Northern Ruby Mountains–East Humboldt Range and Wood Hills, northeastern Nevada: Tectonics, v. 11, p. 154–164, doi:10.1029/91TC01879.

Honjo, N., Bonnichsen, W., Leeman, W.P., and Stormer, J.C., Jr., 1992, Mineralogy and geothermometry of high-temperature rhyolites from the central and western Snake River Plain: Bulletin of Volcanology, v. 54, p. 220–237, doi:10.1007/BF00278390.

Horton, T.W., Sjostrom, D.J., Abruzzese, M.J., Poage, M.A., Waldbauer, J.R., Hren, M., Wooden, J., and Chamberlain, C.P., 2004, Spatial and temporal variation of Cenozoic surface elevation in the Great Basin and Sierra Nevada: American Journal of Science, v. 304, p. 862–888, doi:10.2475/ajs.304.10.862.

Howard, K.A., 2003, Crustal structure in the Elko-Carlin region, Nevada, during Eocene gold mineralization: Ruby–East Humboldt metamorphic core complex as a guide to the deep crust: Economic Geology and the Bulletin of the Society of Economic Geologists, v. 98, p. 249–268, doi:10.2113/gsecongeo.98.2.249.

Howard, K.A., Wooden, J.L., Barnes, C.G., Premo, W.R., Snoke, A.W., and Lee, S.-Y., 2011, Episodic growth of a Late Cretaceous and Paleogene intrusive complex of pegmatitic leucogranite, Ruby Mountains core complex, Nevada, USA: Geosphere, v. 7, p. 1220–1248, doi:10.1130/GES00668.1.

Humphreys, E.D., 1995, Post-Laramide removal of the Farallon slab, western United States: Geology, v. 23, p. 987–990, doi:10.1130/0091-7613(1995)023<0987:PLROTF>2.3.CO;2.

Janecke, S.U., and Snee, L.W., 1993, Timing and episodicity of middle Eocene volcanism and onset of conglomerate deposition, Idaho: Journal of Geology, v. 101, p. 603–621, doi:10.1086/648252.

Janecke, S., McIntosh, W., and Good, S., 1999, Testing models of rift basins: structure and stratigraphy of an Eocene–Oligocene supradetachment basin, Muddy Creek half graben, south-west Montana: Basin Research, v. 11, p. 143–165, doi:10.1046/j.1365-2117.1999.00092.x.

John, D.A., 1995, Tilted middle Tertiary ash-flow calderas and subjacent granitic plutons, southern Stillwater Range, Nevada: Cross sections of an Oligocene igneous center: Geological Society of America Bulletin, v. 107, p. 180–200, doi:10.1130/0016-7606(1995)107<0180:TMTAFC>2.3.CO;2.

John, D.A., Henry, C.D., and Colgan, J.P., 2008, Magmatic and tectonic evolution of the Caetano caldera, north-central Nevada: A tilted, mid-Tertiary eruptive center and source of the Caetano Tuff: Geosphere, v. 4, p. 75–106, doi:10.1130/GES00116.1.

Johnson, J.G., and Pendergast, A., 1981, Timing and mode of emplacement of the Roberts Mountains allochthon, Antler orogeny: Geological Society of America Bulletin, v. 92, p. 648–658, doi:10.1130/0016-7606(1981)92<648:TAMOEO>2.0.CO;2.

Johnson, J.G., and Visconti, R., 1992, Roberts Mountains thrust relationships in a critical area, northern Sulphur Spring Range, Nevada: Geological Society of America Bulletin, v. 104, p. 1208–1220, doi:10.1130/0016-7606(1992)104<1208:RMTRIA>2.3.CO;2.

Ketner, K.B., 1998, The nature and timing of tectonism in the western facies terrane of Nevada and California: An outline of evidence and interpretations derived from geologic maps of key areas: U.S. Geological Survey Professional Paper 1592, 19 p.

Ketner, K.B., and Alpha, A.G., 1992, Mesozoic and Tertiary rocks near Elko, Nevada— Evidence for Jurassic to Eocene folding and low-angle faulting, *in* Evolution of sedimentary basins—Eastern Great Basin: U.S. Geological Survey Bulletin, v. 1988-C, p. C1–C13.

Konstantinou, A., Strickland, A., Miller, E.L., and Wooden, J.P., 2012, Multistage Cenozoic extension of the Albion–Raft River–Grouse Creek metamorphic core complex: Geochronologic and stratigraphic constraints: Geosphere, v. 8, p. 1429–1466, doi:10.1130/GES00778.1.

Konstantinou, A., Strickland, A., Miller, E.L., Vervoort, J.D., Fisher, C.M., Wooden, J.L., and Valley, J.W., 2013, Synextensional magmatism leading to crustal flow in the Albion–Raft River–Grouse Creek metamorphic core complex, northeastern Basin and Range: Tectonics, v. 32, p. 1384–1403, doi:10.1002/tect.20085.

Le Bas, M.J., Le Maitre, R.W., Streckeisen, A., and Zanettin, B., 1986, A chemical classification of volcanic rocks based on the total alkali-silica diagram: Journal of Petrology, v. 27, p. 745–750, doi:10.1093/petrology/27.3.745.

Lewis, C.J., Wernicke, B.P., Selverstone, J., and Bartley, J.M., 1999, Deep burial of the footwall of the northern Snake Range decollement, Nevada: Geological Society of America Bulletin, v. 111, p. 39–51, doi:10.1130/0016-7606(1999)111<0039:DBOTFO>2.3.CO;2.

Long, S.P., 2012, Magnitudes and spatial patterns of erosional exhumation in the Sevier hinterland, eastern Nevada and western Utah, USA: Insights from a Paleogene paleogeologic map: Geosphere, v. 8, p. 881–901, doi:10.1130/GES00783.1.

Longo, A.A., Thompson, T.B., and Harlan, J.B., 2002, Geologic overview of the Rain subdistrict, *in* Thompson, T.B., et al., eds., Gold deposits of the Carlin trend: Nevada Bureau of Mines and Geology Bulletin 111, p. 168–189.

Lund, K., Aleinikoff, J.N., Evans, K.V., duBray, E.A., Dewitt, E.H., and Unruh, D.M., 2010, SHRIMP U-Pb dating of recurrent Cryogenian and Late Cambrian–Early Ordovician alkalic magmatism in central Idaho: Implications for Rodinian rift tectonics: Geological Society of America Bulletin, v. 122, p. 430–453, doi:10.1130/B26565.1.

Lund Snee, J.-E., 2013, Geology and geochronology of Cenozoic units in the Piñon Range and Huntington Valley, Nevada [M.S. thesis]: Stanford, California, Stanford University, 227 p., http://purl.stanford.edu/hx388mg6634.

Lund Snee, J.-E., and Miller, E.L., 2015, Preliminary geologic map of Cenozoic units of the central Robinson Mountain volcanic field and northwestern Huntington Valley, Elko County, Nevada: Nevada Bureau of Mines and Geology Open-File Report 15-2, scale 1:24,000, http://pubs.nbmg.unr.edu/product-p/of2015-02.htm.

MacCready, T., Snoke, A.W., Wright, J.E., and Howard, K.A., 1997, Mid-crustal flow during Tertiary extension in the Ruby Mountains core complex, Nevada: Geological Society of America Bulletin, v. 109, p. 1576–1594, doi:10.1130/0016-7606(1997)109<1576:MCFDTE>2.3.CO;2.

Mattinson, C.G., Colgan, J.P., Metcalf, J.R., Miller, E.L., and Wooden, J.L., 2007, Late Cretaceous to Paleocene metamorphism and magmatism in the Funeral Mountains metamorphic core complex, Death Valley, California, *in* Cloos, M., et al., eds., Convergent margin terranes and associated regions: A tribute to W.G. Ernst: Geological Society of America Special Paper 419, p. 205–223, doi:10.1130/2006.2419(11).

McGrew, A.J., and Snee, L.W., 1994, $^{40}Ar/^{39}Ar$ thermochronologic constraints on the tectonothermal evolution of the northern East Humboldt Range metamorphic core complex, Nevada: Tectonophysics, v. 238, p. 425–450, doi:10.1016/0040-1951(94)90067-1.

McGrew, A.J., and Snoke, A.W., 2010, SHRIMP-RG U-Pb isotopic systematics of zircon from the Angel Lake ortho-

Geosphere, published online on 5 February 2016 as doi:10.1130/GES01198.1

gneiss, East Humboldt Range, Nevada: Is this really Archean crust?: Comment: Geosphere, v. 6, p. 962–965, doi:10.1130/GES00526.1.

McGrew, A.J., and Snoke, A.W., 2015, Geologic map of the Welcome quadrangle and an adjacent part of the Wells quadrangle, Elko County, Nevada: Nevada Bureau of Mines and Geology Map 184, scale 1:24,000, http://pubs.nbmg.unr.edu/product-p/m184.htm.

McGrew, A.J., Peters, M.T., and Wright, J.E., 2000, Thermobarometric constraints on the tectonothermal evolution of the East Humboldt Range metamorphic core complex, Nevada: Geological Society of America Bulletin, v. 112, p. 45–60, doi:10.1130/0016-7606(2000)112<45:TCOTTE>2.0.CO;2.

McKee, E.H., Noble, D.C., and Silberman, M.L., 1970, Middle Miocene hiatus in volcanic activity in the Great Basin area of the western United States: Earth and Planetary Science Letters, v. 8, p. 93–96, doi:10.1016/0012-821X(70)90156-1.

McKee, E.H., Silberman, M.L., Marvin, R.E., and Obradovich, J.D., 1971, A summary of radiometric ages of Tertiary volcanic rocks in Nevada and eastern California—Part 1, central Nevada: Isochron-West, v. 2, p. 21–42.

Miller, E.L., and Gans, P.B., 1989, Cretaceous crustal structure and metamorphism in the hinterland of the Sevier thrust belt, western U.S. Cordillera: Geology, v. 17, p. 59–62, doi:10.1130/0091-7613(1989)017<0059:CCSAMI>2.3.CO;2.

Miller, E.L., Miller, M.M., Stevens, C.H., Wright, J.E., and Madrid, R., 1992, Late Paleozoic paleogeographic and tectonic evolution of the western U.S. Cordillera, *in* Burchfiel, B., et al., eds., The Cordilleran orogen: Conterminous U.S.: Boulder, Colorado, Geological Society of America, Geology of North America, v. 3, p. 57–106.

Miller, E.L., Dumitru, T.A., Brown, R.W., and Gans, P.B., 1999, Rapid Miocene slip on the Snake Range–Deep Creek Range fault system, east-central Nevada: Geological Society of America Bulletin, v. 111, p. 886–905, doi:10.1130/0016-7606(1999)111<0886:RMSOTS>2.3.CO;2.

Miller, E.L., Konstantinou, A., and Strickland, A., 2012, Geodynamics of synconvergent extension and tectonic mode switching: Constraints from the Sevier-Laramide orogen: Comment: Tectonics, v. 31, TC4015, doi:10.1029/2012TC003103.

Mix, H.T., Mulch, A., Kent-Corson, M.L., and Chamberlain, C.P., 2011, Cenozoic migration of topography in the North American Cordillera: Geology, v. 39, p. 87–90, doi:10.1130/G31450.1.

Molnar, P., and Chen, W.-P. 1983, Focal depths and fault plane solutions of earthquakes under the Tibetan Plateau: Journal of Geophysical Research, v. 88, no. B2, p. 1180–1196, doi:10.1029/JB088iB02p01180.

Moore, S.W., Madrid, H.B., and Server, G.T., 1983, Results of oil-shale investigations in northeastern Nevada: U.S. Geological Survey Open-File Report 83-586, 18 p.

Mueller, K.J., and Snoke, A.W., 1993, Progressive overprinting of normal fault systems and their role in Tertiary exhumation of the East Humboldt–Wood Hills metamorphic complex, northeast Nevada: Tectonics, v. 12, p. 361–371, doi:10.1029/92TC01967.

Mulch, A., Chamberlain, C.P., Cosca, M.A., Teyssier, C., Methner, K., Hren, M.T., and Graham, S.A., 2015, Rapid change in high-elevation precipitation patterns of western North America during the Middle Eocene Climatic Optimum (MECO): American Journal of Science, v. 315, p. 317–336, doi:10.2475/04.2015.02.

Palmer, H.C., MacDonald, W.D., and Hayatsu, A., 1991, Magnetic, structural and geochronologic evidence bearing on volcanic sources and Oligocene deformation of ash flow tuffs, northeast Nevada: Journal of Geophysical Research, v. 96, no. B2, p. 2185–2202, doi:10.1029/90JB02224.

Perkins, M.E., and Nash, B.P., 2002, Explosive silicic volcanism of the Yellowstone hotspot: The ash fall tuff record: Geological Society of America Bulletin, v. 114, p. 367–381, doi:10.1130/0016-7606(2002)114<0367:ESVOTY>2.0.CO;2.

Perkins, M.E., Brown, F.H., Nash, W.P., Williams, S.K., and McIntosh, W., 1998, Sequence, age, and source of silicic fallout tuffs in middle to late Miocene basins of the northern Basin and Range province: Geological Society of America Bulletin, v. 110, p. 344–360, doi:10.1130/0016-7606(1998)110<0344:SAASOS>2.3.CO;2.

Phillips, D., and Matchan, E.L., 2013, Ultra-high precision $^{40}Ar/^{39}Ar$ ages for Fish Canyon Tuff and Alder Creek Rhyolite sanidine: New dating standards required?: Geochimica et Cosmochimica Acta, v. 121, p. 229–239, doi:10.1016/j.gca.2013.07.003.

Premo, W.R., Howard, K.A., and Castiñeras, P., 2005, New SHRIMP U-Pb zircon ages and Nd isotopic signatures for plutonism in the northern Ruby–East Humboldt Ranges of NE Nevada: Implications for the timing of Tertiary core complex formation: Geological Society of America Abstracts with Programs, v. 37, no. 7, p. 359.

Premo, W.R., Castiñeras, P., and Wooden, J.L., 2008, SHRIMP-RG U-Pb isotopic systematics of zircon from the Angel Lake orthogneiss, East Humboldt Range, Nevada: Is this really Archean crust?: Geosphere, v. 4, p. 963–975, doi:10.1130/GES00164.1.

Premo, W.R., Moscati, R.J., McGrew, A.J., and Snoke, A.W., 2014, New U-Pb zircon geochronology of Precambrian paragneisses and late Phanerozoic orthogneisses of the Angel Lake–Lizzies Basin region of the East Humboldt Range, northeastern Nevada: A comparison with the thermal chronology at Lamoille Canyon in the adjacent Ruby Mountains: Geological Society of America Abstracts with Programs, v. 46, no. 5, p. 33.

Rahl, J.M., McGrew, A.J., and Foland, K.A., 2002, Transition from contraction to extension in the northeastern Basin and Range: New evidence from the Copper Mountains, Nevada: Journal of Geology, v. 110, p. 179–194, doi:10.1086/338413.

Regnier, J., 1960, Cenozoic geology in the vicinity of Carlin, Nevada: Geological Society of America Bulletin, v. 71, p. 1189–1210, doi:10.1130/0016-7606(1960)71[1189:CGITVO]2.0.CO;2.

Renne, P.R., Mundil, R., Balco, G., Min, K., and Ludwig., K.R., 2010, Joint determination of ^{40}K decay constants and $^{40}Ar^*/^{40}K$ for the Fish Canyon sanidine standard, and improved accuracy for $^{40}Ar/^{39}Ar$ geochronology: Geochimica et Cosmochimica Acta, v. 74, p. 5349–5367, doi:10.1016/j.gca.2010.06.017.

Ressel, M.W., and Henry, C.D., 2006, Igneous geology of the Carlin Trend, Nevada: Development of the Eocene Plutonic Complex and significance for Carlin-type gold deposits: Economic Geology and the Bulletin of the Society of Economic Geologists, v. 101, p. 347–383, doi:10.2113/gsecongeo.101.2.347.

Rey, P.F., Teyssier, C., and Whitney, D.L., 2009, The role of partial melting and extensional strain rates in the development of metamorphic core complexes: Tectonophysics, v. 477, p. 135–144, doi:10.1016/j.tecto.2009.03.010.

Rickwood, P.C., 1989, Boundary lines within petrologic diagrams which use oxides of major and minor elements: Lithos, v. 22, p. 247–263, doi:10.1016/0024-4937(89)90028-5.

Ruksznis, A., 2015, Geology and geochronology of Cenozoic sedimentary basins, east-central Nevada [M.S. thesis]: Stanford, California, Stanford University, 201 p.

Ryan, W.B.F., et al., 2009, Global multi-resolution topography synthesis: Geochemistry, Geophysics, Geosystems, v. 10, Q03014, doi:10.1029/2008GC002332.

Ryskamp, E.B., Abbott, J.T., Christiansen, E.H., Keith, J.D., Vervoort, J.D., and Tingey, D.G., 2008, Age and petrogenesis of volcanic and intrusive rocks in the Sulphur Spring Range, central Nevada: Comparisons with ore-associated Eocene magma systems in the Great Basin: Geosphere, v. 4, p. 496–519, doi:10.1130/GES00113.1.

Sanford, R.F., 2005. Geology and stratigraphy of the Challis Volcanic Group and related rocks, Little Wood River area, south-central Idaho, with a section on geochronology by Lawrence W. Snee: U.S. Geological Survey Bulletin 2064-II, 22 p.

Satarugsa, P., and Johnson, R.A., 2000, Cenozoic tectonic evolution of the Ruby Mountains metamorphic core complex and adjacent valleys, northeastern Nevada: Rocky Mountain Geology, v. 35, p. 205–230, doi:10.2113/35.2.205.

Server, G.T., and Solomon, B.J., 1983, Geology and oil shale deposits of the Elko Formation, Pinon Range, Elko County, Nevada: U.S. Geological Survey Miscellaneous Field Studies Map MF-1546, scale 1:24,000.

Sharp, R.P., 1939, The Miocene Humboldt Formation in northeastern Nevada: Journal of Geology, v. 47, p. 133–160, doi:10.1086/624749.

Smith, J.F., and Howard, K.A., 1977, Geologic map of the Lee quadrangle: U.S. Geological Survey Geologic Quadrangle Map GQ-1393, scale 1:62,500.

Smith, J.F., and Ketner, K.B., 1975, Stratigraphy of Paleozoic rocks in the Carlin-Piñon Range area, Nevada: U.S. Geological Survey Professional Paper 867-A, p. A1–A87.

Smith, J.F., and Ketner, K.B., 1976, Stratigraphy of post-Paleozoic rocks and summary of resources in the Carlin-Piñon Range area, Nevada: U.S. Geological Survey Professional Paper 867-B, p. B1–B48.

Smith, J.F., and Ketner, K.B., 1978, Geologic map of the Carlin-Pinon Range area, Elko and Eureka counties, Nevada: U.S. Geological Survey Miscellaneous Investigations Series I-1028, scale 1:62,500.

Snoke, A.W., 1980, Transition from infrastructure to suprastructure in the northern Ruby Mountains, Nevada, *in* Crittenden, M.D., Jr., et al., eds., Cordilleran metamorphic core complexes: Geological Society of America Memoir 153, p. 287–334, doi:10.1130/MEM153-p287.

Snoke, A.W., Barnes, C.G., Howard, K.A., and Wright, J.E., 2004, Late Eocene and Oligocene intrusions in the Ruby–East Humboldt core complex, Nevada: Magmatic processes in the middle crust in relation to tectonic extension: Geological Society of America Abstracts with Programs, v. 36, no. 4, p. 71.

Solomon, B.J., McKee, E.H., and Andersen, D.W., 1979, Stratigraphy and depositional environments of Paleogene rocks

Geosphere, published online on 5 February 2016 as doi:10.1130/GES01198.1

near Elko, Nevada, *in* Armentrout, J.M., et al., eds., Cenozoic paleogeography of the western United States: Pacific Coast Paleogeography Symposium III: Pacific Section, Society of Economic Paleontologist and Mineralogists, p. 75–88.

Sonder, L.J., and Jones, C.H., 1999, Western United States extension: How the west was widened: Annual Review of Earth and Planetary Sciences, v. 27, p. 417–462, doi:10.1146/annurev.earth.27.1.417.

Stewart, J.H., 1980, Geology of Nevada: Nevada Bureau of Mines and Geology Special Publication 4, 136 p.

Strickland, A., Miller, E.L., and Wooden, J.L., 2011, The timing of Tertiary metamorphism and deformation in the Albion–Raft River–Grouse Creek metamorphic core complex, Utah and Idaho: Journal of Geology, v. 119, p. 185–206, doi:10.1086/658294.

Sullivan, W.A., and Snoke, A.W., 2007, Comparative anatomy of core-complex development in the northeastern Great Basin, USA: Rocky Mountain Geology, v. 42, p. 1–29, doi:10.2113/gsrocky.42.1.1.

Trexler, J.H., and Nitchman, S.P., 1990, Sequence stratigraphy and evolution of the Antler foreland basin, east-central Nevada: Geology, v. 18, p. 422–425, doi:10.1130/0091-7613(1990)018<0422:SSAEOT>2.3.CO;2.

Trexler, J.H., Cashman, P.H., Snyder, W.S., and Davydov, V.I., 2004, Late Paleozoic tectonism in Nevada: Timing, kinematics, and tectonic significance: Geological Society of America Bulletin, v. 116, p. 525–538, doi:10.1130/B25295.1.

Turner, R.J.W., Madrid, R.J., and Miller, E.L., 1989, Roberts Mountains allochthon: Stratigraphic comparison with lower Paleozoic outer continental margin strata of the northern Canadian Cordillera: Geology, v. 17, p. 341–344, doi:10.1130/0091-7613(1989)017<0341:RMASCW>2.3.CO;2.

Van Buer, N.J., Miller, E.L., and Dumitru, T.A., 2009, Early Tertiary paleogeologic map of the northern Sierra Nevada batholith and the northwestern Basin and Range: Geology, v. 37, p. 371–374, doi:10.1130/G25448A.1.

Vandervoort, D.S., and Schmitt, J.G., 1990, Cretaceous to early Tertiary paleogeography in the hinterland of the Sevier thrust belt, east-central Nevada: Geology, v. 18, p. 567–570, doi:10.1130/0091-7613(1990)018<0567:CTETPI>2.3.CO;2.

Walker, J.D., Bowers, T.D., Black, R.A., Glazner, A.F., Farmer, G.L., and Carlson, R.W., 2006, A geochemical database for western North American volcanic and intrusive rocks (NAVDAT), *in* Krishna Sinha, A., ed., Geoinformatics: Data to knowledge: Geological Society of America Special Paper 397, p. 61–71, doi:10.1130/2006.2397(05).

Walker, J.D., Geissman, J.W., Bowring, S.A., and Babcock, L.E., compilers, 2012, Geologic time scale v. 4.0: Boulder, Colorado Geological Society of America, doi:10.1130/2012.CTS004R3C, http://www.geosociety.org/science/timescale/timescl.pdf.

Wallace, A.R., Perkins, M.E., and Fleck, R.J., 2008, Late Cenozoic paleogeographic evolution of northeastern Nevada: Evidence from the sedimentary basins: Geosphere, v. 4, p. 36–74, doi:10.1130/GES00114.1.

Wannamaker, P.E., and Doerner, W.M., 2002, Crustal structure of the Ruby Mountains and southern Carlin Trend region, Nevada, from magnetotelluric data: Ore Geology Reviews, v. 21, p. 185–210, doi:10.1016/S0169-1368(02)00089-6.

Wells, M.L., and Hoisch, T.D., 2008, The role of mantle delamination in widespread Late Cretaceous extension and magmatism in the Cordilleran orogen, western United States: Geological Society of America Bulletin, v. 120, p. 515–530, doi:10.1130/B26006.1.

Wells, M.L., Hoisch, T.D., Cruz-Uribe, A.M., and Vervoort, J.D., 2012, Geodynamics of synconvergent extension and tectonic mode switching: Constraints from the Sevier-Laramide orogen: Tectonics, v. 31, TC1002, doi:10.1029/2011TC002913.

Willden, R., and Kistler, R.W., 1979, Precambrian and Paleozoic stratigraphy in central Ruby Mountains, Elko County, Nevada, *in* Newman, G.W., and Cooke, H.D., eds., RMAG-UGA 1979 Basin and Range Symposium: Rocky Mountain Association of Geologists and Utah Geological Association, p. 221–243.

Willis, M.A., 2014, A metamorphic pressure-temperature time path from the Wood Hills, Elko County, eastern Nevada [M.S. thesis]: Flagstaff, Northern Arizona University, 108 p.

Wolfe, J.A., Forest, C.E., and Molnar, P., 1998, Paleobotanical evidence of Eocene and Oligocene paleoaltitudes in mid-latitude western North America: Geological Society of America Bulletin, v. 110, p. 664–678, doi:10.1130/0016-7606(1998)110<0664:PEOEAO>2.3.CO;2.

Wright, J.E., and Snoke, A.W., 1993, Tertiary magmatism and mylonitization in the Ruby–East Humboldt metamorphic core complex, northeastern Nevada: U-Pb geochronology and Sr, Nd, and Pb isotope geochemistry: Geological Society of America Bulletin, v. 105, p. 935–952, doi:10.1130/0016-7606(1993)105<0935:TMAMIT>2.3.CO;2.

Geosphere

Cenozoic paleogeographic evolution of the Elko Basin and surrounding region, northeast Nevada

J.-E. Lund Snee, E.L. Miller, M. Grove, J.K. Hourigan and A. Konstantinou

Geosphere published online 5 February 2016;
doi: 10.1130/GES01198.1

Notes